Mechanisms Through Which Lithocholic Acid and Caloric Restriction Delay Yeast Chronological Aging

Anna Leonov

A Thesis
in
The Department
of
Biology

Presented in Partial Fulfillment of the Requirements
For the Degree of
Doctor of Philosophy (Biology) at
Concordia University
Montreal, Quebec, Canada

April 2018

CONCORDIA UNIVERSITY

School of Graduate Studies

This is to certify that the thesis prepared

By: Anna Leonov

Entitled: Mechanisms Through Which Lithocholic Acid and Caloric Restriction Delay Yeast Chronological Aging

and submitted in partial fulfillment of the requirements for the degree of

Doctor of Philosophy (Biology)

complies with the regulations of the University and meets the accepted standards with respect to originality and quality.

Signed by the final Examining Committee:

_____Chair
Dr. Andrew Chapman

_____External Examiner
Dr. Thomas Sanderson

_____External to Program
Dr. Paul Joyce

_____Examiner
Dr. Jin Suk Lee

_____Examiner
Dr. Alisa Piekny

_____Thesis Supervisor
Dr. Vladimir Titorenko

Approved by _____
Dr. Grant Brown, Graduate Program Director

May 15, 2018 _____
Dr. André Roy, Dean, Faculty of Arts and Science

ABSTRACT

Mechanisms Through Which Lithocholic Acid and Caloric Restriction Delay Yeast Chronological Aging

Anna Leonov, Ph.D.
Concordia University, 2018

The objective of studies described in this thesis was to investigate mechanisms through which lithocholic acid (LCA) and caloric restriction (CR) delay chronological aging of the budding yeast *Saccharomyces cerevisiae*. My overall hypothesis was that each of these aging-delaying interventions slows down yeast chronological aging by targeting different cell biological processes. Findings presented here support this hypothesis. Indeed, I found that LCA delays the chronological mode of *S. cerevisiae* aging by altering the lipid composition of mitochondrial membranes. I demonstrated that these LCA-driven alterations in mitochondrial membrane lipidome elicit distinct changes in the abundance of many mitochondrial proteins, thereby enabling the establishment of a geroprotective pattern of mitochondrial functionality. These findings provided the first comprehensive evidence that mitochondrial lipidome plays an essential role in defining longevity of chronologically aging yeast. I found that CR slows yeast chronological aging through a different mechanism. This previously unknown mechanism links the chronological mode of *S. cerevisiae* aging to cell cycle regulation and controlled cell differentiation. The key aspects of my hypothesis-driven investigation of these two different mechanisms of aging delay are outlined below.

The Titorenko laboratory has previously found that exogenously added LCA delays yeast chronological aging. The laboratory has demonstrated that LCA enters the yeast cell, is sorted to

mitochondria, resides in both mitochondrial membranes, changes the relative concentrations of different membrane phospholipids, triggers changes in the concentrations of many mitochondrial proteins, and alters some key aspects of mitochondrial functionality. Based on these observations, I hypothesized that the LCA-driven changes in mitochondrial lipidome may have a causal role in the remodeling of mitochondrial proteome, which may in turn alter the functional state of mitochondria to create a mitochondrial pattern that delays yeast chronological aging. To test this hypothesis, I investigated how the *ups1Δ*, *ups2Δ* and *psd1Δ* mutations that eliminate enzymes involved in mitochondrial phospholipid metabolism influence the mitochondrial lipidome. I also assessed how these mutations affect the mitochondrial proteome, influence mitochondrial functionality and impinge on the efficiency of aging delay by LCA. My findings provide evidence that 1) LCA initially creates a distinct pro-longevity pattern of mitochondrial lipidome by proportionally decreasing phosphatidylethanolamine and cardiolipin concentrations to maintain equimolar concentrations of these phospholipids, and by increasing phosphatidic acid concentration; 2) this pattern of mitochondrial lipidome allows to establish a specific, aging-delaying pattern of mitochondrial proteome; and 3) this pattern of mitochondrial proteome plays an essential role in creating a distinctive, geroprotective pattern of mitochondrial functionality.

A yeast culture grown in a nutrient-rich medium initially containing 2% glucose is not limited in calorie supply. When yeast cells cultured in this medium consume glucose, they undergo cell cycle arrest at a checkpoint in late G_1 and differentiate into quiescent and non-quiescent cell populations. Studies of such differentiation have provided insights into mechanisms of yeast chronological aging under conditions of excessive calorie intake. CR is an aging-delaying dietary intervention. I hypothesized that CR may slow down yeast chronological aging by eliciting specific changes in cell cycle regulation and controlled cell differentiation. To test this hypothesis, I

investigated how CR influences the differentiation of chronologically aging yeast cultures into quiescent and non-quiescent cells, and how it affects their properties. I found that CR extends yeast chronological lifespan via a mechanism linking cellular aging to cell cycle regulation, maintenance of quiescence, entry into a non-quiescent state and survival in this state. My findings suggest that CR delays yeast chronological aging by causing specific changes in the following: 1) a checkpoint in G_1 for cell cycle arrest and entry into a quiescent state; 2) a growth phase in which high-density quiescent cells are committed to become low-density quiescent cells; 3) the differentiation of low-density quiescent cells into low-density non-quiescent cells; and 4) the conversion of high-density quiescent cells into high-density non-quiescent cells.

Acknowledgements

I am grateful to my supervisor, Dr. Vladimir Titorenko, for his guidance and support during the years I spent in his laboratory. I would like to thank the members of my committee, Dr. Jin Suk Lee and Dr. Alisa Piekny, for their valuable suggestions during my graduate research and studies, as well as all my current and past lab-mates.

Table of Contents

List of Figures

List of Tables

List of Abbreviations

ACN, acetonitrile
CDP-DAG, cytidine diphosphate-diacylglycerol
CDK, cyclin-dependent kinase
CFU, colony forming units
CLS, chronological lifespan
CL, cardiolipin
CR, caloric restriction
CW, Calcofluor White M2R
DAG, diacylglycerol
DHR, Dihydrorhodamine 123
DIC, differential interference contrast
DTT, dithiothreitol
ER, the endoplasmic reticulum
ETC, electron transport chain
IAA, iodoacetamide
IMM, inner mitochondrial membrane
IMS, the intermembrane space
LCA, lithocholic bile acid
MAM, the mitochondria-associated membrane domain of the endoplasmic reticulum
MFQL, Molecular Fragmentation Query Language
MICOS, the mitochondrial contact site protein complex
MS, mass spectrometry
mtDNA, mitochondrial DNA
nDNA, nuclear DNA
NQ, non-quiescent
OMM, outer mitochondrial membrane
PA, phosphatidic acid
PC, phosphatidylcholine
PCD, programmed cell death
PG, phosphatidylglycerol
PGP, phosphatidylglycerol-phosphate
Pho85, phosphate metabolism, protein 85
PI, phosphatidylinositol
PKA, protein kinase A
POA, palmitoleic acid
PS, phosphatidylserine
PP2ACdc55, the Cdc55 protein phosphatase 2A
Q, quiescent
RLS, replicative lifespan
ROS, reactive oxygen species
RP-HPLC/MS, reverse phase high performance liquid chromatography coupled to mass spectrometry
R123, Rhodamine 123

Snf1, sucrose non-fermenting, protein 1
SSC, statistically significantly changed
SU, statistically unchanged
TCA, tricarboxylic acid
TORC1, target of rapamycin complex 1

1.1 Introduction

Studies of the budding yeast *Saccharomyces cerevisiae*, a unicellular eukaryote amenable to comprehensive molecular analyses, have provided deep insights into mechanisms of cellular aging in multicellular eukaryotes [1-5]. These studies have been instrumental in identifying genes, uncovering signaling pathways and discovering chemical compounds shown to orchestrate a distinct set of cellular processes that define organismal longevity in eukaryotes across phyla [5-21]. These studies have revealed that the key features of the aging process and the mechanisms of its deceleration by certain longevity-extending genetic, dietary and pharmacological interventions are evolutionarily conserved [1-3, 6, 8-10, 15-19].

Two different methods have been established to investigate aging of budding yeast; each of them is designed to monitor a distinct aspect of the aging process. One method measures yeast replicative lifespan (RLS) by assessing the number of asymmetric mitotic divisions a mother cell can undergo prior to cell cycle arrest [2, 3, 5]. Another method measures yeast chronological lifespan (CLS) by assessing the length of time a cell remains viable following cell cycle arrest; a cell is considered to be viable if it can re-enter the cell cycle in response to addition of essential nutrients [2-4, 12, 13]. The use of these two methods has significantly advanced our understanding of mechanisms that underlie the replicative and chronological paradigms of cellular aging in yeast [2-5, 12, 13].

1.1.1 Some traits of mitochondrial functionality are essential for aging of *S. cerevisiae*

An age-related deterioration of mitochondrial functionality is the universal hallmark of aging in eukaryotes across phyla [22]. This age-related deterioration is manifested as a progressive decline of the efficiencies with which mitochondria create the bulk of cellular ATP and generate biosynthetic intermediates for amino acids, nucleotides and lipids [22-31].

The functional state of mitochondria defines the pace of the replicative and chronological modes of aging in the yeast *S. cerevisiae* [32-36]. Some traits of mitochondrial functionality are well known for their essential roles in yeast replicative and chronological aging. These mitochondrial traits include the following: 1) electron transport chain, oxidative phosphorylation and membrane potential [32-43]; 2) reactive oxygen species (ROS) homeostasis [32-34, 38, 44-55]; 3) protein synthesis and proteostasis [32, 48, 56-68]; 4) synthesis and assembly of iron-sulfur

clusters [40, 48, 69-71]; 5) amino acid synthesis [33, 45, 48, 55, 72-77]; and 6) NADPH synthesis [33, 48, 55, 78, 79].

However, prior to studies described in my thesis, it was unknown if such an important trait of mitochondrial functionality as the composition of mitochondrial membrane lipids can play a role in yeast aging. Our high-throughput screen of almost 19,000 chemical compounds from several commercial libraries has previously identified lithocholic bile acid (LCA) as a molecule that delays the onset and decreases the rate of yeast chronological aging [7, 80]. Although LCA delays the chronological mode of aging in *S. cerevisiae*, this yeast is unable to synthesize LCA or any other bile acid [7]. Bile acids are known to be synthesized from cholesterol in mammalian hepatocytes of the liver [7]. In mammals, these amphipathic by their chemical structure molecules operate as 1) trophic factors for the enteric epithelium; 2) detergents for the emulsification and absorption of dietary lipids and fat-soluble vitamins; and 3) signaling molecules that control lipid, glucose and energy homeostasis and stimulate detoxification of xenobiotics [7].

We showed that in *S. cerevisiae*, the aging-delaying efficiency of LCA under caloric restriction (CR) on 0.2% glucose greatly exceeds its aging-delaying efficiency under non-CR conditions on 2% glucose [7]. We demonstrated that exogenously added LCA enters the yeast cell, accumulates in mitochondria, resides mainly in the inner mitochondrial membrane (IMM), and associates with the outer mitochondrial membrane (OMM) [81]. We provided evidence that mitochondria-associated LCA alters the abundance and relative concentrations of different classes of membrane phospholipids [81], elicits age-related changes in the concentrations of many mitochondrial proteins [82], and modifies the age-related chronology of some key aspects of mitochondrial functionality [81]. Based on these findings, we proposed the following hypotheses: 1) LCA delays yeast chronological aging because it initially causes specific changes in the composition of mitochondrial membrane lipids; 2) as outlined in Figure 1.1, these changes in mitochondrial membrane lipidome include an increase in the concentrations of phosphatidic acid (PA), phosphatidylglycerol (PG), phosphatidylcholine (PC) and phosphatidylserine (PS), as well as a decrease in the concentrations of cardiolipin (CL), monolysocardiolipin (MLCL) and phosphatidylethanolamine (PE); 3) the LCA-driven changes in mitochondrial lipidome then alter mitochondrial proteome; and 4) these changes in protein composition of mitochondria lead to specific alterations in mitochondrial functionality, thus creating a mitochondrial pattern that delays the onset and slows down the progression of yeast chronological aging (Figure 1.1) [82, 83].

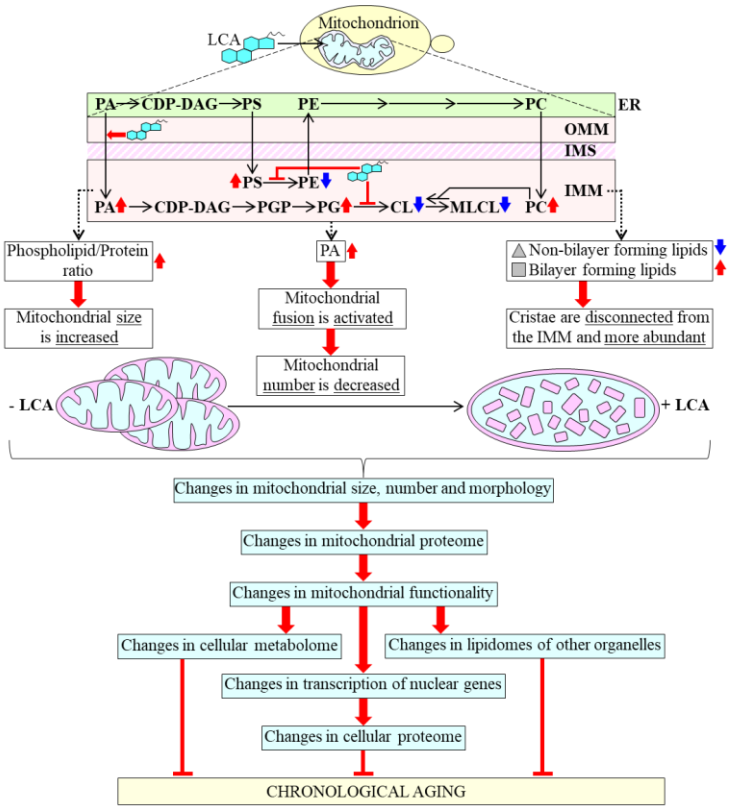

Figure 1.1. Our hypothesis on how LCA delays yeast chronological aging by altering the composition of mitochondrial membrane phospholipids. See text for more details. Abbreviations: Abbreviations: CDP-DAG, cytidine diphosphate-diacylglycerol; CL, cardiolipin; DAG, diacylglycerol; ER, the endoplasmic reticulum; IMM, the inner mitochondrial membrane; IMS, the intermembrane space; MAM, the mitochondria-associated membrane domain of the ER; OMM, the outer mitochondrial membrane; PA, phosphatidic acid; PC, phosphatidylcholine; PG, phosphatidylglycerol; PGP, phosphatidylglycerol-phosphate; PI, phosphatidylinositol; PS, phosphatidylserine.

The relative concentrations of different classes of membrane phospholipids in yeast mitochondria depend on several processes known to be accelerated by enzymes confined to both mitochondria and the endoplasmic reticulum (ER) [192-199]. Among these processes are the following steps of phospholipid synthesis and transfer: 1) the synthesis of PA, cytidine diphosphate-diacylglycerol (CDP-DAG), diacylglycerol (DAG), PS, PC and phosphatidylinositol (PI) in the ER; 2) the movement of PA from the ER to the outer mitochondrial membrane (OMM) through mitochondria-ER contact sites at zones of a juxtaposition between the OMM and the mitochondria-associated membrane (MAM) domain of the ER; 3) the transfer of PA from the OMM across the intermembrane space (IMS) to the inner mitochondrial membrane (IMM; 4) the conversion of ER-derived PA into CDP-DAG, phosphatidylglycerol-phosphate (PGP), PG, CL and MLCL in a series of reactions that occur in the IMM; 5) the transfer of PS from the ER to the OMM via mitochondria-ER contact sites; 6) the transport of PS from the OMM via the IMS to the IMM, where PS is converted into PE; 7) the synthesis of PE from PS in the OMM, which requires a close apposition between the two mitochondrial membranes; 8) the transfer of PC and PI from the ER to the OMM via mitochondria-ER contact sites, which is followed by the movement of PC

and PI from the OMM to the IMM; and 9) the movement of DAG and CDP-DAG from the ER to the OMM across mitochondria-ER contact sites, and the subsequent transfer of these two phospholipids to the IMM (Figure 1.1) [192-199].

We have previously demonstrated that mitochondrial membranes of yeast treated with LCA have decreased concentrations of non-bilayer forming phospholipids and increased concentrations of bilayer forming phospholipids [81]. The shape of a phospholipid molecule is known to be defined by the relative sizes of the cross-sectional areas of its hydrophilic head group and hydrophobic acyl chains, as follows: 1) if the cross-sectional areas of the hydrophilic head group and hydrophobic acyl chains of a phospholipid are equally sized, it has a cylindrical shape; 2) if the cross-sectional area of the hydrophilic head group of a phospholipid is smaller than the cross-sectional area of its hydrophobic acyl chains, it has a cone shape; and 3) if the cross-sectional area of the hydrophilic head group of a phospholipid is larger than the cross-sectional area of its hydrophobic acyl chains, it has an inverted cone shape [81]. Moreover, the relative concentrations of cylinder-, cone- and inverted cone-shaped phospholipids in a membrane have been shown to define membrane curvature; therefore, changes in the relative concentration of these differently shaped lipids can elicit changes in membrane curvature [81]. For the IMM, an increase in the relative concentrations of phospholipids having the bilayer forming shape of a cylinder decreases the extent of membrane curving [81]. This, in turn, causes the following three kinds of simultaneous changes in mitochondrial morphology: 1) an increase in the abundance of the IMM domains exhibiting so-called "flat" bilayer conformation; 2) a decrease in the abundance of the IMM domains displaying negative curvature (*i.e.*, membrane curving away from the mitochondrial matrix) characteristic of mitochondrial contact sites between the IMM and OMM; and 3) a decrease in the abundance of the IMM domains having positive curvature (*i.e.*, membrane curving towards the mitochondrial matrix) characteristic of mitochondrial cristae formed by the IMM [81]. Furthermore, the simultaneous increase in the relative concentrations of cone- and inverted cone-shaped phospholipids, both being non-bilayer forming species, increases the extent of membrane curving thus increasing the abundance of mitochondrial contact sites and mitochondrial cristae [18, 73, 74]. We have previously found that LCA 1) decreases the relative concentrations of non-bilayer forming phospholipids; 2) increases the relative concentrations of bilayer forming phospholipids; 3) decreases the abundance of the IMM domains having negative curvature characteristic of mitochondrial contact sites between the IMM and OMM; 4) decreases the

abundance of the IMM domains that have positive curvature typical of mitochondrial cristae formed by the IMM; and 5) increases the abundance of the IMM domains having flat bilayer conformation [81].

1.1.2 Chronologically aging yeast cultures contain populations of quiescent and non-quiescent cells

A body of knowledge about mechanisms underlying chronological aging of the yeast *Saccharomyces cerevisiae* has been provided by studies in which yeast cells were cultured in a nutrient-rich liquid medium initially containing 2% glucose [84, 85]. Under these so-called non-caloric restriction (non-CR) conditions yeast cells are not limited in the supply of calories [84, 86, 87]. When glucose is exhausted at the diauxic shift, cells in a non-CR yeast culture undergo arrest at the checkpoint START A in the late G_1 phase of the cell cycle [97]. The non-CR yeast culture then differentiates into several cell populations [88-91].

One of these cell populations is a population of quiescent (Q) cells (Figure 1.2); these cells exist in a distinct non-proliferative state called G_0 [88-94]. Q cells are mainly daughter cells [88-90]. They are unbudded and uniformly sized, are refractive by phase-contrast microscopy and enclosed by a rigid cell wall, have high buoyant density, store glycogen and trehalose in bulk quantities, are highly metabolically active, exhibit high rates of mitochondrial respiration and low concentrations of reactive oxygen species (ROS), are able to form colonies when plated on fresh solid medium, can re-enter mitosis when nutrients become available following transfer to fresh liquid medium, are resistant to long-term thermal and oxidative stresses, exhibit low rates of mutations that impair mitochondrial functionality, and display a delayed onset of the apoptotic and necrotic modes of programmed cell death (PCD) [88-91, 93, 94].

The differentiation of a non-CR yeast culture following glucose exhaustion at the diauxic shift also yields at least three subpopulations of non-quiescent (NQ) cells (Figure 1.2), most or all of which are first- and higher-generation mother cells [88-96, 93, 94]. One subpopulation of NQ cells consists of metabolically active cells that exhibit high reproductive (colony-forming) capacities, high ROS concentrations, impaired mitochondrial respiration and elevated frequencies of mutations impairing mitochondrial functionality (Figure 1.2) [88-91, 93, 94]. Another subpopulation of NQ cells includes metabolically active cells that are impaired in reproductive (clonogenic) ability and are likely to be descended from NQ cells of the first subpopulation (Figure

1.2) [88-91, 93, 94]. The third subpopulation of NQ cells is composed of cells that exhibit hallmarks of the apoptotic and/or necrotic modes of PCD and may derive from NQ cells of the second subpopulation (Figure 1.2) [88-91, 91, 94].

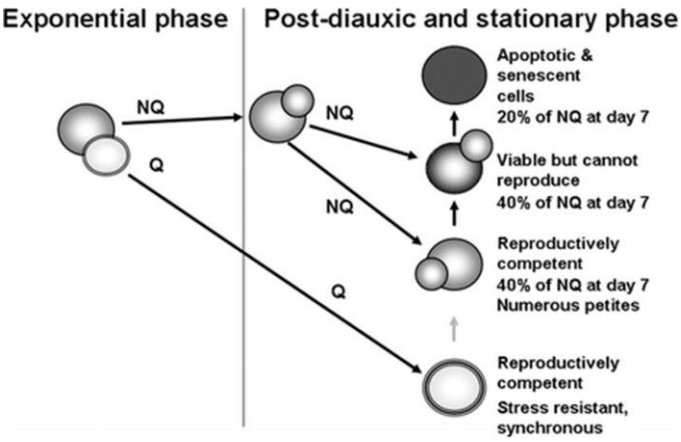

Figure 1.2. When glucose is exhausted at the diauxic shift in a yeast culture grown on 2% glucose, cells in this culture undergo arrest at the G_1 phase of the cell cycle; this culture then differentiates into four cell populations. One of these cell populations is a population of quiescent (Q) cells. In addition, there are at least three subpopulations of non-quiescent (NQ) cells. From: Reference [90].

In response to a depletion of glucose (as well as nitrogen, phosphate or sulfur), a signaling network of certain proteins and protein complexes orchestrates cell cycle arrest at the G_1 phase of the cell cycle, the differentiation of a chronologically aging non-CR yeast culture into populations of Q and NQ cells, and quiescence maintenance. Proteins and protein complexes integrated into this signaling network operate as network nodes, many of which are connected by physical links known to be predominantly phosphorylations and dephosphorylations that activate or inhibit specific target proteins [92, 95-100]. The core hubs of this signaling network of a quiescence program are four nutrient-sensing protein complexes, each of which exhibits a protein kinase activity and modulates many downstream effector proteins integrated into the network (Figure 1.3). These core hubs of the network are: 1) TORC1 (target of rapamycin complex 1), a key regulator of cell metabolism, growth, division and stress resistance in response to changes in the availabilities of nitrogen and carbon sources; 2) PKA (protein kinase A), an essential controller of cell metabolism, proliferation and stress resistance in response to changes in carbon source availability; 3) Snf1 (sucrose non-fermenting, protein 1), a heterotrimeric protein complex required for cell growth support and energy homeostasis maintenance after glucose exhaustion; and 4) Pho85 (phosphate metabolism, protein 85), a protein kinase associated with various cyclins to promote phosphate metabolism, glycogen and trehalose synthesis, oxidative stress response and

cellular proteostasis in response to changes in the accessibility of a phosphate source or following glucose exhaustion (Figure 1.3) [92, 95, 97, 101, 102].

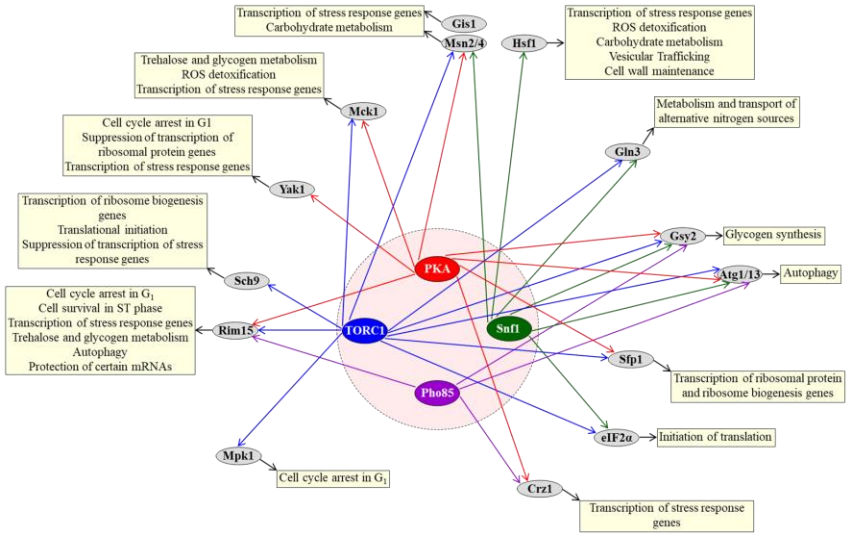

Figure 1.3. In response to a depletion of glucose, a signaling network of certain proteins and protein complexes orchestrates cell cycle arrest at the G_1 phase of the cell cycle, the differentiation of a chronologically aging non-CR yeast culture into populations of quiescent and non-quiescent cells, and quiescence maintenance. See text for more details.

The four core hubs of the signaling network of the quiescence program modulate many downstream effector proteins, including the following: 1) Rim15, a serine-threonine protein kinase which, following glucose exhaustion at the diauxic shift, is essential for cell cycle arrest at G_1, cell survival during stationary growth phase, transcription of many stress response genes, trehalose and glycogen accumulation, autophagy, and post-transcriptional protection of a subset of mRNAs needed for entry into quiescence; Rim15 is controlled by the TORC1, PKA and Pho85 core hubs of the network (Figure 1.3) [101, 103-114]; 2) Sch9, a serine-threonine protein kinase which, prior to glucose exhaustion at the diauxic shift, prevents entry into quiescence by stimulating transcription of genes essential for ribosome biogenesis, promoting translation initiation and suppressing transcription of many stress response genes; Sch9 is modulated by TORC1 (Figure 1.3) [99, 101, 106, 111, 115-119]; 3) Yak1, a serine-threonine protein kinase which in yeast cells entering SP phase is required for cell cycle arrest at G_1, suppresses transcription of genes encoding ribosomal proteins and activates transcription of many stress response genes; Yak1 is under the control of PKA (Figure 1.3) [120-123]; 4) Mck1, a dual-specificity serine-threonine and tyrosine protein kinase which, after glucose exhaustion at the diauxic shift, is essential for the accumulation of trehalose and glycogen, ROS detoxification and transcription of many stress response genes;

Mck1 is likely to be controlled by TORC1 and PKA (Figure 1.3) [125-127]; 5) Msn2/4 and Gis1, transcription factors that activate expression of stress-responsive element- and post-diauxic shift-controlled (respectively) genes involved in protection against thermal, oxidative and osmotic stresses, as well as in carbohydrate metabolism; these transcription factors are modulated by TORC1, PKA and Snf1 (Figure 1.3) [108, 109, 112, 128-138]; 6) Hsf1, a transcription factor which activates expression of many heat shock element-controlled genes involved in protein folding, protein synthesis and modification, ROS detoxification, energy generation, carbohydrate metabolism, intracellular vesicular trafficking, and cell wall maintenance; Hsf1 is controlled by Snf1 (Figure 1.3) [139-142]; 7) Gln3, a transcriptional activator of nitrogen catabolite-repressible genes involved in the metabolism and transport of alternative nitrogen sources; Gln3 is under the control of TORC1 and Snf1 (Figure 1.3) [130, 143-147]; 8) Gsy2, glycogen synthase which is induced upon glucose exhaustion or nitrogen starvation; Gsy2 is modulated by TORC1, PKA, Snf1 and Pho85 (Figure 1.3) [146, 148-155]; 9) the Atg1-Atg13 complex, which initiates autophagy by enabling phagophore assembly site formation; this complex is controlled by TORC1, PKA, Snf1 and Pho85 (Figure 1.3) [156-163]; 10) Sfp1, a transcription activator of genes encoding ribosomal proteins and protein components of ribosome biogenesis machinery; Sfp1 is under the control of TORC1 and PKA (Figure 1.3) [116, 118, 159, 164-170]; 11) eIF2α, a subunit of a protein complex involved in the initiation of protein synthesis on the ribosome; eIF2α is modulated by TORC1 and Snf1 (Figure 1.3) [171, 172];]; 12) Crz1, a transcription factor activating expression of stress response genes; Crz1 is modulated by PKA and Pho85 (Figure 1.3) [173-177]; 13) Igo1 and Igo2, two paralogues proteins whose Rim15-diven phosphorylation upon glucose exhaustion protects from degradation a specific set of mRNAs required for entry into quiescence; phosphorylated Igo1 and Igo2 also inhibit the Cdc55 protein phosphatase 2A (PP2ACdc55) to prevent dephosphorylation of the transcription factor Gis1, thereby enabling phosphorylated Gis1 to activate transcription of many stress response and carbohydrate metabolism genes, as well as transcription of the XBP1 gene encoding a global transcriptional repressor of genes involved in cell cycle progression, transition to the Q state and recovery from it; additionally, the Igo1/2-dependent inhibition of PP2ACdc55 prevents dephosphorylation of the cyclin-dependent kinase (CDK) inhibitor Sic1 to protect it from proteolysis - so that phosphorylated Sic1 can elicit cell cycle arrest at late G_1 (Figure 1.3) [91, 113, 114, 178-184]; and 14) Mpk1, a mitogen-activated protein kinase which phosphorylates the CDK inhibitor Sic1 to prevent its proteolytic degradation

and to allow phosphorylated Sic1 to assist in arresting cell cycle at a checkpoint in late G_1; Mpk1 is controlled by TORC1 (Figure 1.3) [183, 184].

CR is a dietary intervention that delays aging in yeast and other evolutionarily distant eukaryotic organisms [84, 85, 185-189]. Mechanisms linking yeast chronological aging to the quiescence program under non-CR conditions are well established [88-92, 94, 126, 127, 180, 190]. However, prior to studies described in my thesis, it was unknown if the aging-delaying effect of CR in chronologically aging yeast is due in part to the ability of this low-calorie diet to control the above quiescence program.

1.2 Thesis outline and contributions of colleagues

The objective of studies described in Chapter 2 was to test my hypothesis that LCA may delay the chronological mode of *S. cerevisiae* aging by altering the lipid composition of mitochondrial membranes. To attain this objective, I investigated how the *ups1Δ*, *ups2Δ* and *psd1Δ* mutations eliminating different enzymes involved in mitochondrial phospholipid metabolism influence the following: 1) mitochondrial lipidome and proteome; 2) mitochondrial functionality; and 3) the geroprotective (aging-delaying) efficiency of LCA in chronologically aging yeast. These analyses revealed a distinct LCA-dependent pro-longevity pattern of mitochondrial lipidome, which consists in a proportional decrease of phosphatidylethanolamine and cardiolipin concentrations to maintain equimolar concentrations of these phospholipids, and in an increase of phosphatidic acid concentration. I found that this pattern of mitochondrial lipidome enables a sustained specific aging-delaying pattern of mitochondrial proteome. Studies described in Chapter 2 provide evidence that the mitochondrial lipidome defines not only the rate of yeast chronological aging but also the geroprotective efficiency of LCA in chronologically aging yeast. I conducted experiments shown in figures 2.1-2.5 and 2.9-2.18, and prepared these figures. The experiments shown in figures 2.6, 2.7 and 2.8 were carried out by Anthony Arlia-Ciommo, Simon Bourque, Olivia Koupaki and Karamat Mohammad. Pavlo Kyryakov, Paméla Dakik, Mélissa McAuley, Younes Medkour and Tamara Di Maulo conducted experiments shown in figures 2.19 and 2.20. All findings described in Chapter 2 have been published in *Oncotarget* (2017) 8:30672-30691. Dr. Titorenko provided intellectual leadership of this project; he also edited the first draft of Chapter 2 and the entire manuscript of the above article.

The objective of studies described in Chapter 3 was to test my hypothesis that CR may slow down yeast chronological aging by eliciting specific changes in cell cycle regulation and controlled cell differentiation. To attain this objective, I investigated how CR influences the differentiation of chronologically aging yeast cultures into quiescent and non-quiescent cells, and how it affects their properties. Findings presented in Chapter 3 demonstrated that CR extends yeast chronological lifespan via a mechanism that links cellular aging to cell cycle regulation, maintenance of the Q state, entry into the NQ state and survival in the NQ state. My comparative analyses of physical, morphological, reproductive, biochemical and physiological properties of Q and NQ cells from differently aged CR or non-CR yeast cultures suggested a hypothetical model for this mechanism. This model is critically discussed in Chapter 3. I conducted experiments shown in figures 3.1-3.6 and prepared these figures. I designed a model shown in figure 3.11 and prepared this figure. Rachel Feldman, Amanda Piano, Anthony Arlia-Ciommo, Vicky Lutchman, Masoumeh Ahmadi, Sarah Elsaser, Hana Fakim, Mahdi Heshmati-Moghaddam, Asimah Hussain, Sandra Orfali, Harshvardhan Rajen, Negar Roofigari-Esfahani and Leana Rosanelli conducted experiments shown in figures 3.7-3.10. All findings described in Chapter 3 have been published in *Oncotarget* (2017) 8:69328-69350. Dr. Titorenko provided intellectual leadership of this project; he also edited the first draft of Chapter 3 and the entire manuscript of the above article.

In Chapter 4 of my thesis I critically analyzed recent progress in understanding how various intercompartmental (i.e., organelle-organelle and organelle-cytosol) communications regulate cellular aging in evolutionarily distant eukaryotes. My analysis suggested several models for an intricate network of intercompartmental communications that underlie cellular aging in eukaryotic organisms across phyla. My models posit that the numerous directed, coordinated and regulated organelle-organelle and organelle-cytosol communications integrated into this network define the long-term viability of a eukaryotic cell and, thus, are critical for regulating cellular aging. I designed models shown in figures 4.1-4.4 and prepared these figures. Chapter 4 has been published as a review article in *International Union of Biochemistry and Molecular Biology Life* (2013) 65:665-674]. Dr. V. Titorenko provided intellectual leadership of this project; he also edited the first draft of Chapter 4 and the entire manuscript of the above review article.

2 Specific changes in mitochondrial lipidome alter mitochondrial proteome and increase the geroprotective efficiency of lithocholic acid in chronologically aging yeast

2.1 Introduction

As described in the ″Introduction″ section, we hypothesized that 1) the observed LCA-dependent specific changes in the composition of mitochondrial membrane lipids [81] may have a causal role in the age-related remodeling of mitochondrial proteome; 2) certain mitochondrial proteins whose abundance is altered in response to LCA-driven changes in mitochondrial lipidome may play essential roles in creating a distinct, aging-delaying pattern of mitochondrial functionality; and 3) these changes in mitochondrial functionality may alter the geroprotective (aging-delaying) efficiency of LCA in chronologically aging yeast. This chapter summarizes my studies aimed at testing these hypotheses.

2.2 Materials and methods

2.2.1 Yeast strains and growth conditions

The WT strain BY4742 (*MATα his3Δ1 leu2Δ0 lys2Δ0 ura3Δ0*) and single-gene-deletion mutant strains in the BY4742 genetic background (all from Thermo Scientific/Open Biosystems) were grown in YP medium (1% yeast extract, 2% peptone) initially containing 0.2% glucose with 50 μM LCA or without it. Cells were cultured at 30^{o}C with rotational shaking at 200 rpm in Erlenmeyer flasks at a ″flask volume/medium volume″ ratio of 5:1.

2.2.2 Isolation of crude mitochondrial fractions

Yeast cells were harvested at 3,000 × g for 5 min at room temperature, washed with water and resuspended in DTT buffer (100 mM Tris-H_2SO_4, pH 9.4, 10 mM dithiothreitol [DTT]). Cells were incubated in DTT buffer incubated for 20 min at 30°C to weaken the cell wall. The cells then were washed with Zymolyase buffer (1.2 M sorbitol, 20 mM potassium phosphate, pH 7.4) and centrifuged at 3,000 × g for 5 min at room temperature. Cells were then incubated with 3 mg/g (wet weight) of Zymolyase-100T in 7 ml/g (wet weight) Zymolyase buffer for 45 min at 30°C. Following an 8-min centrifugation at 2,200 × g at 4°C, the isolated spheroplasts were washed in ice-cold homogenization buffer (5 ml/g) (0.6 M sorbitol, 10 mM Tris-HCl, pH7.4, 1 mM EDTA, 0.2% (w/v) BSA) and centrifuged at 2,200 × g for 8 min at 4°C. Spheroplasts were homogenized

in ice-cold homogenization buffer using 15 strokes. Cell debris was removed by centrifuging the resulting homogenates at 3,000 × g for 10 min at 4°C. The resulting supernatant was then centrifuged at 12,000 × g for 15 min at 4°C to pellet mitochondria. The remnant cell debris was removed by centrifuging the mitochondrial fraction at 3,000 × g for 5 min at 4°C. The resulting supernatant was then centrifuged at 12,000 × g for 15 min at 4°C to obtain the crude mitochondrial pellet, which was then resuspended in 3 ml of SEM Buffer (250 mM sucrose, 1 mM EDTA, 10 mM MOPS, pH 7.2) and used for the purification of mitochondria as described below.

2.2.3 Purification of mitochondria devoid of microsomal and cytosolic contaminations

A sucrose gradient was made by overlaying 1.5 ml of 60% sucrose with 4 ml of 32% sucrose, 1.5 ml of 23% sucrose, and then 1.5 ml of 15% sucrose (all in EM buffer; 1 mM EDTA, 10 mM MOPS, pH 7.2). Finally, a 3-ml aliquot of the crude mitochondrial fraction in SEM buffer was applied to the gradient and centrifuged at 134,000 × g (33,000 rpm) for three hours at 4°C in vacuum (Rotor SW40Ti, Beckman). The purified mitochondria found at the 60%/32% sucrose interface were carefully removed and stored at - 80°C until lipids were extracted for mass spectrometry.

2.2.4 Lipid extraction from yeast cells [191]

Yeast cells were harvested by centrifugation in a Centra CL2 clinical centrifuge at 3,000 × g for 5 min at room temperature. The cell pellet was resuspended in ice-cold 155 mM ammonium bicarbonate (pH 8.0), and the cells were subjected to centrifugation at 16,000 × g for 1 min at 4^{o}C. The cell pellet was stored at -80^{O}C until lipid extraction. For lipid extraction, the pelleted cells kept at -80^{O}C were thawed on ice before being resuspended in 1 ml of ice-cold nanopure water. The volume that contained 5 × 10^{7} cells was transferred to a 15-ml high-strength glass screw top centrifuge tube with a Teflon lined cap (#0556912; Fisher Scientific). The volume of each sample was topped off to 1 ml with ice-cold nanopure water. To each tube the following was added: 20 µl of the internal standard mix prepared in Chromasolv HPLC (>99.9%) chloroform (Sigma-Aldrich) (Table 2.1), 800 µl of 425-600 µM acid-washed glass beads to break open the cells (#G8772; Sigma-Aldrich) and 3 ml of a Chromasolv HPLC (>99.9%) chloroform-methanol mixture (both from Sigma-Aldrich) at a 17:1 ratio. The samples were then vortexed vigorously for 2 h at 4^{O}C and subjected to centrifugation in a Centra CL2 clinical centrifuge at 3,000 × g for 5 min at room

temperature; this centrifugation allowed to separate the upper aqueous phase from the lower organic phase, which contained nonpolar lipids TAG, PC, PE and PG. The lower organic phase was then transferred to another 15-ml high-strength glass screw top centrifuge tube using a glass Pasteur pipette with careful attention not to disrupt the glass beads or upper aqueous phase. 1.5 ml of chloroform-methanol (2:1) solution was added to the remaining upper aqueous phase to allow the separation of polar lipids PA, PS, PI and CL. The samples were again vortexed vigorously at 4^{o}C for 1 h. The initial separated organic band was kept at 4^{o}C for the duration of the second vortexing. At the end of 1 h, the samples were again centrifuged for 5 min at 3,000 × rpm at room temperature; the lower organic phase was then separated and added to the corresponding initial organic phase with a glass Pasteur pipette. With both lower organic phases combined, the solvent was evaporated off by nitrogen gas flow. Once all solvent was evaporated, the remaining lipid film was dissolved in 100 µl of chloroform-methanol (1:2) and immediately transferred into 2-ml glass vials with Teflon screw tops to avoid evaporation until samples were analyzed by mass spectrometry. Samples were then stored at -80^{o}C and ran on the LTQ Orbitrap Mass Spectrometer within one week of the extraction.

Table 2.1. Internal standard mix composition (modified from [191])

Detection mode	Class of lipid standard	Lipid chain composition (number carbons: number double bonds on fatty acid chain)	Exact mass molecular weight (g/mol)	M/Z (mass/ion charge)	Concentration in mix (mg/µL)
Negative	CL	14:0 / 14:0 / 14:0 /14:0	1274.9000	619.4157	0.10
	FFA	19:0	298.2872	297.2711	0.02
	PA	14:0 / 14:0	614.3920	591.4026	0.10
	PE	14:0 / 14:0	635.4526	634.4448	0.10
	PG	14:0 / 14:0	688.4290	665.4394	0.10
	PS	14:0 / 14:0	701.4240	678.4271	0.02
Positive	TAG	13:0 / 13:0 / 13:0	680.5955	698.6299	0.10
	PC	13:0 / 13:0	649.4683	650.4761	0.10

Internal standards CL, PA, PE, PG, PS and PC were all from Avanti Polar Lipid, Alabaster, AL, USA. TAG internal standard originates from Larodan, Malmo, Sweden.

2.2.5 Lipid identification and quantitation using mass spectrometry

Samples were diluted (1:1) with 1:2 chloroform-methanol supplemented with 0.1% ammonium hydroxide for improved ionization efficiency. Samples were injected one at a time using a Thermo Orbitrap Velos Mass Spectrometer equipped with HESI-II ion source (Thermo Scientific) at a flow rate of 5 µl/ min. The instrument settings for the Orbitrap used the optimized settings, as described in reference 191 (Table 2.2).

Table 2.2. Thermo Orbitrap Velos mass spectrometer's tune file instrument settings (from [191])

Instrument polarity	Positive	Negative
Source voltage (kV)	3.9	4
Capillary temperature (^{O}C)	275	275
Sheath gas flow	5	5
Aux gas flow	1	1
FT-MS injection time (ms)	100	500
FT-MS microscans	3	1

Data were acquired according to the Instrument Method for data-dependent acquisition for 5 min in both positive and negative modes by the FT-MS analyzer at a resolution of 100,000 for both MS and MS/MS data (Table 2.3).

Table 2.3. Instrument method for data-dependent acquisition (from [191])

Acquisition time	5 min (with a 0.25-min delay)	
Instrument polarity	Positive	Negative
MS (Segment I)		
Analyzer	FTMS	FTMS
Mass range	Normal	Normal
Resolution	100,000	100,000
Data type	Centroid	Centroid
Scan range	400-1,200	400-1,200
Data-dependent MS/MS (segments 2-10)		
Analyzer	FTMS	FTMS
Resolution	30,000	30,000
Data type	Centroid	Centroid
Activation	HCD	HCD
Activation time (ms)	0.1	0.1
Isolation width	1	1
Collision energy	35	65
Mass range	Normal	Normal
Data type	Centroid	Centroid
Scan range	-	-

Between each sample, the line was flushed with chloroform-methanol (1:2) mixture until the ion detection steadied and returned back into the baseline level. Diluted internal standard mix was injected multiple times throughout the acquisition to ensure no sensitivity loss throughout the run.

Once all data was acquired, raw files were converted to open format mzXML using ProteoWizard MSConvert software (http://proteowizard.sourceforge.net/), the file format used by the Lipid Identification Software LipidXplorer (https://wiki.mpi-cbg.de/lipidx/Main_Page). Data files were then imported into this software using settings described in Table 2.4; all lipids in the PA, PC, PE, PI, PS, CL and TAG lipid classes were identified with the help of Molecular Fragmentation Query Language (MFQL) files. MFQL files were obtained from the LipidXplorer page listed above and aided in the identification of lipids by their m/z ratio as well as their fragmentation patterns.

LipidXplorer's output data was then opened under a Microsoft Excel file and all detected lipids were quantified by comparison with the intensity of the corresponding lipid class' internal standard's known concentration in the sample. Each quantified lipid had a corresponding internal standard from the same lipid class, allowing the calculation of molar percentage of each identified lipid species and, therefore, of each lipid class.

Table 2.4. Lipid identification by LipidXplorer import settings for data acquired under positive and negative mode (from [191])

	Positive mode	Negative mode
Selection Window (Da)	1	1
Time range (sec.)	0-350	0-350
Calibration masses		
MS	0	0
MS/MS	0	0
m/z range (m/z-m/z)		
MS	140-1,200	100-400
MS/MS	200-1,400	200-1200
Resolution (FMHW)		
MS	100,000	100,000
MS/MS	30,000	30,000
Tolerance (ppm)		
MS	10	10
MS/MS	10	10
Resolution Gradient (res/(m/z))		
MS	0	-55
MS/MS	0	0
Minimum Occupation (0<1)		
MS	0.5	0.5
MS/MS	0	0
MS1 offset (Da)	0	0

2.2.6 A plating assay for the analysis of chronological lifespan

Cells were grown in YEPD (0.2% glucose) medium at 30ºC with rotational shaking at 200 rpm in Erlenmeyer flasks at a flask volume/medium volume ratio of 5:1. A sample of cells was removed from each culture at various time points. A fraction of the cell sample was diluted to determine the total number of cells per ml of culture using a hemacytometer. 10 µl of serial dilutions (1:10 to $1:10^3$) of cells were applied to the hemacytometer, where each large square is calibrated to hold 0.1 µl. The number of cells in 4 large squares was then counted and an average was taken to ensure greater accuracy. The concentration of cells was calculated as follows: number of cells per large square x dilution factor x 10 x 1,000 = total number of cells per ml of culture. A second fraction of the cell sample was diluted and serial dilutions ($1:10^2$ to $1:10^5$) of cells were plated onto YEPD (2% glucose) plates in triplicate to count the number of viable cells per ml of each culture. 100 µl of diluted culture was plated onto each plate. After a 48-h incubation at 30ºC, the number of colonies per plate was counted. The number of colony forming units (CFU) equals to the number of viable cells in a sample. Therefore, the number of viable cells was calculated as follows: number of colonies x dilution factor x 10 = number of viable cells per ml. For each culture assayed, % viability of the cells was calculated as follows: number of viable cells per ml / total number of cells per ml x 100%. The % viability of cells in mid-logarithmic phase was set at 100% viability for that culture. The life span curves for wild-type and some of the mutant strains were also validated using a LIVE/DEAD yeast viability kit (Invitrogen) following the manufacturer's instructions for stationary-phase cultures.

2.2.7 Total cell lysates preparation

Total cell lysates were made by vortexing the cells in TCL buffer (25 mM Tris/HCl pH 8.5, 150 mM NaCl, 1 mM EDTA, 0.1 mM DTT, 4% CHAPS, 1 mM PMSF, protease inhibitor cocktail (Sigma)) with glass beads three times for 1 min. Lysates were then centrifuged and supernatants collected.

2.2.8 Identification and quantification of proteins by mass spectrometry (MS)

Protein bands stained with QC Colloidal Coomassie Blue was cut out from an SDS-PAGE gel with a razor blade. The gel pieces were placed in individual 0.5-ml siliconized Eppendorf tubes. The bands were destained by washing twice with distilled water for 1 h. The bands were then incubated in 50 µl of acetonitrile (ACN) for 5 min at 37°C, after which ACN was removed and the bands were dried at 37°C. Next, the destained bands were incubated in 50 µl of 10 mM dithiothreitol for 30 min at 37°C to reduce thiol groups in peptides. DTT was discarded and the bands were incubated in 50 µl of 55 mM iodoacetamide (IAA) for 20 min at 37°C in the dark to remove the residual DTT. IAA was removed and the bands were incubated in 50 µl of a 1:1 mixture of 100 mM ABC and 50% acetonitrile for 10 min at 37°C. The mixture was discarded and the bands were incubated twice in 50 µl of ACN under the same conditions and dried at 37°C. The trypsin and trypsin buffer were prepared as follows: (1) 1.6 ml of a 1:1 mixture of 100 mM ABC and 10mM $CaCl_2$ were used to resuspend 20 µg of trypsin; and (2) for protein digest, 50 µl of trypsin solution (1 mg/ml) was added to the bands, which were then incubated overnight at 37°C.

The following day, the samples were spun down and the supernatants containing peptides were transferred to new 0.5-ml siliconized Eppendorf tubes. To extract more peptides, the gel pieces were subjected to several washes and treatments at room temperature; the supernatants were conserved and combined with the first set to extracted peptides. For the first extraction, the bands were initially incubated in 50 µl of 25 mM ABC for 10 min and then in 50 µl of ACN for 10 min. The samples were spun down and the supernatant were added to the first set of extracted peptides. For the second extraction, the bands were incubated in 50 µl of 5% formic acid for 10 min and then in 50 µl of ACN for 10 min. The samples were spun down and the supernatant were combined with the first set of extracted peptides. The gel pieces were no longer used and discarded. To prevent possible oxidation during storage, 12.5 µl of 100 mM DTT was added to each set of peptides. The peptides were completely dried in a Speed-Vac at medium temperature settings (37°C) for 2 h and stored at -20°C until MS analysis.

Dried peptides were resuspended in 20 µl of 5% ACN. For each recovered protein band, an aliquot of 10 µl of dried peptides in 5% ACN was diluted 2-fold in Nano pure water for MS analysis. Samples can be stored at -20°C until being subjected to MS analysis. Individual proteins composing each band were then identified by reverse phase high performance liquid

chromatography coupled to mass spectrometry (RP-HPLC/MS) using an LTQ Orbitrap. 3-µl aliquots of peptides were separated in ACN gradient using a 100-µM capillary column packed with C18 mobile phase.

Once acquiring time was completed using the LTQ Orbitrap, the raw mass spectrometry data file obtained by Xcalibur were analyzed using the Thermo Scientific Xcalibur Proteome Discoverer application (version 1.3) hereafter referred to as the Proteome Discoverer. The Proteome Discoverer was used to identify individual proteins by comparing the raw data of mass spectra of digested fragments to the mass spectra of peptides within the Uniprot FASTA database. The analysis by the Proteome Discoverer coupled to the FASTA database was enabled by using the peak-finding search engine SEQUEST. The SEQUEST engine processes MS data using a peak-finding algorithm to search the raw data for generating a peak probability list with relative protein abundances.

The following settings of the SEQUEST search wizard within the Proteome Discoverer application were used:

Raw file and Scan Range Selection Parameters: The raw file was selected and the Base peak ion chromatogram appeared to reveal: 1) the "Intensity (counts)" corresponding to the intensity of the largest peak in the spectrum; and 2) the "Time (min)" showing the retention time (RT). The following algorithm and settings were used:

Lower RT Limit (min): The beginning of the RT of the scan range of interest: 10 min.

Upper RT Limit (min): The end of the retention time of the scan range of interest: 18 min.

Scan Extraction Parameters

First mass: The mass of the first precursor ion in the range of ion fragments to search for in the database: 350 Daltons (Da).

Last mass: The mass of the last precursor ion in the range of ion fragments to search for in the database: 5000 Daltons (Da).

Activation type: The fragmentation method to use for activating the scan: Collision Induced Dissociation (CID).

Unrecognized charge replacement: Specifies the charge number of the precursor ions: Automatic (Default), assigns a charge number of +2 and +3 to the spectrum.

Intensity threshold: Specifies the intensity threshold below which ions are filtered out. The default value of 0.0 was used.

Minimum ion count: The minimum ion count corresponds to the minimum number of ions that must be present in an MS/MS spectrum for it to be included in a search. The default value of 1 was used.

S/N threshold: The signal-to-noise threshold is the intensity of the signal to the intensity of the background noise. The use of this threshold filters out low-intensity ions that function as a noise. The value of 1.5 was used.

Database: Uniprot_sprot FASTA

Enzyme: Trypsin

Missed Cleavages: The maximum number of internal cleavage sites per peptide fragment that is acceptable for an enzyme to miss during proteolytic digest. The default value of 2 was used.

Precursor mass tolerance: The precursor mass tolerance value used for finding peptide candidates. The possible range of values is 0.01 to 5000 ppm. The default value of 10 ppm was used.

Fragment mass tolerance: The default mass tolerance value of 0.8 Da was used for matching fragment peaks. The possible range of values was 0.0001 to 2.0 Da.

Ions series calculated: Specifies the ion factors for a, b, c, x, y, and z ions for the experiment type. The possible range is 0 through 1.0 for all ion factors. The ion factors used are b ions: 1 and y ions :1.

Search against decoy database: Specifies if the application uses a decoy database in the search; the "yes" was used.

Target FDR (strict): Specifies a strict target false discovery rate (FDR) for peptide matches with high confidence. The possible value range of 0.0 to 1.0 was used. The default value of 0.01 (1% FDR) was used.

Target FDR (relaxed): Specifies a relaxed target false discovery rate (FDR) for peptide matches with moderate confidence. The possible value ranges from 0.0 to 1.0 was used. The default value of 0.05 (5% FDR) was used.

The Thermo Proteome Search Results Report for the identification of proteins was created. The protein page displays all the proteins and their corresponding peptides found in the sample during the database search. For each protein, the report shows the following results:

Accession: The unique identifier was assigned to the protein by the Uniprot FASTA database.

Description: The name and description of the protein of the identifier appeared in the corresponding Accession column.

Score: The SEQUEST protein score is the sum of all peptide XCorr values above the specified score threshold. The score threshold was calculated as *"0.8 + peptide charge * peptide relevance factor", where peptide relevance factor* has a default value of 0.4. For each spectrum, only the highest-scoring match was used. For each spectrum and sequence, the Proteome Discoverer application uses only the highest scored peptide.

Coverage: Represents the percentage of the protein sequence covered by the identified peptides.

 # *Proteins:* Represents the number of identified proteins in the protein group of a master protein. When the Protein Grouping setting is disabled, the #Proteins is always equal to 1.

 # *Unique Peptides:* Represents the number of peptide sequences unique to a protein.

 # *Peptides:* Represents the number of different peptide sequences identified in the protein.

 # *PSMs:* The peptide spectrum matches (PSMs) value corresponds to the total number of identified peptide sequences for the protein, including those that have been identified redundantly.

 # *AAs:* Represents the number of amino acid in the sequence length of the protein.

MW kDa: Represents the calculated molecular weight of the protein.

Calc. pI: Represents the theoretically calculated isoelectric point, *i.e.* the pH value at which a molecule carries no net electrical charge.

Peptides Results Parameters: For each identified peptide, the report shows the following results:

Protein Descriptions: Identifies a protein associated with the peptides. This description is taken from the Uniprot FASTA file.

 # *Proteins:* Represents the total number of proteins in which this peptide can be found.

Probability: Represents the probability score for the peptide.

SpScore (search-dependent): Represents the raw value of the preliminary score of the SEQUEST algorithm.

XCorr (search-dependent): Scores the number of fragment ions that are common to two different peptides with the same precursor mass; calculates the cross-correlation score for all candidate peptides queried from the database.

Δ Score: A measure of the difference between the top two scores for the peptides identified by that spectrum; the Proteome Discoverer application calculates this score as follows: ΔScore = Score (Rank N Peptide) – Score (Rank 1 Peptide)/Score (Rank 1 Peptide).

ΔCn: Represents the normalized score difference between the currently selected PSM and the highest-scoring PSM for that spectrum.

 # Missed Cleavages: Represents the number of cleavage sites in a peptide sequence that trypsin did not cleave, excluding the cases where the presence of proline prevents trypsin from cleaving the peptide bond.

Peptides Matched: Represents the number of peptides included in the precursor mass tolerance window set for the search.

Charge: Represents the charge state of the peptide.

Intensity: Represents the intensity of the precursor ion.

MH+ ^{Da}: Represents the protonated monoisotopic mass of the peptide, in Daltons.

ΔM ^{ppm}: Represents the difference between the theoretical mass of the peptide and the experimental mass of the precursor ion.

RT ^{min}: Represents the retention time when the peptide was observed, in minutes.

Xcalibur is a registered trademark of Thermo Fisher Scientific Inc. in the United States. SEQUEST is a registered trademark of the University of Washington in the United States.

The ″Proteome Discoverer″ software was used to calculate the exponentially modified protein abundance index (emPAI), a measure of the relative abundance of mitochondrial proteins in a pair of analyzed datasets.

2.2.9 Oxygen consumption assay (cellular respiration measurement)

A sample of cells was taken from a culture at a certain time-point. Cells were pelleted by centrifugation and resuspended in 1 ml of fresh YP medium containing 0.05% glucose. Oxygen uptake by cells was measured continuously in a 2-ml stirred chamber using a custom-designed biological oxygen monitor (Science Technical Center of Concordia University) equipped with a Clark-type oxygen electrode.

2.2.10 Mitochondrial membrane potential measurement

The mitochondrial membrane potential (ΔΨ) was measured in live yeast by fluorescence microscopy of Rhodamine 123 (R123) staining. For R123 staining, 5×10^6 cells were harvested by centrifugation for 1 min at 21,000 × g at room temperature and then resuspended in 100 µl of 50 mM sodium citrate buffer (pH 5.0) containing 2% glucose. R123 (Invitrogen) was added to a

final concentration of 10 μM. Following incubation in the dark for 30 min at room temperature, the cells were washed twice in 50 mM sodium citrate buffer (pH 5.0) containing 2% glucose and then analyzed by fluorescence microscopy. Images were collected with a Zeiss Axioplan fluorescence microscope (Zeiss) mounted with a SPOT Insight 2-megapixel color mosaic digital camera (Spot Diagnostic Instruments). For evaluating the percentage R123-positive cells, the UTHSCSA Image Tool (Version 3.0) software was used to calculate both the total number of cells and the number of stained cells. Fluorescence of individual R123-positive cells in arbitrary units was determined by using the UTHSCSA Image Tool software (Version 3.0). In each of 3 independent experiments, the value of median fluorescence was calculated by analyzing at least 800-1000 cells that were collected at each time-point. The median fluorescence values were plotted as a function of the number of days cells were cultured.

2.2.11 Monitoring the formation of ROS

ROS production in wild-type and mutant cells grown in YEPD (0.2% glucose) with LCA was tested microscopically by incubation with Dihydrorhodamine 123 (DHR). In the cell, this non-fluorescent compound can be oxidized to the fluorescent chromophore rhodamine 123 by ROS. Cells were also probed with a fluorescent counterstain Calcofluor White M2R (CW), which stains the yeast cell walls fluorescent blue. CW was added to each sample to label all cells for their proper visualization. DHR was stored in the dark at –20^{o}C as 50 μl aliquots of a 1 mg/ml solution in ethanol. CW was stored in the dark at –20^{o}C as the 5-mM stock solution in anhydrous DMSO (dimethyl sulfoxide). The concurrent staining of cells with DHR and CW was carried out as follows. The required amounts of the 50 μl DHR aliquots (1 mg/ml) and of the 5-mM stock solution of CW were taken out of the freezer and warmed to room temperature. The solutions of DHR and CW were then centrifuged at 21,000 × g for 5 min to clear them of any aggregates of fluorophores. For cell cultures with a titer of ~ 10^7 cells/ml, 100 μl was taken out of the culture to be treated. If the cell titer was lower, proportionally larger volumes were used. 6 μl of the 1 mg/ml DHR and 1 μl of the 5-mM CW solutions were added to each 100 μl aliquot of culture. After a 2-h incubation in the dark at room temperature, the samples were centrifuged at 21,000 × g for 5 min. Pellets were resuspended in 10 μl of PBS buffer (20 mM KH_2PO_4/KOH, pH 7.5, and 150 mM NaCl). Each sample was then supplemented with 5 μl of mounting medium, added to a microscope slide, covered with a coverslip, and sealed using nail polish. Once the slides were

prepared, they were visualized under the Zeiss Axioplan fluorescence microscope mounted with a SPOT Insight 2-megapixel color mosaic digital camera. Several pictures of the cells on each slide were taken, with two pictures taken of each frame. One of the two pictures was of the cells seen through a rhodamine filter to detect cells dyed with DHR. The second picture was of the cells seen through a DAPI filter to visualize CW, and therefore all the cells present in the frame. For evaluating the percentage of DHR-positive cells, the UTHSCSA Image Tool (Version 3.0) software was used to calculate both the total number of cells and the number of stained cells. Fluorescence of individual DHR-positive cells in arbitrary units was determined by using the UTHSCSA Image Tool software (Version 3.0). In each of 3-5 independent experiments, the value of median fluorescence was calculated by analyzing at least 800-1000 cells that were collected at each time point. The median fluorescence values were plotted as a function of the number of days cells were cultured.

2.2.12 ATP measurement

2×10^9 cells were harvested by centrifugation for 1 min at 16,000 × g at 4ºC. The cell pellet was washed three times in ice-cold PBS (20 mM KH_2PO_4/KOH (pH 7.5) and 150 mM NaCl) and then resuspended in 200 µl of ice-cold SHE solution (50 mM NaOH and 1 mM EDTA). 800 µl of ice-cold SHE solution were added to the cell suspension. The resulting alkali extract was incubated at 60ºC for 30 min to destroy endogenous enzyme activities and pyridine nucleotides. The extract was neutralized by adding 500 µl of THA solution (100 mM Tris/HCl (pH 8.1) and 50 mM HCl). The extract was then divided into 150 µl aliquots, quickly frozen in liquid nitrogen and stored at -80ºC prior to use. For ATP measurement, 1 µl of alkali extract was added to 1 µl ATP reagent (50 mM Tris-HCl (pH 8.1), 3 mM $MgCl_2$, 0.2 mM glucose, 0.04% BSA, 0.05 mM NADP+, 10 µg/ml hexokinase, 2 µg/ml glucose-6-phosphate dehydrogenase). Following a 30-min incubation at 25ºC, the reaction was stopped by adding 1 µl of 0.15 M NaOH and heating at 80º C for 20 min. A 1 µl aliquot was transferred 100 µl of reagent containing 100 µg/ml hexokinase and 20 µg/ml glucose-6-phosphate dehydrogenase. The reaction mixture was incubated for 1 h at 38ºC. The NADPH generated from NADP+ was measured fluorimetrically (excitation at 365 nm, emission monitored at 460 nm).

2.2.13 Statistical analysis

Statistical analysis was performed using Microsoft Excel's (2010) Analysis ToolPak - VBA. All data on cell survival are presented as mean ± SEM. The *p* values for comparing the means of two groups using an unpaired two-tailed *t* test were calculated with the help of the GraphPad Prism 7 statistics software. The logrank test for comparing each pair of survival curves was performed with GraphPad Prism 7. Two survival curves were considered statistically different if the *p* value was less than 0.05.

2.3 Results

2.3.1 The relative concentrations of different classes of membrane phospholipids in yeast mitochondria depend on several processes of phospholipid synthesis and transfer

My first objective was to test a hypothesis that the composition of mitochondrial membrane lipids may define the efficiency with which LCA delays yeast chronological aging. To attain this objective, I examined how single-gene-deletion mutations eliminating proteins involved in different aspects of phospholipid metabolism and transfer in mitochondrial membranes influence mitochondrial lipidome. I also assessed how these mutations affect the efficiency of yeast chronological aging delay by LCA.

A spatiotemporal dynamic of processes that define the relative concentrations of different classes of membrane phospholipids in yeast mitochondria is well-understood [192-199]. These processes are catalyzed by enzymes that reside in both mitochondria and the endoplasmic reticulum (ER). These processes include the following steps of phospholipid synthesis and transfer: 1) the synthesis of phosphatidic acid (PA), cytidine diphosphate-diacylglycerol (CDP-DAG), diacylglycerol (DAG), phosphatidylserine (PS), phosphatidylcholine (PC) and phosphatidylinositol (PI) in the ER; 2) the movement of PA from the ER to the OMM through mitochondria-ER contact sites at zones of a juxtaposition between the OMM and the mitochondria-associated membrane (MAM) domain of the ER; 3) the transfer of PA from the OMM across the intermembrane space (IMS) to the IMM, which is catalyzed by the Ups1/Mdm35 protein complex and inhibited by CL; 4) the conversion of ER-derived PA into CDP-DAG, phosphatidylglycerol-phosphate (PGP), phosphatidylglycerol (PG), cardiolipin (CL) and monolysocardiolipin (MLCL) in a series of reactions that are catalyzed by Tam41, Pgs1, Gep4, Crd1, Cld1 and Taz1

(respectively) in the IMM; 5) the transfer of PS from the ER to the OMM via mitochondria-ER contact sites by an unidentified mechanism; 6) the Ups2/Mdm35-dependent transport of PS from the OMM via the IMS to the IMM, where PS is converted into phosphatidylethanolamine (PE) in a reaction catalyzed by Psd1; 7) the synthesis of PE from PS in the OMM, which is catalyzed by Psd1, requires a close apposition between the two mitochondrial membranes and is assisted by the mitochondrial contact site (MICOS) protein complex; 8) the transfer of PC and PI from the ER to the OMM via mitochondria-ER contact sites, which is followed by the movement of PC and PI from the OMM to the IMM; mechanisms of both these processes remain obscure; and 9) the movement of DAG and CDP-DAG from the ER to the OMM across mitochondria-ER contact sites, and the subsequent transfer of these two phospholipids to the IMM by currently unknown mechanisms (Figure 2.1) [192-199].

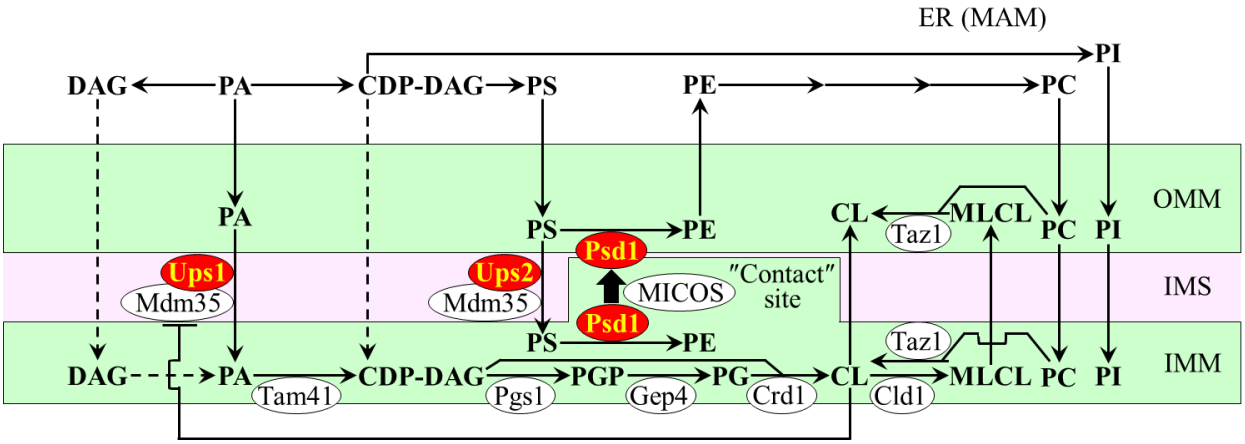

Figure 2.1. The relative concentrations of different classes of membrane phospholipids in yeast mitochondria depend on several processes of phospholipid synthesis and transfer. These processes are catalyzed by enzymes that reside in the inner mitochondrial membrane (IMM), intermembrane space (IMS), outer mitochondrial membrane (OMM) and endoplasmic reticulum (ER). Only enzymes catalyzing these processes in the IMM, IMS and OMM are shown. A T bar denotes a cardiolipin (CL)-dependent inhibition of phosphatidic acid (PA) transfer from the OMM across the IMS to the IMM. In this study, I investigated various effects of single-gene-deletion mutations that eliminate enzymes displayed in red color. See text for more details. Abbreviations: CDP-DAG, cytidine diphosphate-diacylglycerol; DAG, diacylglycerol; MAM, the mitochondria-associated membrane domain of the ER; MICOS, the mitochondrial contact site protein complex; MLCL, monolysocardiolipin; PC, phosphatidylcholine; PG, phosphatidylglycerol; PGP, phosphatidylglycerol-phosphate; PI, phosphatidylinositol; PS, phosphatidylserine.

2.3.2 The *ups1Δ* mutation alters mitochondrial membrane lipidome and lowers the geroprotective efficiency of LCA

I used quantitative mass spectrometry to compare lipidomes of mitochondria purified from wild-type (WT) yeast cells cultured with or without LCA to those from *ups1Δ* cells. Both WT and *ups1Δ* cells were recovered on day 2, 4 or 7 of cell culturing, i.e. at different stages of chronological aging. The *ups1Δ* mutation eliminates a component of the Ups1/Mdm35 protein complex, which catalyzes the transfer of PA from the OMM across the IMS to the IMM [192, 200, 201]. I found that 1) akin to the effect of LCA on mitochondrial membrane lipidome in WT, LCA increases the concentrations of PS, PI, PC and PA in mitochondria of *ups1Δ* in an age-related manner; 2) similar to its effect in WT, LCA decreases the concentration of PE in mitochondrial membranes of *ups1Δ* at different stages of chronological aging; and 3) unlike an age-related decrease in the concentration of CL elicited by LCA in WT, this bile acid does not cause significant changes in CL concentration in *ups1Δ* (compare Figures 2.2 and 2.3).

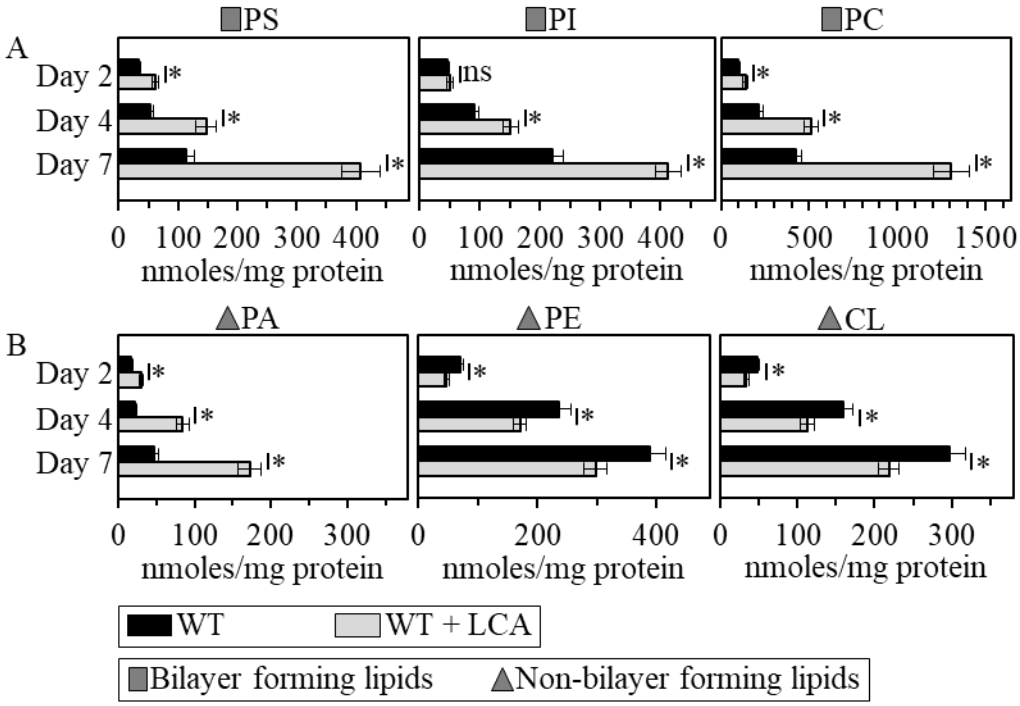

Figure 2.2. LCA exhibits age-related differential effects on the concentrations of different classes of mitochondrial membrane phospholipids in chronologically aging wild-type (WT) yeast. WT cells were cultured in the nutrient-rich YP medium initially containing 0.2% glucose with 50 μM LCA or without it. Mitochondria were purified from cells recovered on day 2, 4 or 7 of cell culturing. Extraction of mitochondrial membrane lipids, and mass spectrometric identification and quantitation of the extracted phospholipid classes were carried out as described in Materials and methods. The concentrations of phospholipids were calculated as nmoles phospholipid/mg protein. (A)

PS, PI and PC are phospholipid classes that exhibit the bilayer forming shape of a cylinder; they decrease the extent of membrane curving for the IMM. (B) PA, PE and CL are phospholipid classes that have the non-bilayer forming shape of a cone; they increase the extent of membrane curving for the IMM. Data are presented as means ± SEM (n = 3; *$p < 0.05$; ns, not significant). Abbreviations: CL, cardiolipin; PA, phosphatidic acid; PC, phosphatidylcholine; PE, phosphatidylethanolamine; PA, phosphatidic acid; PI, phosphatidylinositol; PS, phosphatidylserine.

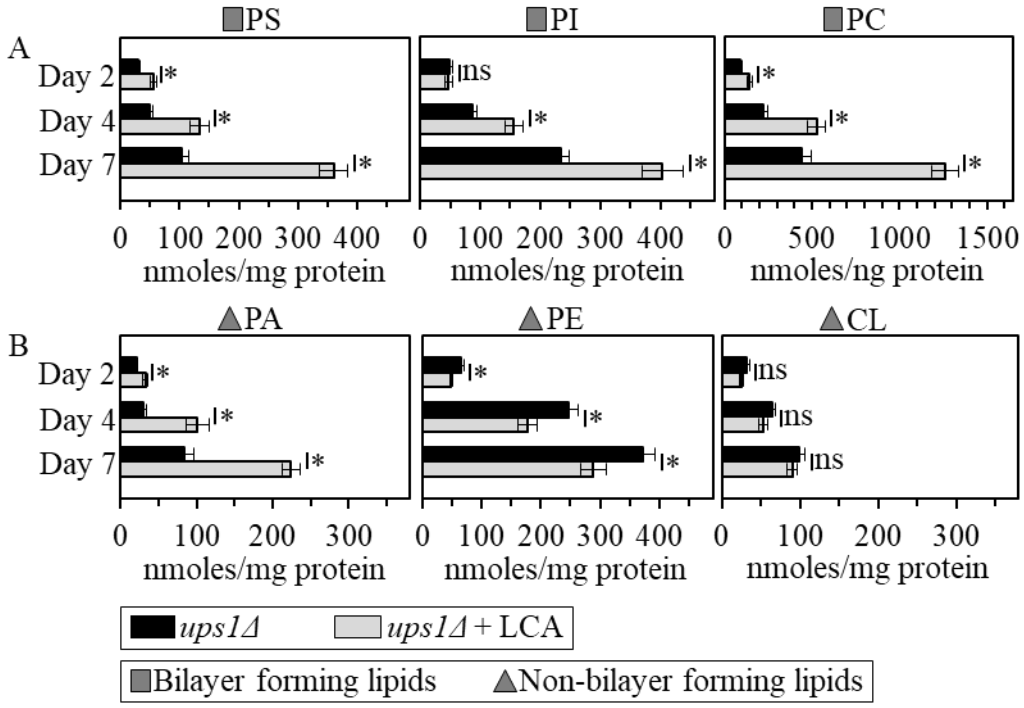

Figure 2.3. LCA exhibits age-related differential effects on the concentrations of different classes of mitochondrial membrane phospholipids in chronologically aging *ups1Δ* yeast. Cells of the *ups1Δ* mutant strain were cultured in the nutrient-rich YP medium initially containing 0.2% glucose with 50 μM LCA or without it. Mitochondria were purified from cells recovered on day 2, 4 or 7 of cell culturing. Extraction of mitochondrial membrane lipids, and mass spectrometric identification and quantitation of the extracted phospholipid classes were carried out as described in Materials and methods. The concentrations of phospholipids were calculated as nmoles phospholipid/mg protein. (A) PS, PI and PC are phospholipid classes that exhibit the bilayer forming shape of a cylinder; they decrease the extent of membrane curving for the IMM. (B) PA, PE and CL are phospholipid classes that have the non-bilayer forming shape of a cone; they increase the extent of membrane curving for the IMM. Data are presented as means ± SEM (n = 3; *$p < 0.05$; ns, not significant). Abbreviations: CL, cardiolipin; PA, phosphatidic acid; PC, phosphatidylcholine; PE, phosphatidylethanolamine; PA, phosphatidic acid; PI, phosphatidylinositol; PS, phosphatidylserine.

I then used these data to compare the ratios between concentrations of all possible pairwise combinations of phospholipid classes in mitochondrial membranes of WT and *ups1Δ* cells cultured

with or without LCA. Of note, PA, PE and CL are phospholipid classes that have the non-bilayer forming shape of a cone; they increase the extent of membrane curving for the IMM, thereby raising the abundance of mitochondrial cristae (formed by the IMM) and mitochondrial contact cites (formed between the IMM and OMM) [81, 198, 199, 202-207]. In contrast, PS, PC and PI are phospholipid classes that exhibit the bilayer forming shape of a cylinder; they decrease the extent of membrane curving for the IMM, thus 1) increasing the abundance of the IMM domains having ″flat″ bilayer conformation; 2) decreasing the abundance of the IMM domains exhibiting negative curvature typical of mitochondrial contact sites; and 3) decreasing the abundance of the IMM domains displaying positive curvature characteristic of mitochondrial cristae [81, 198, 199, 202-207]. I found that, in cells cultured with or without LCA, the *ups1Δ* mutation 1) increases the PA/PS, PA/PC and PA/PI ratios for non-bilayer forming PA vs. bilayer forming PS, PC and PI; 2) does not alter the PE/PS, PE/PC and PE/PI ratios for non-bilayer forming PE vs. PS, PC and PI; 3) decreases the CL/PS, CL/PC and CL/PI ratios for non-bilayer forming CL vs. PS, PC and PI; 4) does not change the PS/PI, PS/PC and PI/PC ratios for all these bilayer forming phospholipid classes; and 5) increases the PA/PE, PA/CL and PE/CL ratios for all these non-bilayer forming phospholipid classes (Figure 2.4). Thus, while this mutation alters the relative to each other concentrations for all non-bilayer forming phospholipids, it has no effect on the relative to each other concentrations for phospholipids that exhibit the bilayer forming shape.

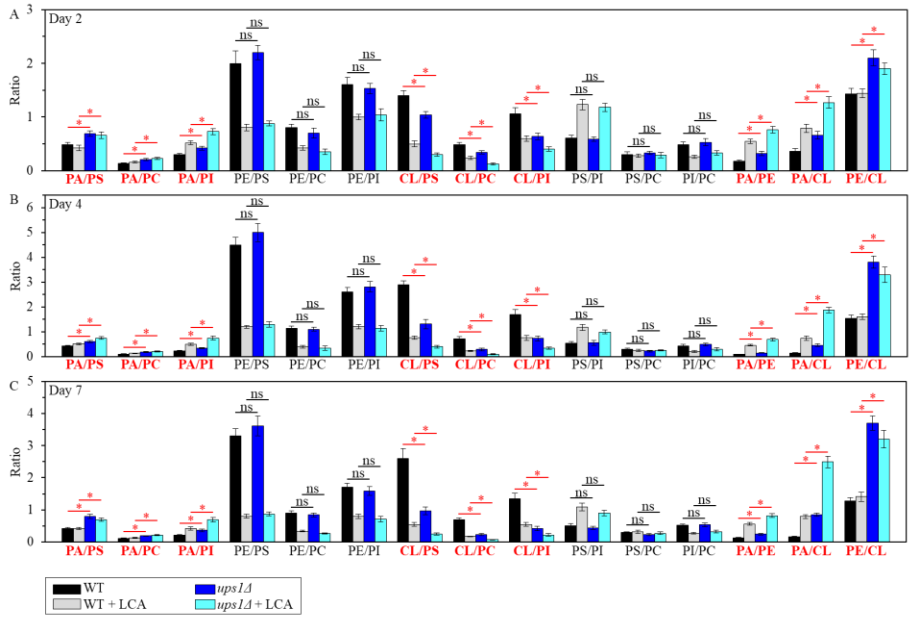

Figure 2.4. The *ups1Δ* mutation differently affects the ratios between concentrations of pairwise combinations of different phospholipid classes in mitochondrial membranes of chronologically aging yeast. *ups1Δ* cells were

cultured in the nutrient-rich YP medium initially containing 0.2% glucose with 50 μM LCA or without it. Mitochondria were purified from cells recovered on day 2 (A), 4 (B) or 7 (C) of cell culturing. Extraction of mitochondrial membrane lipids, and mass spectrometric identification and quantitation of the extracted phospholipid classes were carried out as described in Materials and methods. Based on these data, the ratios between concentrations of all possible pairwise combinations of phospholipid classes were calculated. Data are presented as means ± SEM (n = 3; *$p < 0.05$; ns, not significant).

I then assessed the effect of the *ups1Δ* mutation on the chronological lifespan (CLS) of yeast cultured with or without LCA. I found that *ups1Δ* 1) significantly shortens yeast CLS in the absence of LCA (Figures 2.5A and 2.5B); and 2) substantially lowers the geroprotective efficiency of LCA by almost eliminating the ability of LCA to increase both the mean and the maximum CLS (Figures 2.5A-2.5D).

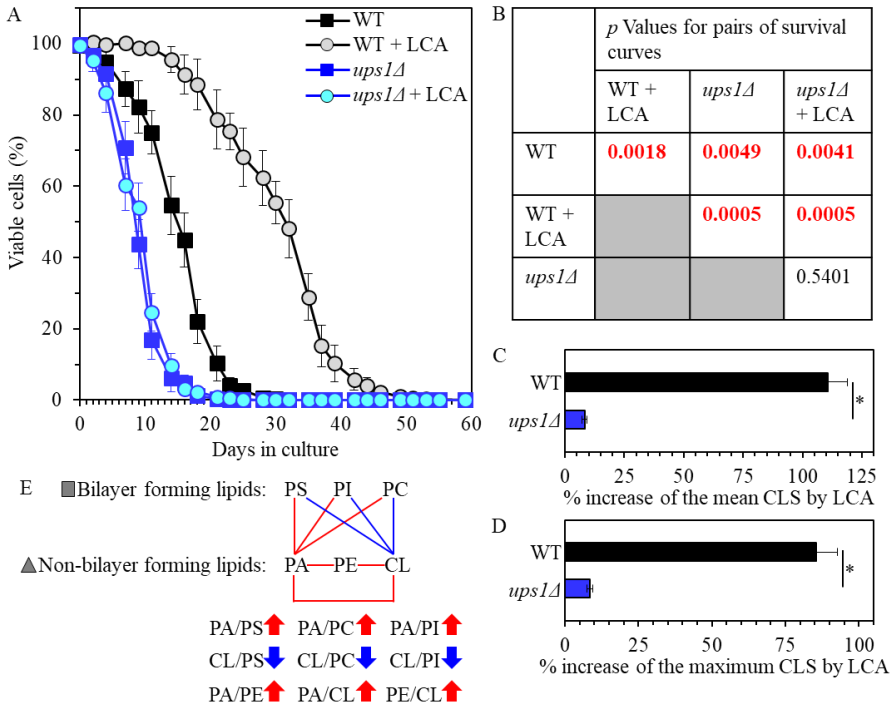

Figure 2.5. The *ups1Δ* mutation shortens yeast CLS in the absence of LCA and lowers the aging-delaying efficiency of LCA. WT and *ups1Δ* cells were cultured in the nutrient-rich YP medium initially containing 0.2% glucose with 50 μM LCA or without it. (A) Survival curves of chronologically aging WT and *ups1Δ* strains are shown. Data are presented as means ± SEM (n = 3). (B) *p* Values for different pairs of survival curves of WT and *ups1Δ* strains cultured with or without LCA. Survival curves shown in (A) were compared. Two survival curves were considered statistically different if the *p* value was less than 0.05. The *p* values for comparing pairs of survival curves using the logrank test were calculated as described in Materials and methods. (C and D) Survival curves shown in (A) were used to calculate the percentage of increase of the mean and maximum CLS by LCA for WT and *ups1Δ* strains.

Data are presented as means ± SEM (n = 3; *$p < 0.05$). (E) The pattern of mitochondrial lipidome characteristic of the *ups1Δ* mutation is shown. Arrows next to the ratios between concentrations of different pairwise combinations of phospholipid classes indicate ratios that are increased (red arrows) or decreased (blue arrows) in *ups1Δ* cells (as compared to WT cells) cultured with or without LCA. Each colored line connects the names of two phospholipid classes whose concentration ratio is increased (red lines) or decreased (blue lines) by the *ups1Δ* mutation and cannot be restored by LCA.

In sum, these findings suggest that the *ups1Δ* mutation may accelerate yeast chronological aging and decrease the geroprotective efficiency of LCA because it creates a distinct pro-aging pattern of mitochondrial lipidome. This characteristic of *ups1Δ* pattern may include the following specific changes in the relative concentrations of different classes of membrane phospholipids: 1) an increase of the PA/PS, PA/PC and PA/PI ratios for non-bilayer forming PA vs. bilayer forming PS, PC and PI; 2) a decrease of the CL/PS, CL/PC and CL/PI ratios for non-bilayer forming CL vs. bilayer forming PS, PC and PI; and 3) an increase of the PA/PE, PA/CL and PE/CL ratios for all these non-bilayer forming phospholipid classes (Figure 2.5E).

2.3.3 The *ups2Δ* mutation changes the composition of mitochondrial membrane lipids and amplifies the aging-delaying effect of LCA

Using quantitative mass spectrometry, I compared lipidomes of mitochondria purified from WT and *ups2Δ* cells. Both WT and mutant strains were cultured with or without LCA and recovered on day 2, 4 or 7 of cell culturing. The *ups2Δ* mutation eliminates a component of the Ups2/Mdm35 protein complex; Ups2/Mdm35 catalyzes the transfer of PS from the OMM across the IMS to the IMM, where PS is converted into PE in a Psd1-dependent reaction [195, 196, 199]. I found that, similar to the effect of LCA on mitochondrial membrane lipidome in WT, LCA causes an age-related increase in the concentrations of PS, PI, PC and PA in mitochondria of *ups2Δ*; however, the concentration of PA in mitochondria of ups2Δ exceeds that in WT mitochondria of cells cultured with or without LCA (compare Figures 2.2 and 2.6). I also observed that, akin to the effect of LCA on mitochondrial membrane lipidome in WT, LCA elicits an age-related decline in the concentrations of PE and CL in mitochondria of *ups2Δ*; yet, the concentrations of both these phospholipids in mitochondria of *ups2Δ* are lower than in WT mitochondria of cells cultured with or without LCA (compare Figures 2.2 and 2.6).

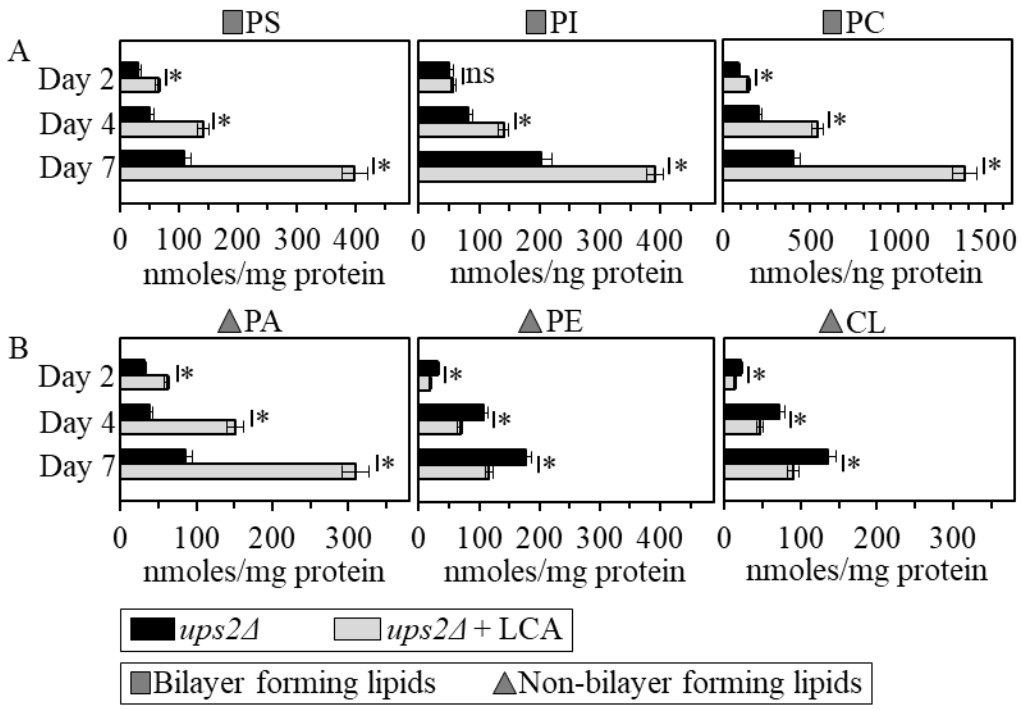

Figure 2.6. LCA exhibits age-related differential effects on the concentrations of different classes of mitochondrial membrane phospholipids in chronologically aging *ups2Δ* yeast. Cells of the *ups2Δ* mutant strain were cultured in the nutrient-rich YP medium initially containing 0.2% glucose with 50 μM LCA or without it. Mitochondria were purified from cells recovered on day 2, 4 or 7 of cell culturing. Extraction of mitochondrial membrane lipids, and mass spectrometric identification and quantitation of the extracted phospholipid classes were carried out as described in Materials and methods. The concentrations of phospholipids were calculated as nmoles phospholipid/mg protein. (A) PS, PI and PC are phospholipid classes that exhibit the bilayer forming shape of a cylinder; they decrease the extent of membrane curving for the IMM. (B) PA, PE and CL are phospholipid classes that have the non-bilayer forming shape of a cone; they increase the extent of membrane curving for the IMM. Data are presented as means ± SEM (n = 3; *$p < 0.05$; ns, not significant). Abbreviations: CL, cardiolipin; PA, phosphatidic acid; PC, phosphatidylcholine; PE, phosphatidylethanolamine; PA, phosphatidic acid; PI, phosphatidylinositol; PS, phosphatidylserine. These experiments were conducted by Anthony Arlia-Ciommo, Simon Bourque, Olivia Koupaki and Karamat Mohammad.

Using the above data, I then compared the ratios between concentrations of all conceivable pairwise combinations of different phospholipids in membranes of mitochondria purified from WT and *ups2Δ* cells; these cells were cultured with or without LCA. I found that, in cells cultured in the presence or absence of LCA, the *ups2Δ* mutation 1) raises the PA/PS, PA/PC and PA/PI ratios for non-bilayer forming PA vs. bilayer forming PS, PC and PI; 2) lowers the PE/PS, PE/PC and PE/PI ratios for non-bilayer forming PE vs. PS, PC and PI; 3) lessens the CL/PS, CL/PC and CL/PI ratios for non-bilayer forming CL vs. PS, PC and PI; 4) does not alter the PS/PI, PS/PC and PI/PC

ratios for all these bilayer forming classes of phospholipids; 5) rises the PA/PE and PA/CL ratios for all these non-bilayer forming phospholipid classes; and 6) does not alter the PE/CL ratio for these two non-bilayer forming phospholipids (Figure 2.7). Thus, unlike the *ups1Δ* mutation, *ups2Δ* allows to maintain the equimolar concentrations of two non-bilayer forming phospholipids, PE and CL, by proportionally decreasing their concentrations.

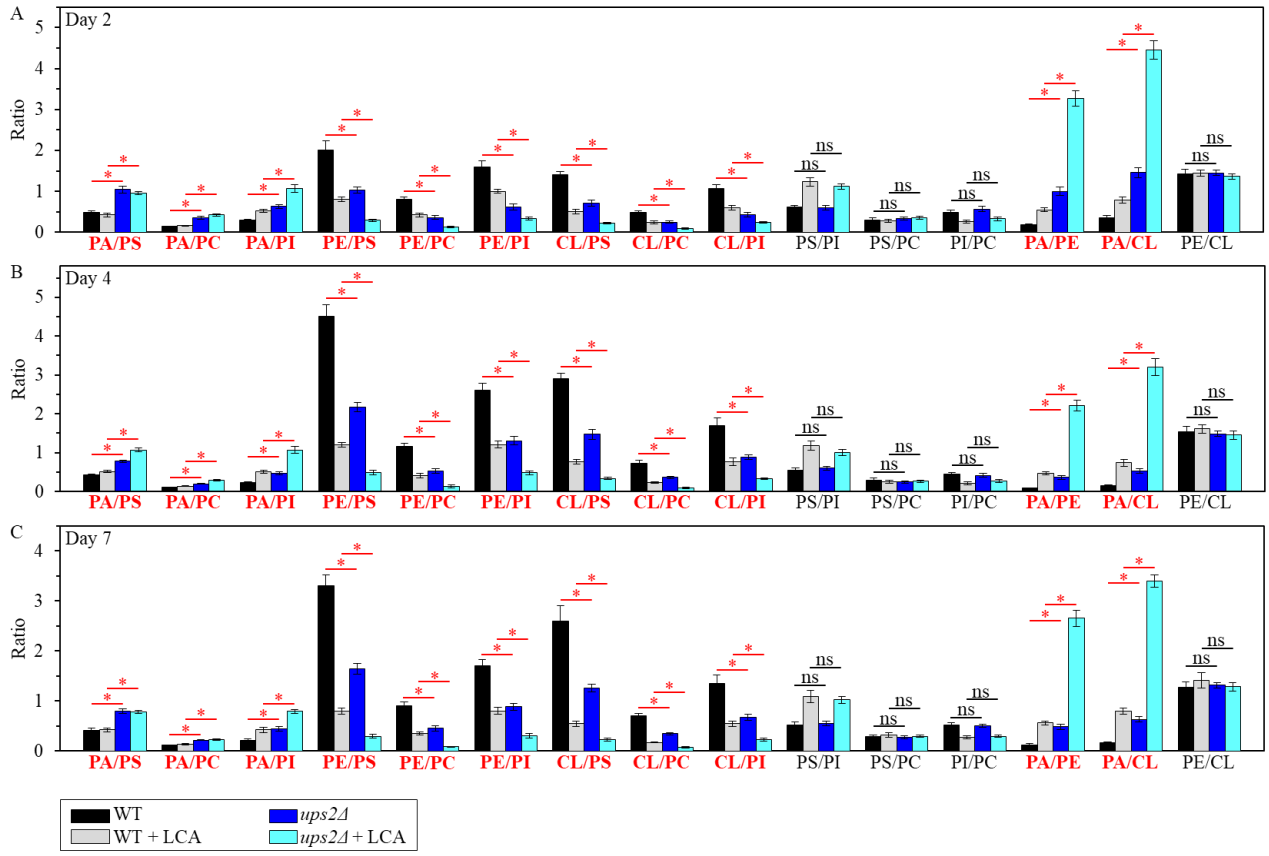

Figure 2.7. The *ups2Δ* mutation exhibits differential effects on the ratios between concentrations of different pairwise combinations of phospholipid classes in mitochondrial membranes of chronologically aging yeast. *ups2Δ* cells were cultured in the nutrient-rich YP medium initially containing 0.2% glucose with 50 μM LCA or without it. Mitochondria were purified from cells recovered on day 2 (A), 4 (B) or 7 (C) of cell culturing. Extraction of mitochondrial membrane lipids, and mass spectrometric identification and quantitation of the extracted phospholipid classes were carried out as described in Materials and methods. Based on these data, the ratios between concentrations of all possible pairwise combinations of phospholipid classes were calculated. Data are presented as means ± SEM (n = 3; *$p < 0.05$; ns, not significant). These experiments were conducted by Anthony Arlia-Ciommo, Simon Bourque, Olivia Koupaki and Karamat Mohammad.

My assessment of the effect of the *ups2Δ* mutation on the CLS of yeast cultured with or without LCA revealed that *ups2Δ* 1) extends yeast CLS in the absence of LCA (Figures 2.8A and 2.8B); and 2) significantly amplifies the geroprotective efficiency of LCA by enhancing the ability of this bile acid to increase both the mean and the maximum CLS (Figures 2.8A-2.8D).

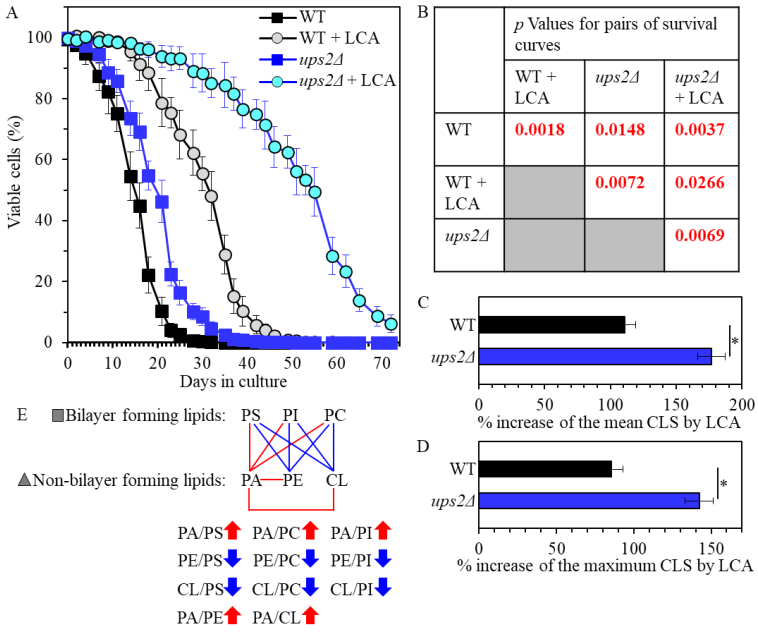

Figure 2.8. The *ups2Δ* mutation extends yeast CLS in the absence of LCA and amplifies the geroprotective efficiency of LCA. WT and *ups2Δ* cells were cultured in the nutrient-rich YP medium initially containing 0.2% glucose with 50 μM LCA or without it. (A) Survival curves of chronologically aging WT and *ups2Δ* strains are shown. Data are presented as means ± SEM (n = 3). (B) *p* Values for different pairs of survival curves of WT and *ups2Δ* strains cultured with or without LCA. Survival curves shown in (A) were compared. Two survival curves were considered statistically different if the *p* value was less than 0.05. The *p* values for comparing pairs of survival curves using the logrank test were calculated as described in Materials and methods. (C and D) Survival curves shown in (A) were used to calculate the percentage of increase of the mean and maximum CLS by LCA for WT and *ups2Δ* strains. Data are presented as means ± SEM (n = 3; $*p < 0.05$). (E) The pattern of mitochondrial lipidome characteristic of the *ups2Δ* mutation is shown. Arrows next to the ratios between concentrations of different pairwise combinations of phospholipid classes indicate ratios that are increased (red arrows) or decreased (blue arrows) in *ups2Δ* cells (as compared to WT cells) cultured with or without LCA. Each colored line connects the names of two phospholipid classes whose concentration ratio is increased (red lines) or decreased (blue lines) by the *ups2Δ* mutation and cannot be restored by LCA. These experiments were conducted by Anthony Arlia-Ciommo, Simon Bourque, Olivia Koupaki and Karamat Mohammad.

Taken together, the above findings indicate that the *ups2Δ* mutation may slow down yeast chronological aging and increase the geroprotective efficiency of LCA because it establishes a distinctive aging-delaying pattern of mitochondrial lipidome. This *ups2Δ*-specific pattern may

consist of the following distinct changes in the relative concentrations of different phospholipid classes: 1) an increase of the PA/PS, PA/PC and PA/PI ratios for non-bilayer forming PA vs. bilayer forming PS, PC and PI; 2) a decrease of the PE/PS, PE/PC and PE/PI ratios for non-bilayer forming PE vs. bilayer forming PS, PC and PI; 3) a decline of the CL/PS, CL/PC and CL/PI ratios for non-bilayer forming CL vs. bilayer forming PS, PC and PI; and 4) a rise of the PA/PE and PA/CL ratios for these non-bilayer forming classes of phospholipids (Figure 2.8E).

2.3.4 The *psd1Δ* mutation elicits changes in mitochondrial membrane lipidome and lessens the geroprotective efficiency of LCA

I compared lipidomes of purified mitochondria from WT cells cultured with or without LCA to those from *psd1Δ* cells. These cells were recovered for purification of mitochondria on day 2, 4 or 7 of cell culturing. The *psd1Δ* mutation eliminates phosphatidylserine decarboxylase which catalyzes the conversion of PS to PE in the IMM and OMM [195, 196, 199, 208, 209]. I found that, similar to the effect of LCA on mitochondrial membrane lipidome in WT, LCA causes an age-related rise in the concentrations of PS, PI, PC and PA in mitochondria of *psd1Δ*; however, the concentration of PA in mitochondria of *psd1Δ* is higher than in mitochondria of WT cultured with or without LCA (compare Figures 2.2 and 2.9). I also observed that, akin to the effect of LCA on mitochondrial membrane lipidome in WT, LCA triggers an age-related decline in the concentrations of PE and CL in mitochondria of *psd1Δ*; however, the concentrations of both PE and CL in mitochondria of *psd1Δ* are lower than in mitochondria of WT cultured with or without LCA (compare Figures 2.2 and 2.9).

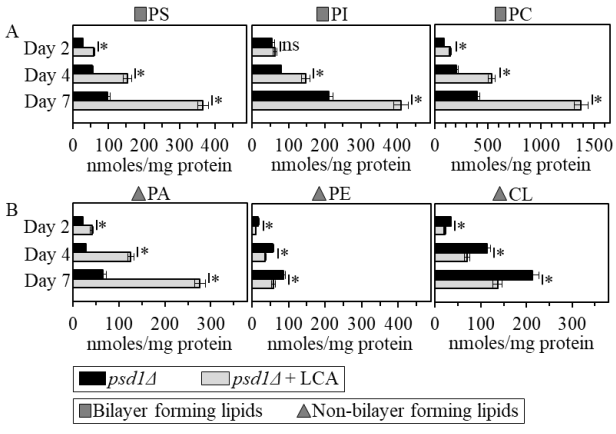

Figure 2.9. LCA exhibits age-related differential effects on the concentrations of different classes of mitochondrial membrane phospholipids in chronologically aging *psd1Δ* yeast. Cells of the *psd1Δ* mutant strain

were cultured in the nutrient-rich YP medium initially containing 0.2% glucose with 50 μM LCA or without it. Mitochondria were purified from cells recovered on day 2, 4 or 7 of cell culturing. Extraction of mitochondrial membrane lipids, and mass spectrometric identification and quantitation of the extracted phospholipid classes were carried out as described in Materials and methods. The concentrations of phospholipids were calculated as nmoles phospholipid/mg protein. (A) PS, PI and PC are phospholipid classes that exhibit the bilayer forming shape of a cylinder; they decrease the extent of membrane curving for the IMM. (B) PA, PE and CL are phospholipid classes that have the non-bilayer forming shape of a cone; they increase the extent of membrane curving for the IMM. Data are presented as means ± SEM (n = 3; *$p < 0.05$; ns, not significant). Abbreviations: CL, cardiolipin; PA, phosphatidic acid; PC, phosphatidylcholine; PE, phosphatidylethanolamine; PA, phosphatidic acid; PI, phosphatidylinositol; PS, phosphatidylserine.

I then used the above data to compare the ratios between concentrations of all possible pairwise combinations of phospholipid classes in mitochondrial membranes of WT and *psd1Δ* cells cultured in the presence or absence of LCA. I found that, in cells cultured with or without LCA, the psd1Δ mutation 1) augments the PA/PS, PA/PC and PA/PI ratios for non-bilayer forming PA vs. bilayer forming PS, PC and PI; 2) reduces the PE/PS, PE/PC and PE/PI ratios for non-bilayer forming PE vs. PS, PC and PI; 3) lessens the CL/PS, CL/PC and CL/PI ratios for non-bilayer forming CL vs. PS, PC and PI; 4) does not change the PS/PI, PS/PC and PI/PC ratios for all these bilayer forming classes of phospholipids; 5) rises the PA/PE and PA/CL ratios for all these non-bilayer forming phospholipid classes; and 6) decreases the PE/CL ratio for these two non-bilayer forming phospholipids (Figure 2.10). Thus, unlike *ups2Δ* and similar to *ups1Δ*, the *psd1Δ* mutation does not allow to maintain the equimolar concentrations of two non-bilayer forming phospholipids, PE and CL.

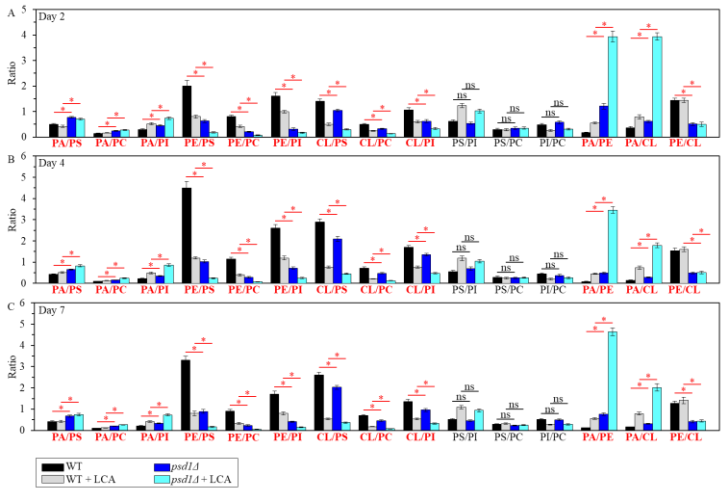

Figure 2.10. The *psd1Δ* mutation differently affects the ratios between concentrations of pairwise combinations of different phospholipid classes in mitochondrial membranes of chronologically aging yeast. *psd1Δ* cells were

cultured in the nutrient-rich YP medium initially containing 0.2% glucose with 50 μM LCA or without it. Mitochondria were purified from cells recovered on day 2 (A), 4 (B) or 7 (C) of cell culturing. Extraction of mitochondrial membrane lipids, and mass spectrometric identification and quantitation of the extracted phospholipid classes were carried out as described in Materials and methods. Based on these data, the ratios between concentrations of all possible pairwise combinations of phospholipid classes were calculated. Data are presented as means ± SEM (n = 3; *$p < 0.05$; ns, not significant).

My assessment of how the *psd1Δ* mutation influences the CLS of yeast cultured with or without LCA showed that *psd1Δ* 1) shortens yeast CLS in the absence of LCA (Figures 2.11A and 2.11B); and 2) substantially decreases the aging-delaying efficiency of LCA by significantly lowering the ability of this bile acid to increase both the mean and the maximum CLS (Figures 2.11A-2.11D).

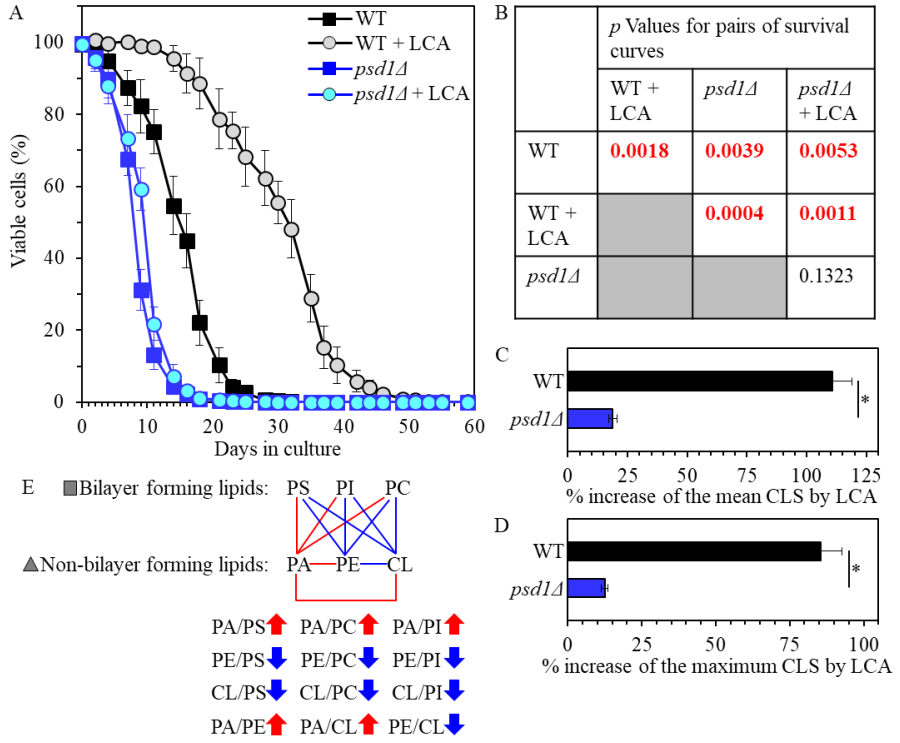

Figure 2.11. The *psd1Δ* mutation shortens yeast CLS in the absence of LCA and considerably decreases the geroprotective efficiency of LCA. WT and *psd1Δ* cells were cultured in the nutrient-rich YP medium initially containing 0.2% glucose with 50 μM LCA or without it. (A) Survival curves of chronologically aging WT and *psd1Δ* strains are shown. Data are presented as means ± SEM (n = 3). (B) *p* Values for different pairs of survival curves of WT and *psd1Δ* strains cultured with or without LCA. Survival curves shown in (A) were compared. Two survival curves were considered statistically different if the *p* value was less than 0.05. The *p* values for comparing pairs of

survival curves using the logrank test were calculated as described in Materials and methods. (C and D) Survival curves shown in (A) were used to calculate the percentage of increase of the mean and maximum CLS by LCA for WT and *psd1Δ* strains. Data are presented as means ± SEM (n = 3; **p* < 0.05). (E) The pattern of mitochondrial lipidome characteristic of the *psd1Δ* mutation is shown. Arrows next to the ratios between concentrations of different pairwise combinations of phospholipid classes indicate ratios that are increased (red arrows) or decreased (blue arrows) in *psd1Δ* cells (as compared to WT cells) cultured with or without LCA. Each colored line connects the names of two phospholipid classes whose concentration ratio is increased (red lines) or decreased (blue lines) by the *psd1Δ* mutation and cannot be restored by LCA.

Collectively, these findings suggest that the *psd1Δ* mutation may accelerate yeast chronological aging and decrease the geroprotective efficiency of LCA because it establishes a distinct pro-aging pattern of mitochondrial lipidome. This characteristic for *psd1Δ* pattern may include the following specific changes in the relative concentrations of different classes of membrane phospholipids: 1) an increase of the PA/PS, PA/PC and PA/PI ratios for non-bilayer forming PA vs. bilayer forming PS, PC and PI; 2) a decrease of the PE/PS, PE/PC and PE/PI ratios for non-bilayer forming PE vs. bilayer forming PS, PC and PI; 3) a decline of the CL/PS, CL/PC and CL/PI ratios for non-bilayer forming CL vs. bilayer forming PS, PC and PI; 4) an increase of the PA/PE and PA/CL ratios for these non-bilayer forming phospholipid classes; and 5) a decrease in the PE/CL ratio for these two non-bilayer forming classes of phospholipids (Figure 2.11E).

2.3.5 A distinct pro-longevity pattern of mitochondrial lipidome extends yeast CLS in the absence of LCA and amplifies the geroprotective efficiency of LCA

I noticed that the *ups1Δ*, *ups2Δ* and *psd1Δ* mutations cause some similar changes to the ratios between concentrations of various pairwise combinations of mitochondrial membrane phospholipids (compare Figures 2.5E, 2.8E and 2.11E). I therefore compared the datasets of such ratios that have been statistically significantly changed (SSC) by the *ups1Δ*, *ups2Δ* and *psd1Δ* mutations in yeast cultured with or without LCA. I found the following for the total of 12 SSC ratios: 1) 8 SSC ratios overlap between the *ups1Δ*, *ups2Δ* and *psd1Δ* datasets; 2) 3 SSC ratios are common to the datasets of the CLS-extending *ups2Δ* mutation that amplifies the geroprotective efficiency of LCA and the CLS-shortening *psd1Δ* mutation that lessens such efficiency; and 3) 1 SSC ratio, namely PE/CL, is common to the datasets of the *ups1Δ* and *psd1Δ* mutations, both of

which are CLS-shortening mutations that lower the geroprotective efficiency of LCA (*ups1Δ* increases the PE/CL ratio, whereas *psd1Δ* decreases it) (Figure 2.12A).

I also noticed that some ratios between concentrations of various pairwise combinations of mitochondrial membrane phospholipids are not statistically changed by the *ups1Δ*, *ups2Δ* and *psd1Δ* mutations. My analysis of these statistically unchanged (SU) ratios revealed the following: 1) 3 SU ratios overlap between the *ups1Δ*, *ups2Δ* and *psd1Δ* datasets; 2) 3 SU ratios are unique to the dataset of *ups1Δ*, a CLS-shortening mutation that lowers the geroprotective efficiency of LCA; and 3) 1 SU ratio, namely PE/CL, is unique to the dataset of *ups2Δ*, a CLS-extending mutation that amplifies the geroprotective efficiency of LCA (Figure 2.12B).

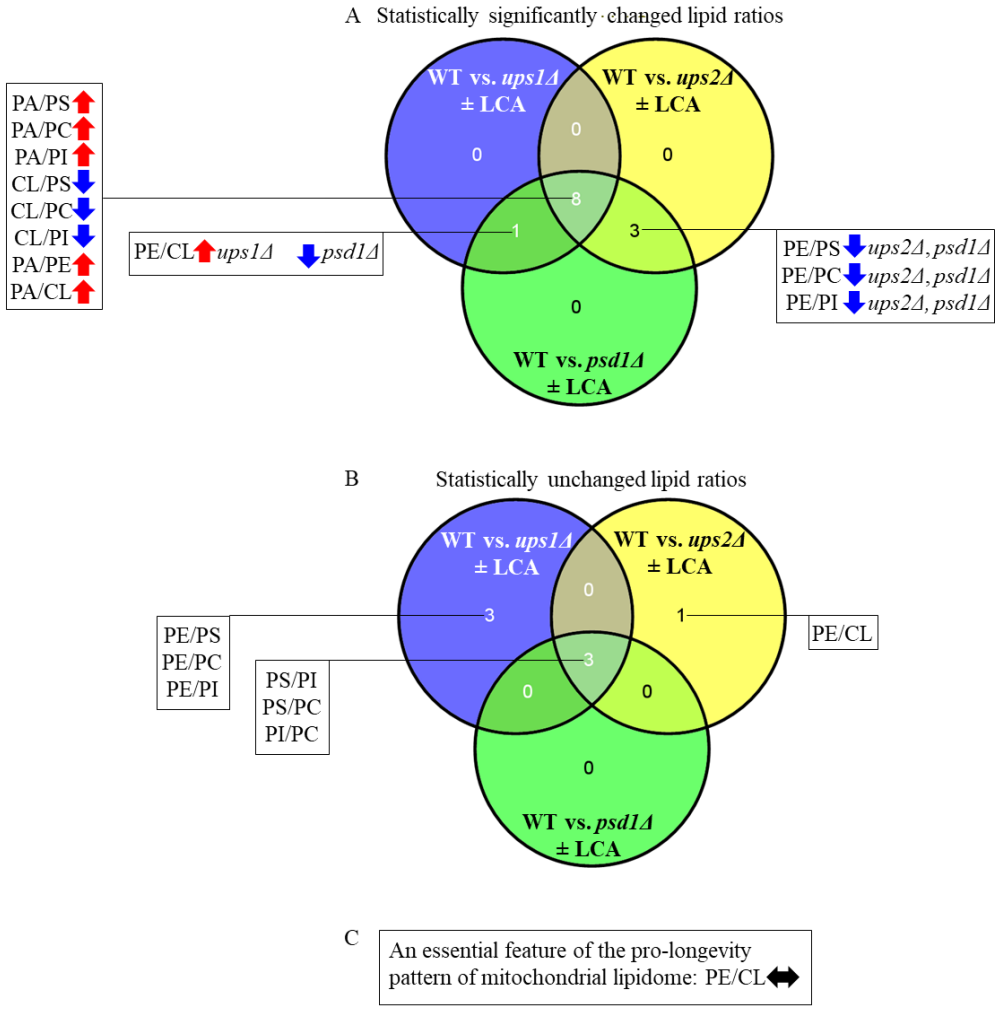

Figure 2.12. Venn diagrams showing a comparison of the effects of the *ups1Δ*, *ups2Δ* and *psd1Δ* mutations on the ratios between concentrations of various pairwise combinations of mitochondrial membrane phospholipids. A comparison of the datasets for the ratios that have been statistically significantly changed (A) or statistically

unchanged (B) by the *ups1Δ*, *ups2Δ* and *psd1Δ* mutations in yeast cultured with or without LCA are shown. (C) The maintenance of equimolar concentrations of PE and CL is an essential feature of the pro-longevity pattern of mitochondrial lipidome. Arrows next to the ratios between concentrations of different pairwise combinations of phospholipid classes indicate ratios that are increased (red arrows) or decreased (blue arrows) in *ups1Δ*, *ups2Δ* or *psd1Δ* cells (as compared to WT cells) cultured with or without LCA.

In sum, these findings suggest that the maintenance of equimolar concentrations of two non-bilayer forming and cone-shaped phospholipids, PE and CL, may be critical feature of the pro-longevity pattern of mitochondrial lipidome (Figure 2.12C). This feature is a longevity assurance trait in the absence of LCA. This feature is also required for the delay of yeast chronological aging by exogenous LCA.

The maintenance of equimolar concentrations of PE and CL is a trait that is common to WT and *ups2Δ*, a mutant strain that not only lives longer than WT but also exhibits an amplified (as compared to WT) geroprotective efficiency of LCA (Figure 2.8). It is conceivable, therefore, that some traits distinguishing mitochondrial lipidome of *ups2Δ* from that of WT may represent additional features of the pro-longevity pattern of mitochondrial lipidome. These additional features are likely to be responsible for the ability of the *ups2Δ* mutation to extend longevity in the absence of LCA and also to increase the geroprotective efficiency of LCA. Among these additional features are the ones that differentiate mitochondrial lipidome of *ups2Δ* from that of WT; they include the following: 1) an increased concentration of PA, another non-bilayer forming and cone-shaped phospholipid; 2) a decreased concentration of PE; and 3) a proportionally (as compared to PE) decreased concentration of CL (compare Figures 2.2 and 2.6). I therefore hypothesize that the proportional decrease in the concentrations of PE and CL in mitochondrial membranes of *ups2Δ* may be responsible for the increased concentration of PA in these membranes.

2.3.6 The *ups1Δ* and *ups2Δ* mutations alter the concentrations of many mitochondrial proteins in yeast cultured with or without LCA

My hypothesis posits that the LCA-dependent establishment and maintenance of a distinct pro-longevity pattern of mitochondrial lipidome may have a causal role in the age-related remodeling of mitochondrial proteome. I therefore used quantitative mass spectrometry to compare the identities and relative concentrations of proteins that were recovered in mitochondria purified from WT, *ups1Δ* and *ups2Δ* cells cultured with or without LCA. The *ups1Δ* mutation

establishes and maintains a distinct pro-aging pattern of mitochondrial lipidome (Figures 2.4, 2.5 and 2.12), shortens CLS (Figure 2.5), and lowers the geroprotective efficiency of LCA (Figure 2.5). In contrast, the *ups2Δ* mutation institutes and preserves a specific pro-longevity pattern of mitochondrial lipidome (Figures 2.7, 2.8 and 2.12), extends CLS (Figure 2.8), and amplifies the geroprotective efficiency of LCA (Figure 2.8).

I found that both mutations, *ups1Δ* and *ups2Δ*, alter the age-related chronology of changes in concentrations of numerous mitochondrial proteins in yeast cultured in the presence of LCA or in its absence; these proteins have been implicated in many essential mitochondrial functions (see Figure 2.13 for *ups1Δ* and Figure 2.14 for *ups2Δ*).

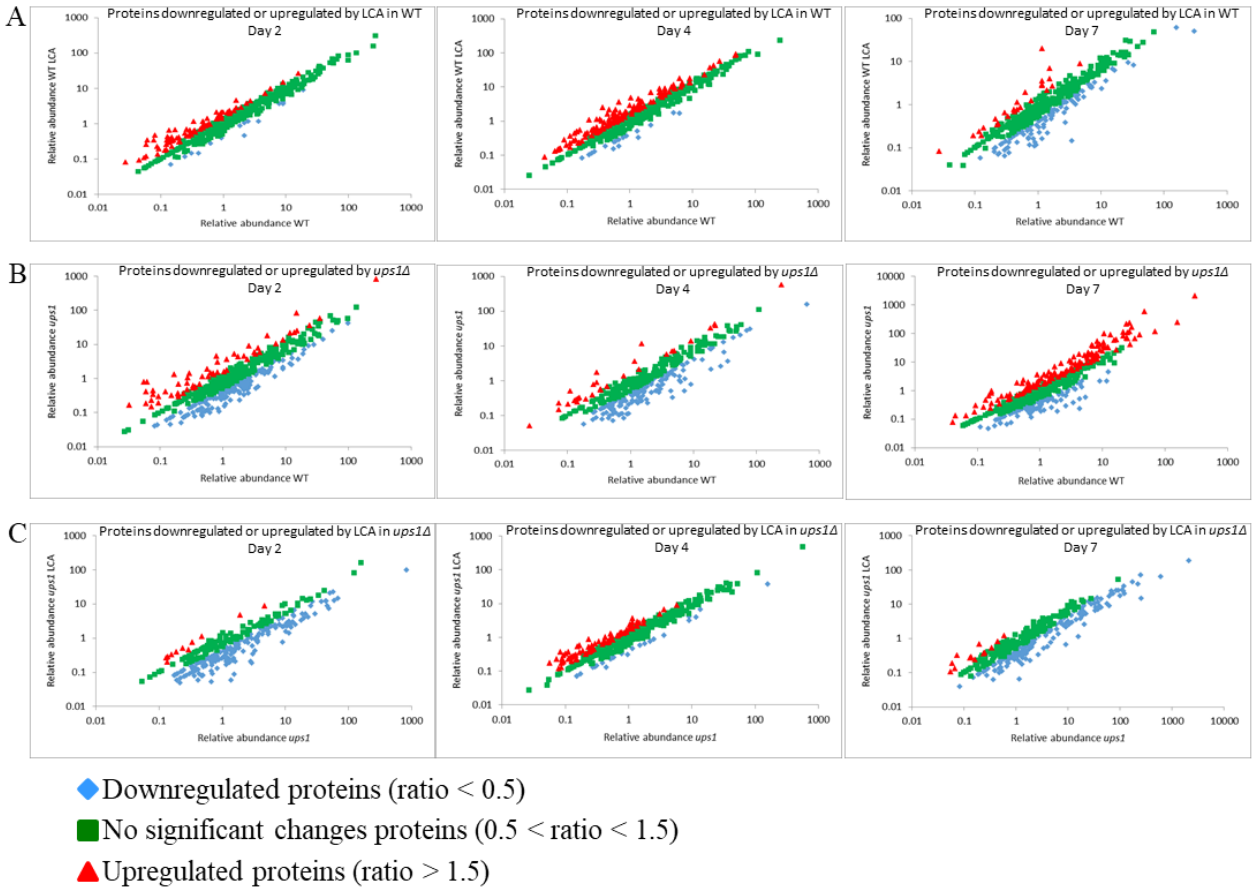

Figure 2.13. Scatter plots comparing the relative concentrations of proteins in mitochondria purified from WT or *ups1Δ* (short-lived) cells cultured with or without LCA. Mitochondria were purified from WT or *ups1Δ* cells recovered on day 2, 4 or 7 of cell culturing. Mass spectrometry-based identification and quantitation of proteins recovered in purified mitochondria were performed as described in Materials and methods. Scatter plots comparing the relative abundance of mitochondrial proteins between specified datasets were plotted on a log-log scale spanning

six orders of magnitude. Data on the relative abundance of mitochondrial proteins are presented as means of 2 independent experiments.

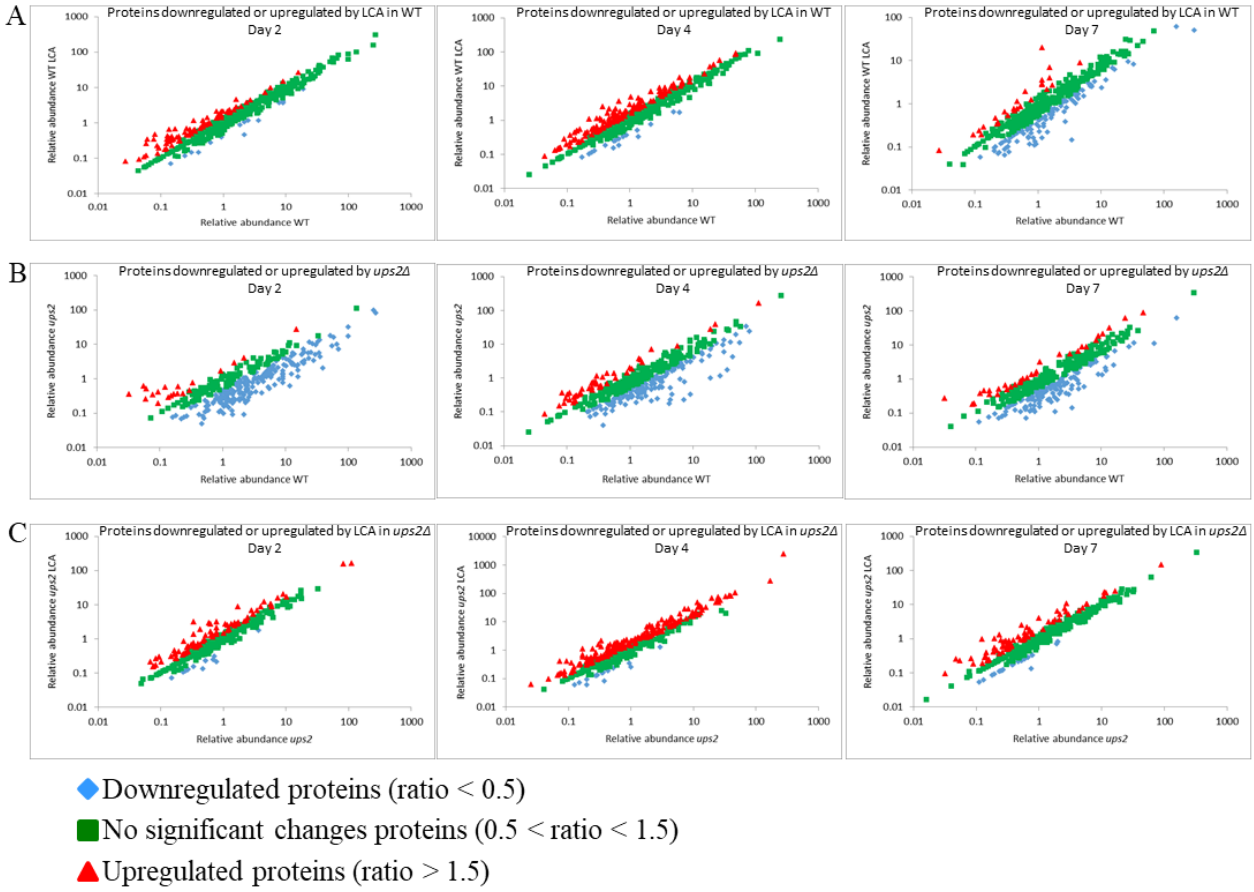

Figure 2.14. Scatter plots comparing the relative concentrations of proteins in mitochondria purified from WT or *ups2Δ* (long-lived) cells cultured with or without LCA. Mitochondria were purified from WT or *ups2Δ* cells recovered on day 2, 4 or 7 of cell culturing. Mass spectrometry-based identification and quantitation of proteins recovered in purified mitochondria were performed as described in Materials and methods. Scatter plots comparing the relative abundance of mitochondrial proteins between specified datasets were plotted on a log-log scale spanning six orders of magnitude. Data on the relative abundance of mitochondrial proteins are presented as means of 2 independent experiments.

I then compared the datasets of relative concentrations of mitochondrial proteins that are statistically significantly downregulated or upregulated 1) by LCA in WT; 2) by the *ups1Δ* or *ups2Δ* mutation in the absence of LCA; and 3) by LCA in *ups1Δ* or *ups2Δ* cells.

My comparative analysis of these datasets for *ups1Δ* revealed the following: 1) many mitochondrial proteins that are downregulated or upregulated in *ups1Δ* cells cultured without LCA are unique to these datasets (i.e. these proteins are not present in the datasets of mitochondrial

proteins that are downregulated or upregulated by LCA in WT or by LCA in *ups1Δ* cells) (Figures 2.15A – 2.15F); and 2) the total number and identities of mitochondrial proteins that are downregulated or upregulated in *ups1Δ* cells cultured with or without LCA fluctuate significantly in cells recovered on day 2, 4 or 7 of cell culturing (i.e. at different stages of chronological aging) (Figures 2.15H – 2.15L).

For *ups2Δ*, I found that: 1) a number of mitochondrial proteins that are downregulated or upregulated in *ups2Δ* cells cultured in the absence of LCA cannot be found in the datasets of mitochondrial proteins downregulated or upregulated by LCA in WT or by LCA in *ups2Δ* cells (Figures 2.16A – 2.16F); 2) the total number and identities of mitochondrial proteins that are downregulated or upregulated in *ups2Δ* cells cultured in the absence of LCA vary substantially with the chronological age of cells (Figures 2.16H and 2.16K); 3) numerous mitochondrial proteins that are downregulated or upregulated by LCA in *ups2Δ* cells are unique to these datasets as they cannot be found in the datasets of mitochondrial proteins downregulated or upregulated by LCA in WT or by the *ups2Δ* mutation in the absence of LCA (Figures 2.16A – 2.16F); and 4) the total number and identities of mitochondrial proteins that are downregulated or upregulated by LCA in *ups2Δ* cells fluctuate significantly with the chronological age of cells (Figures 2.16I and 2.16L).

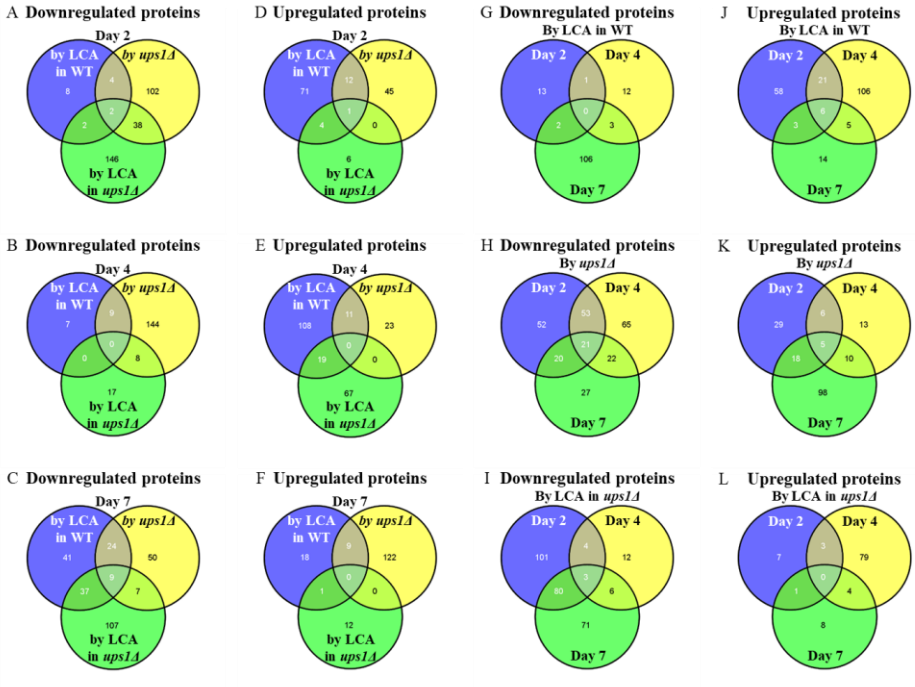

Figure 2.15. The *ups1Δ* mutation alters the concentrations of many mitochondrial proteins in yeast cultured with or without LCA. (A – F) Venn diagrams showing a comparison of the datasets of relative concentrations of

mitochondrial proteins that are statistically significantly downregulated or upregulated by LCA in WT, by the *ups1Δ* mutation in the absence of LCA, and by LCA in *ups1Δ* cells; WT cells were recovered on day 2, 4 or 7 of culturing. (G and J) Venn diagrams showing a comparison of the datasets of relative concentrations of mitochondrial proteins that are statistically significantly downregulated or upregulated by LCA in WT cells recovered on day 2, 4 or 7 of culturing. (H and K) Venn diagrams showing a comparison of the datasets of relative concentrations of mitochondrial proteins that are statistically significantly downregulated or upregulated by the *ups1Δ* mutation in the absence of LCA; *ups1Δ* cells were recovered on day 2, 4 or 7 of culturing. (I and L) Venn diagrams showing a comparison of the datasets of relative concentrations of mitochondrial proteins that are statistically significantly downregulated or upregulated by LCA in *ups1Δ* cells recovered on day 2, 4 or 7 of culturing.

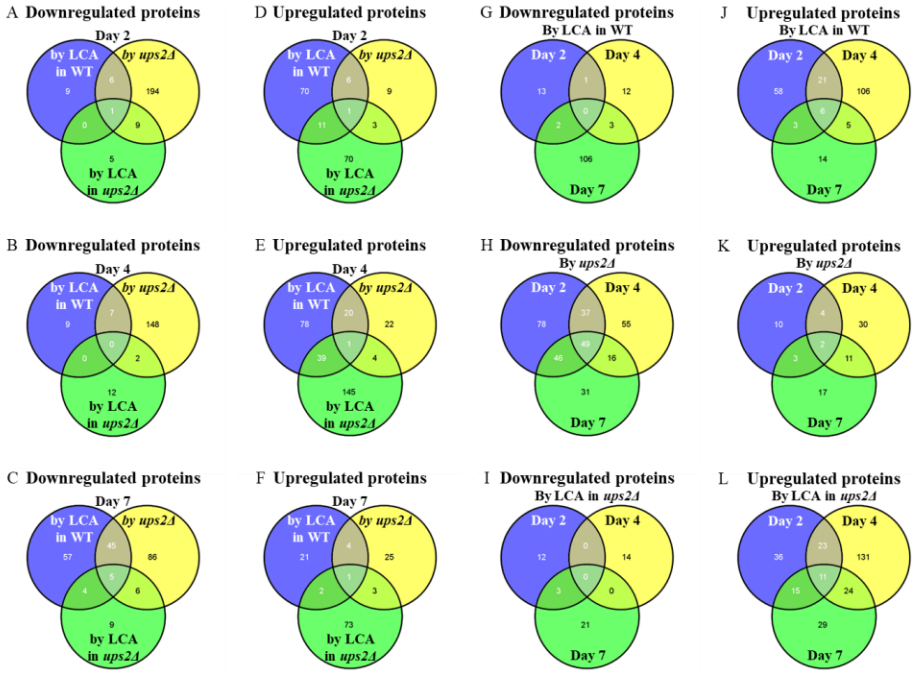

Figure 2.16. The *ups2Δ* mutation alters the concentrations of many mitochondrial proteins in yeast cultured with or without LCA. (A – F) Venn diagrams showing a comparison of the datasets of relative concentrations of mitochondrial proteins that are statistically significantly downregulated or upregulated by LCA in WT, by the *ups2Δ* mutation in the absence of LCA, and by LCA in *ups2Δ* cells; WT cells were recovered on day 2, 4 or 7 of culturing. (G and J) Venn diagrams showing a comparison of the datasets of relative concentrations of mitochondrial proteins that are statistically significantly downregulated or upregulated by LCA in WT cells recovered on day 2, 4 or 7 of culturing. (H and K) Venn diagrams showing a comparison of the datasets of relative concentrations of mitochondrial proteins that are statistically significantly downregulated or upregulated by the *ups2Δ* mutation in the absence of LCA; *ups2Δ* cells were recovered on day 2, 4 or 7 of culturing. (I and L) Venn diagrams showing a comparison of the datasets of relative concentrations of mitochondrial proteins that are statistically significantly downregulated or upregulated by LCA in *ups2Δ* cells recovered on day 2, 4 or 7 of culturing.

Taken together, these findings indicate that in yeast cultured with or without LCA 1) the establishment and maintenance of a distinct pro-aging pattern of mitochondrial lipidome in short-lived *ups1Δ* cells (Figures 2.4, 2.5 and 2.12) correlate with the establishment and maintenance of a specific aging-accelerating pattern of mitochondrial proteome in these mutant cells; and 2) the institution and preservation of a specific pro-longevity pattern of mitochondrial lipidome in long-lived *ups2Δ* cells (Figures 2.7, 2.8 and 2.12) correlate with the institution and preservation of a distinctive aging-delaying pattern of mitochondrial proteome in these mutant cells.

2.3.7 The mitochondrial proteomes of *ups1Δ* and *ups2Δ* differ substantially

Because my findings suggest that in yeast cultured with or without LCA the *ups1Δ* and *ups2Δ* mutations can establish and maintain either an aging-accelerating or an aging-delaying (respectively) pattern of mitochondrial proteome, I compared the datasets of relative concentrations of mitochondrial proteins that are statistically significantly downregulated or upregulated in *ups1Δ* or *ups2Δ* cells in the absence or presence of LCA.

For *ups1Δ* and *ups2Δ* cells cultured without LCA, I found the following: 1) many mitochondrial proteins that are downregulated or upregulated in long-lived *ups2Δ* cells are not present in the datasets of mitochondrial proteins that are downregulated or upregulated in short-lived *ups1Δ* cells (Figures 2.17A – 2.17F); and 2) the total number and identities of mitochondrial proteins that are downregulated or upregulated only in long-lived *ups2Δ* cells fluctuate significantly in cells recovered at different stages of chronological aging (Figures 2.17A – 2.17F). Functions of some mitochondrial proteins that are downregulated or upregulated only in long-lived *ups2Δ* cells remain to be established (Figures 2.17G – 2.17L). Many mitochondrial proteins that are downregulated or upregulated only in long-lived *ups2Δ* cells have been implicated in essential mitochondrial functions, including the electron transport chain (ETC), respiration, the tricarboxylic acid (TCA) cycle, ribosome assembly, amino acid metabolism, carbohydrate metabolism, protein import, proteostasis, metabolite synthesis, protein synthesis, ATP synthesis, metabolite transport, lipid metabolism, contact sites and cristae maintenance, redox homeostasis, mitochondrial DNA (mtDNA) maintenance, stress response, mRNA synthesis and processing, the maintenance of contact sites between mitochondria and vacuoles, and mitochondrial fusion (Figures 2.17G – 2.17L).

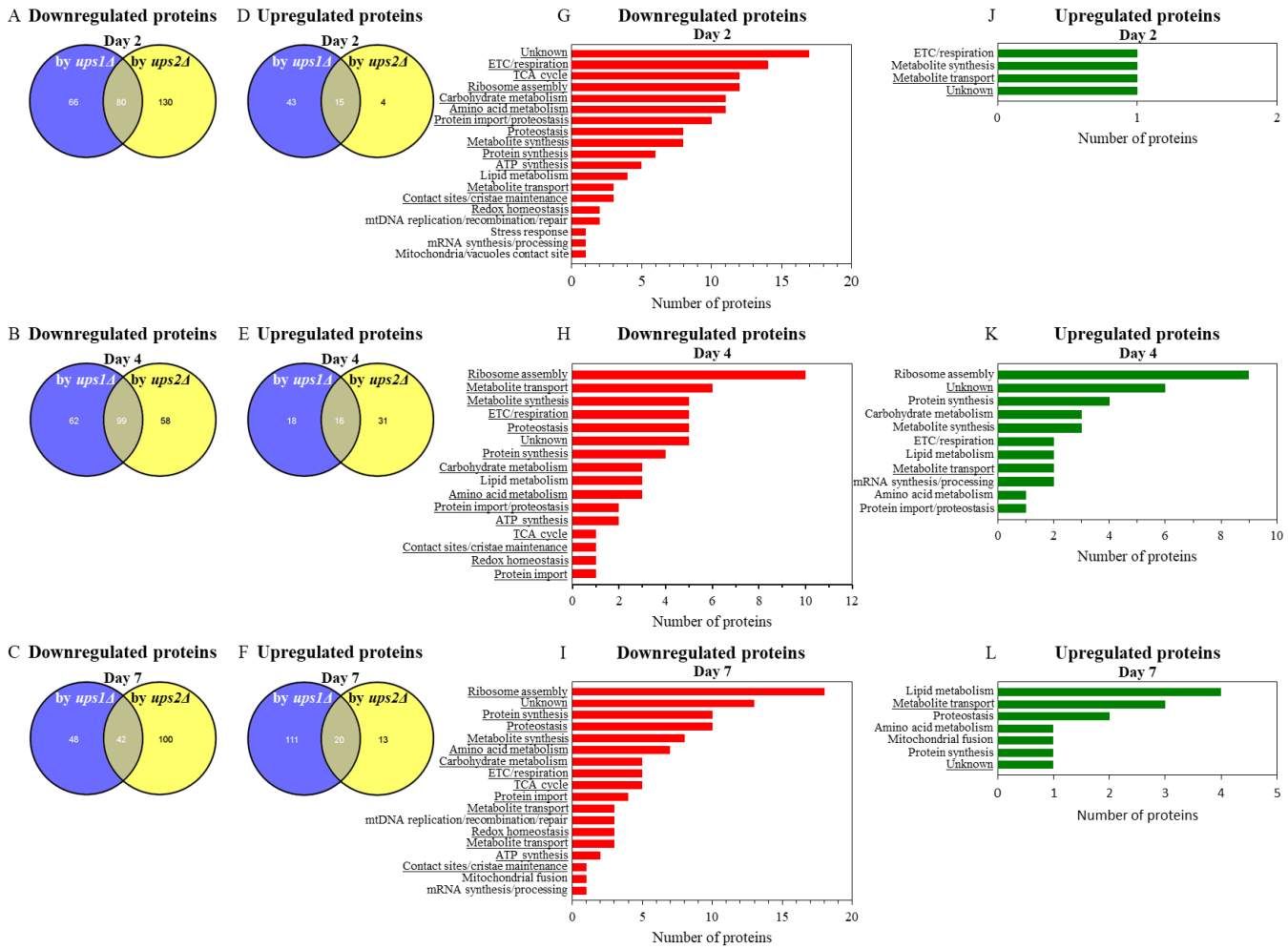

Figure 2.17. In cells cultured without LCA, many mitochondrial proteins that are downregulated or upregulated in long-lived *ups2Δ* cells are not downregulated or upregulated in short-lived *ups1Δ* cells. (A – F) Venn diagrams showing a comparison of the datasets of relative concentrations of mitochondrial proteins that are statistically significantly downregulated or upregulated in *ups1Δ* or *ups2Δ* cells cultured in the absence of LCA; cells were recovered on day 2, 4 or 7 of culturing. (G – L) Mitochondrial proteins that are downregulated or upregulated only in long-lived *ups2Δ* cells belong to various functional categories. The names of functional categories whose protein representatives were downregulated or upregulated in *ups2Δ* cells recovered on every of the three days are underlined. Functions of some mitochondrial proteins that are downregulated or upregulated only in *ups2Δ* cells are currently unknown. Abbreviations: ETC, electron transport chain; mtDNA, mitochondrial DNA; TCA, the tricarboxylic acid cycle.

For *ups1Δ* and *ups2Δ* cells cultured with LCA, I found the following: 1) a number of mitochondrial proteins that are downregulated or upregulated by LCA in long-lived *ups2Δ* cells cannot be found in the datasets of mitochondrial proteins that are downregulated or upregulated

by LCA in WT or short-lived *ups1Δ* cells (Figures 2.18A – 2.18F); and 2) the total number and identities of mitochondrial proteins that are downregulated or upregulated by LCA only in long-lived *ups2Δ* cells vary notably in cells recovered at different stages of chronological aging (Figures 2.18A – 2.18F). Functions of some mitochondrial proteins that are downregulated or upregulated by LCA only in long-lived *ups2Δ* cells remain unknown (Figures 2.18G – 2.18L). Numerous mitochondrial proteins that are downregulated or upregulated by LCA only in long-lived *ups2Δ* cells are known for their essential roles in the same set of mitochondrial functions as the ones played by proteins that are downregulated or upregulated only in long-lived *ups2Δ* cells culture without LCA (compare Figures 2.17G – 2.17L to Figures 2.18G – 2.18L).

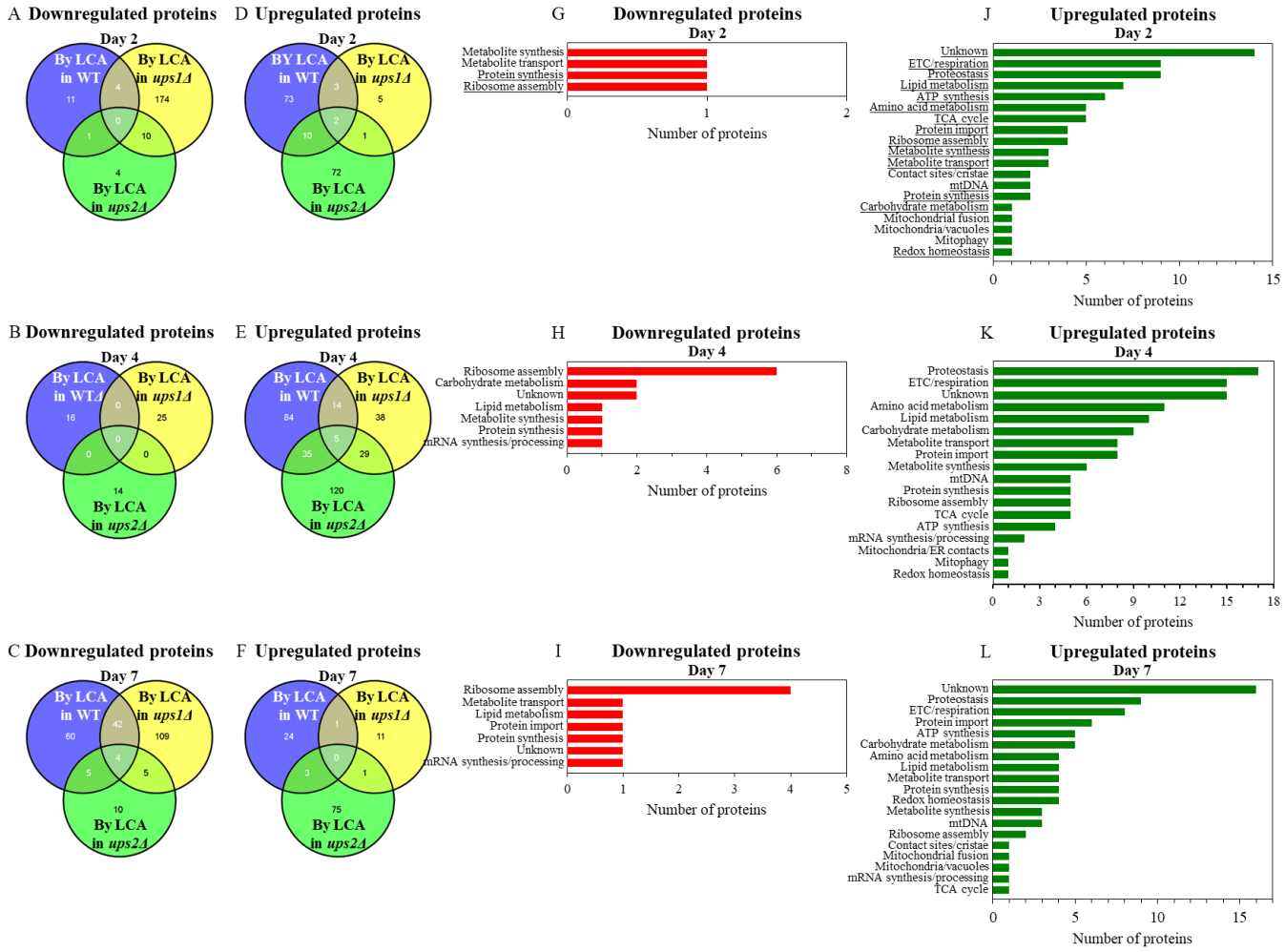

Figure 2.18. In cells cultured with LCA, many mitochondrial proteins that are downregulated or upregulated by LCA in long-lived *ups2Δ* cells are not downregulated or upregulated by LCA in WT or short-lived *ups1Δ* cells. (A – F) Venn diagrams showing a comparison of the datasets of relative concentrations of mitochondrial proteins

that are statistically significantly downregulated or upregulated by LCA in WT, *ups1Δ* or *ups2Δ*; cells were recovered on day 2, 4 or 7 of culturing. (G – L) Mitochondrial proteins that are downregulated or upregulated by LCA only in long-lived *ups2Δ* cells belong to many different functional categories. The names of functional categories whose protein representatives were downregulated or upregulated by LCA in *ups2Δ* cells recovered on every of the three days are underlined. Functions of some mitochondrial proteins that are downregulated or upregulated by LCA only in *ups2Δ* cells are currently unknown. Abbreviations: ETC, electron transport chain; mtDNA, mitochondrial DNA; TCA, the tricarboxylic acid cycle.

In sum, these findings suggest that in yeast cultured with or without LCA the *ups2Δ* mutation may establish and maintain an aging-delaying pattern of mitochondrial proteome.

2.3.8 Many mitochondrial proteins that are downregulated or upregulated by LCA only in long-lived *ups2Δ* cells play essential roles in aging delay by LCA

Because my findings suggest that in yeast cultured with LCA the *ups2Δ* mutation may establish and maintain a distinct pattern of mitochondrial proteome that is essential for the ability of LCA to delay aging, I investigated how single-gene-deletion mutations eliminating the key proteins constituting such pattern affect the geroprotective efficiency of LCA.

I thought that some of the proteins downregulated by LCA in *ups2Δ* may function in attenuating the geroprotective efficiency of LCA, and thus the elimination of these proteins by mutations may increase such efficiency. I also thought that some of the proteins upregulated by LCA in *ups2Δ* may act as facilitators of aging delay by LCA, and therefore the elimination of these proteins by mutations may decrease the geroprotective efficiency of LCA.

I found that mutants that lack 10 out of 12 proteins most highly downregulated by LCA in *ups2Δ* exhibit a statistically significantly increase of the aging-delaying efficiency of LCA; a slight increase of such efficiency seen in mutants that lack 2 other downregulated by LCA proteins was not statistically significant (Figures 2.19A – 2.19C). I also found that mutants that lack 11 out of 12 proteins vastly upregulated by LCA in *ups2Δ* display a statistically significantly decrease of the geroprotective efficiency of LCA; a minor decrease of such efficiency observed in a mutant lacking one of the downregulated by LCA proteins was not statistically significant (Figures 2.19D – 2.19F). Of note, none of these mutants exhibits such robust change of the aging-delaying efficiency of LCA as the changes seen in the *ups1Δ*, *ups2Δ* and *psd1Δ* mutants (compare Figures 2.5, 2.8, 2.11 and 2.19). This finding suggests that Ups1, Ups2 and Psd1 may function as upstream

regulators of various mitochondrial processes whose synergistic action defines the efficiency of aging delay by LCA.

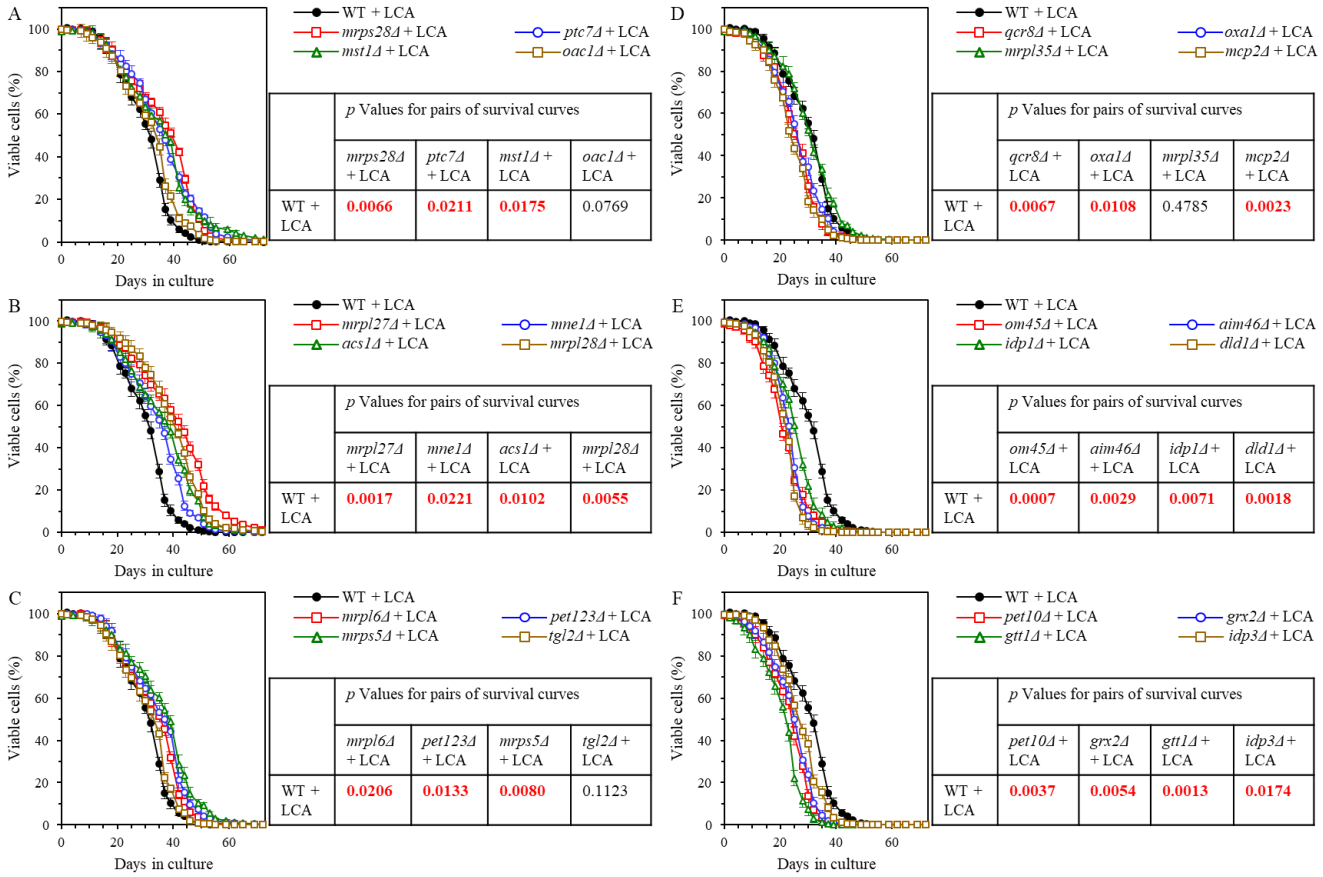

Figure 2.19. Many mutations eliminating proteins downregulated by LCA in *ups2Δ* increase the aging-delaying efficiency of LCA, while many mutations eliminating proteins upregulated by LCA in *ups2Δ* decrease such efficiency. WT and mutant cells were cultured in the nutrient-rich YP medium initially containing 0.2% glucose with 50 μM LCA. (A - C) Survival curves of chronologically aging WT and mutant strains that lack proteins most highly downregulated by LCA in *ups2Δ* are shown. Data are presented as means ± SEM (n = 3). Also shown are *p* values for different pairs of survival curves of WT and mutant strains cultured with LCA. Survival curves shown in (A - C) were compared. Two survival curves were considered statistically different if the *p* value was less than 0.05. The p values for comparing pairs of survival curves using the logrank test were calculated as described in Materials and methods. (D - F) Survival curves of chronologically aging WT and mutant strains that lack proteins most substantially upregulated by LCA in *ups2Δ* are shown. Data are presented as means ± SEM (n = 3). Also shown are *p* values for different pairs of survival curves of WT and mutant strains cultured with LCA. Survival curves shown in (D - F) were compared. Two survival curves were considered statistically different if the *p* value was less than 0.05. The *p* values for comparing pairs of survival curves using the logrank test were calculated as described in Materials and methods. Pavlo Kyryakov, Paméla Dakik, Mélissa McAuley, Younes Medkour and Tamara Di Maulo conducted experiments

Taken together, these findings further support the notion that the *ups2Δ* mutation may allow to sustain a distinct aging-delaying pattern of mitochondrial proteome that is essential for the ability of LCA to delay aging.

2.3.9 The *ups1Δ* and *ups2Δ* mutations have different effects on some key aspects of mitochondrial functionality in yeast cultured with LCA

My hypothesis posits that the LCA-dependent remodeling of mitochondrial lipidome and the resulting changes in mitochondrial proteome may create an aging-delaying pattern of mitochondrial functionality that is essential for the ability of LCA to delay aging. To test this hypothesis, I monitored the age-related chronology of changes in four vital cellular processes confined to and regulated by mitochondria. These processes include the following: 1) mitochondrial respiration; 2) the maintenance of electrochemical potential ($\Delta\Psi$) across the IMM; 3) the maintenance of the homeostasis of cellular ROS known to be produced primarily as by-products of mitochondrial respiration [210, 211]; and 4) the modulation of cellular concentrations of ATP, which in yeast cultured in media with low (0.2%) glucose concentration is generated mainly in mitochondria [210, 211]. These vital processes were monitored in chronologically aging WT, *ups1Δ* and *ups2Δ* cells cultured with LCA.

I found that in WT cells cultured with LCA the rate of mitochondrial respiration 1) is increased when cells enter diauxic (D) growth phase that begins on day 2 of culturing; 2) reaches a plateau in post-diauxic (PD) growth phase that occurs between days 3 and 7 of culturing; and 3) slightly declines during the subsequent stationary (ST) growth phase that follows PD phase and begins after day 7 of culturing (Figure 2.20A). In *ups2Δ* cells cultured with LCA the rate of mitochondrial respiration 1) is increased to a significantly higher extent during D phase than in WT cells; and 2) reaches a plateau in PD phase and then additionally rises in ST phase to a substantially higher level than that in WT cells (Figure 2.20A). In *ups1Δ* cells cultured with LCA the rate of mitochondrial respiration 1) is increased to a significantly lower degree during D phase than in WT cells; and 2) substantially declines in PD and ST phases to reach a markedly lower level than that in WT cells (Figure 2.20A).

In WT cells cultured with LCA the value of $\Delta\Psi$ 1) is increased during D phase; 2) reaches a plateau during PD phase; and 3) slightly rises during ST phase (Figure 2.20B). In *ups2Δ* cells

cultured with LCA the value of ΔΨ 1) is increased to a similar extent during D phase as in WT cells; 2) further rises during PD phase to reach a level significantly exceeding that in WT cells; and 3) slightly declines but remains higher than that in WT cells during ST phase (Figure 2.20B). In *ups1Δ* cells cultured with LCA the value of ΔΨ 1) is increased to a significantly lower degree during D phase than in WT cells; and 2) slightly rises during PD phase and then declines in ST phase to reach a substantially lower level than that in WT cells (Figure 2.20B).

In WT cells cultured with LCA the concentration of ROS 1) is increased during D phase; 2) reaches a plateau during PD phase; and 3) remains mainly unchanged during ST phase (Figure 2.20C). In *ups2Δ* cells cultured with LCA the concentration of ROS 1) is increased to a lower degree during D phase than in WT cells; and 2) undergoes minor changes during PD and ST phases to reach a level that is significantly lower than that in WT cells (Figure 2.20C). In *ups1Δ* cells cultured with LCA the concentration of ROS 1) is increased to a similar extent during D phase as in WT cells; and 2) further rises during PD and ST phases to reach a level significantly exceeding that in WT cells (Figure 2.20C).

In WT cells cultured with LCA the concentration of ATP 1) is increased during D phase; 2) reaches a plateau during PD phase; and 3) slightly declines during ST phase (Figure 2.20D). In *ups2Δ* cells cultured with LCA the concentration of ATP 1) is increased to a similar degree during D phase as in WT cells; 2) further rises during PD phase to reach a level significantly higher than that in WT cells; and 3) slightly declines but remains higher than that in WT cells during ST phase (Figure 2.20D). In *ups1Δ* cells cultured with LCA the concentration of ATP 1) is increased to a significantly lower extent during D phase than in WT cells; and 2) remains unchanged during PD phase and then declines in ST phase to reach a substantially lower level than that in WT cells (Figure 2.20D).

In sum, these findings support the notion that the LCA-dependent remodeling of mitochondrial lipidome and the resulting changes in mitochondrial proteome can create an aging-delaying pattern of mitochondrial functionality that is essential for the ability of LCA to delay aging.

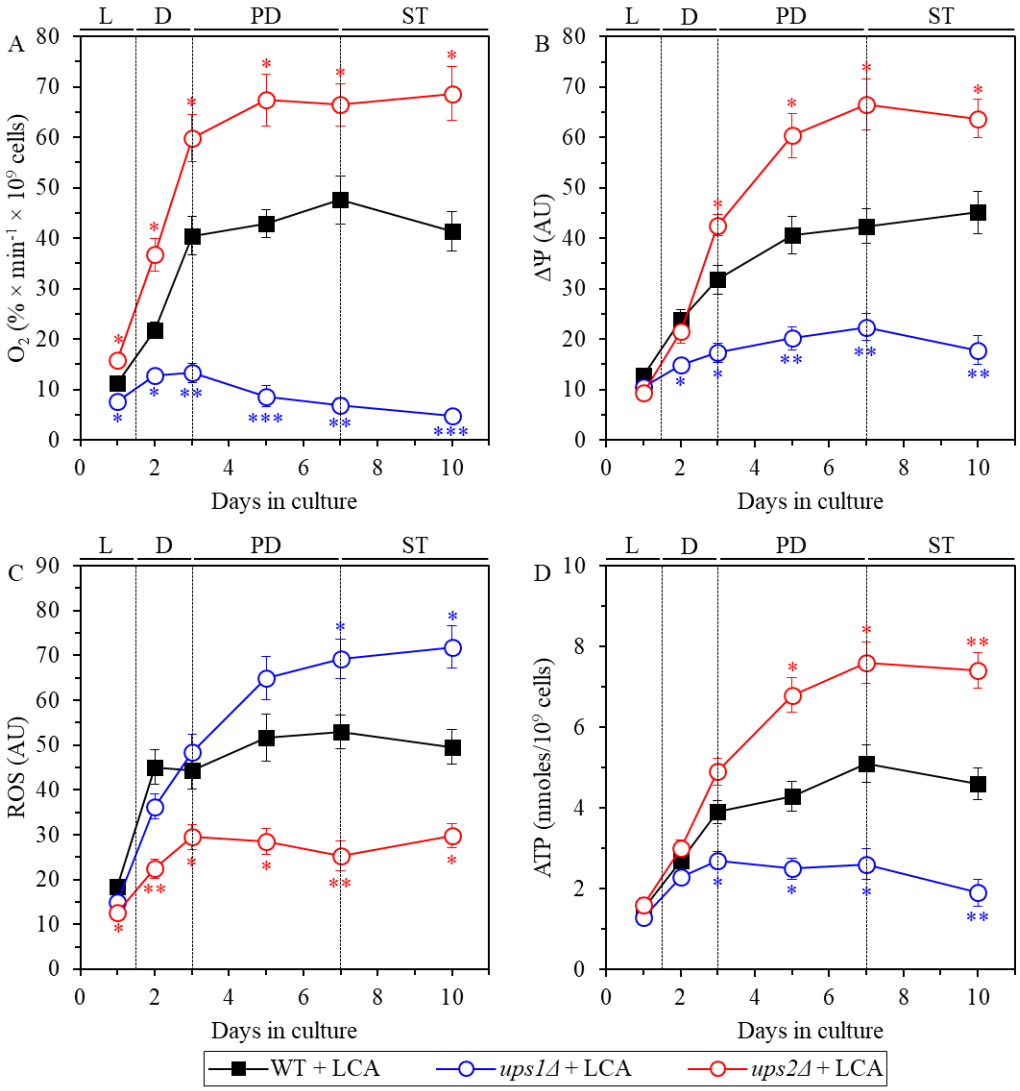

Figure 2.20. In yeast cultured with LCA, the *ups1Δ* and *ups2Δ* mutations differently affect four key aspects of mitochondrial functionality. WT and mutant cells were cultured in the nutrient-rich YP medium initially containing 0.2% glucose with 50 μM LCA. The dynamics of age-related changes in the rate of oxygen consumption my cells (A), electrochemical potential (ΔΨ) across the IMM (B), cellular concentration of ROS (C) and cellular concentration of ATP (D) during chronological aging of yeast. Data are presented as means ± SEM (n = 3; **p* < 0.05; **p < 0.01; ***p < 0.001). Pavlo Kyryakov, Paméla Dakik, Mélissa McAuley, Younes Medkour and Tamara Di Maulo conducted experiments.

2.4 Discussion

This study provides evidence that the mitochondrial lipidome defines not only the rate of yeast chronological aging but also the geroprotective efficiency of LCA in chronologically aging yeast. I demonstrate the existence of a distinct pro-longevity pattern of mitochondrial lipidome,

which extends yeast CLS in the absence of LCA and amplifies the geroprotective efficiency of LCA. This pattern consists in a proportional decrease of PE and CL concentrations, and in a concomitant increase of PA concentration. PE, CL and PA are non-bilayer forming, cone-shaped phospholipid classes that increase the extent of membrane curving for the IMM to rise the abundance of mitochondrial cristae (formed by the IMM) and mitochondrial contact cites (formed between the IMM and OMM) [81, 198, 199, 202-207]. I also show that these LCA-driven specific changes in the composition of mitochondrial membrane lipids cause a distinct remodeling of mitochondrial proteome by decreasing and increasing concentration of many mitochondrial proteins. These proteins have been implicated in such vital mitochondrial functions as the ETC and respiration, the TCA cycle, ribosome assembly, amino acid metabolism, carbohydrate metabolism, protein import, proteostasis, metabolite synthesis, protein synthesis, ATP synthesis, metabolite transport, lipid metabolism, contact sites and cristae maintenance, redox homeostasis, mtDNA maintenance, stress response, mRNA synthesis and processing, the maintenance of contact sites between mitochondria and vacuoles, and mitochondrial fusion. I provide evidence that the LCA-dependent remodeling of mitochondrial lipidome and the resulting changes in mitochondrial proteome allow to change the age-related chronology of changes in such vital mitochondrial processes as respiration, electrochemical potential maintenance, ROS homeostasis preservation and ATP synthesis. These changes facilitate the establishment and maintenance of an aging-delaying pattern of mitochondrial functionality that is essential for the ability of LCA to delay aging.

3 Caloric restriction extends yeast chronological lifespan via a mechanism linking cellular aging to cell cycle regulation, maintenance of a quiescent (Q) state, entry into a non-quiescent (NQ) state and survival in the NQ state

3.1 Introduction

CR is a dietary intervention that delays aging in yeast and other evolutionarily distant eukaryotic organisms [84, 85, 185-189]. Mechanisms linking yeast chronological aging to a quiescence program under non-CR conditions are well established; these mechanisms are discussed in Chapter 1 of my thesis [88-92, 94, 126, 127, 180, 190]. It was unknown, however, if the aging-delaying effect of CR in chronologically aging yeast is due in part to the ability of this low-calorie diet to control the quiescence program. To test if the ability of CR to slow down yeast chronological aging, I investigated how the CR diet influences the differentiation of chronologically aging yeast cultures into Q and NQ cells, and how it affects their properties.

3.2 Materials and methods

3.2.1 Yeast strains, media and growth conditions

The wild-type strain *Saccharomyces cerevisiae* BY4742 (*MATα his3Δ1 leu2Δ0 lys2Δ0 ura3Δ0*) from Open Biosystems/Dharmacon (a part of GE Healthcare) was grown in YP medium (1% yeast extract, 2% peptone; both from Fisher Scientific; #BP1422-2 and #BP1420-2, respectively) initially containing 0.2% or 2% glucose (#D16-10; Fisher Scientific) as carbon source. Cells were cultured at 30°C with rotational shaking at 200 rpm in Erlenmeyer flasks at a ″flask volume/medium volume″ ratio of 5:1.

3.2.2 A plating assay for the analysis of chronological lifespan

Cells were grown in YEPD (0.2% glucose or 2% glucose, as specified in the text) medium at 30°C with rotational shaking at 200 rpm in Erlenmeyer flasks at a flask volume/medium volume ratio of 5:1. A sample of cells was removed from each culture at various time points. A fraction of the cell sample was diluted to determine the total number of cells per ml of culture using a hemacytometer. 10 μl of serial dilutions (1:10 to $1:10^3$) of cells were applied to the hemacytometer, where each large square is calibrated to hold 0.1 μl. The number of cells in 4 large squares was then counted and an average was taken to ensure greater accuracy. The concentration of cells was

calculated as follows: number of cells per large square x dilution factor x 10 x 1,000 = total number of cells per ml of culture. A second fraction of the cell sample was diluted and serial dilutions ($1:10^2$ to $1:10^5$) of cells were plated onto YEPD (2% glucose) plates in triplicate to count the number of viable cells per ml of each culture. 100 µl of diluted culture was plated onto each plate. After a 48-h incubation at 30°C, the number of colonies per plate was counted. The number of colony forming units (CFU) equals to the number of viable cells in a sample. Therefore, the number of viable cells was calculated as follows: number of colonies x dilution factor x 10 = number of viable cells per ml. For each culture assayed, % viability of the cells was calculated as follows: number of viable cells per ml / total number of cells per ml x 100%. The % viability of cells in mid-logarithmic phase was set at 100% viability for that culture. The life span curves for wild-type and some of the mutant strains were also validated using a LIVE/DEAD yeast viability kit (Invitrogen) following the manufacturer's instructions for stationary-phase cultures.

3.2.3 Separation of Q and NQ cells by centrifugation in Percoll density gradient

1 ml of 1.5 M NaCl (#S7653; Sigma) was placed into a 50-ml conical polypropylene centrifuge tube (#055398; Fisher Scientific), and 8 ml of the Percoll solution (#P1644; Sigma) was added to this tube. The NaCl and Percoll solutions were then mixed by pipetting. To form two Percoll density gradients, 4 ml of the NaCl/Percoll mixture was put into each of the two polyallomer tubes for an MLS-50 rotor for an Optima MAX ultracentrifuge (all from Beckman Coulter, Inc.). The tubes were centrifuged at 25,000 × g (16,000 rpm) for 15 min at 4°C in an Optima MAX ultracentrifuge. A sample of yeast cells was taken from a culture at a certain time-point. A fraction of the sample was diluted to determine the total number of cells per ml of culture using a hemacytometer (#0267110; Fisher Scientific). For each Percoll density gradient, 1×10^9 yeast cells were placed into a 15-ml conical polypropylene centrifuge tube (#0553912; Fisher Scientific) and then pelleted by centrifugation at 5,000 rpm for 7 min at room temperature in an IEC Centra CL2 clinical centrifuge (Thermo Electron Corporation). Pelleted cells were resuspended in 500 µl of 50 mM Tris/HCl buffer (pH 7.5), overlaid onto the preformed Percoll gradient and centrifuged at 2,300 × g (5,000 rpm) for 30 min at 25oC in an Optima MAX ultracentrifuge. The upper and lower fractions of cells were collected with a pipette, Percoll was removed by washing cells twice with 50 mM Tris/HCl buffer (pH 7.5) and cells were resuspended in 50 mM Tris/HCl buffer (pH 7.5) for subsequent assays.

3.2.4 Reproductive (colony forming) capability assay for Q and NQ cells separated by centrifugation in Percoll density gradient

An aliquot of the upper or lower fraction of cells recovered from the Percoll gradient and washed twice with 50 mM Tris/HCl buffer (pH 7.5) was diluted to determine the total number of cells per fraction using a hemacytometer (#0267110; Fisher Scientific). Serial dilutions ($1:10^2$ to $1:10^5$) of cells were also plated onto YEPD (1% yeast extract, 2% peptone, 2% glucose) plates in duplicate to count the number of viable cells per ml of each cell fraction. 100 µl of diluted culture was plated onto each plate. After 48-h incubation at 30°C, the number of colonies per plate was counted. The number of colony forming units (CFU) equals to the number of reproductively capable cells in a sample. Therefore, the number of reproductively capable cells was calculated as follows: number of CFU × dilution factor × 10 = number of reproductively capable cells per ml. For each cell fraction assayed, % reproductive capability of the cells was calculated as follows: number of CFU per ml/total number of cells per ml × 100%.

3.2.5 Synchronous reentry into mitosis assay for Q and NQ cells separated by centrifugation in Percoll density gradient

5×10^6 cells recovered in the upper or lower fraction of the Percoll gradient and washed twice with 50 mM Tris/HCl buffer (pH 7.5) were harvested by centrifugation for 1 min at 21,000 × g at room temperature. Pelleted cells were washed twice with water and then inoculated into 50 ml of YP medium (1% yeast extract, 2% peptone; both from Fisher Scientific; #BP1422-2 and #BP1420-2, respectively) initially containing 0.2% or 2% glucose (#D16-10; Fisher Scientific) as carbon source. Cells were cultured for 4 h at 30°C with rotational shaking at 200 rpm in Erlenmeyer flasks at a "flask volume/medium volume" ratio of 5:1. A sample of cells was taken from a culture at a certain time-point and examined microscopically for the percentage of cells with new buds. At least 500 cells were examined per time point, and the budding percentage was calculated as follows: (number of cells with new buds per ml/total number of cells per ml) × 100%.

3.2.6 Measurement of trehalose and glycogen concentrations

2×10^9 cells were harvested by centrifugation for 1 min at 16,000 × g at 4°C. The cell pellet was washed three times in ice-cold PBS (20 mM KH_2PO_4/KOH (pH 7.5) and 150 mM NaCl) and

then resuspended in 200 µl of ice-cold SHE solution (50 mM NaOH and 1 mM EDTA). 800 µl of ice-cold SHE solution were added to the cell suspension. The resulting alkali extract was incubated at 60°C for 30 min to destroy endogenous enzyme activities and pyridine nucleotides. The extract was neutralized by adding 500 µl of THA solution (100 mM Tris/HCl (pH 8.1) and 50 mM HCl). The extract was then divided into 150 µl aliquots, quickly frozen in liquid nitrogen and stored at -80°C prior to use.

To measure trehalose concentration, 50 µl of alkali extract were added to 150 µl of trehalose reagent (25 mM KH_2PO_4/KOH (pH 7.5) and 0.02% BSA) with or without 15 mU trehalase. The mixture was incubated for 60 min at 37°C. 800 µl of glucose reagent (100 mM Tris/HCl (pH 8.1), 2 mM $MgCl_2$, 1 mM DTT, 1 mM ATP, 0.2 mM $NADP^+$, and mixture of hexokinase (7 U) and glucose-6-phosphate dehydrogenase (8 U)) were added, and the mixture was incubated for 30 min at 25°C. The NADPH generated from NADP+ was measured fluorimetrically (excitation at 365 nm, emission monitored at 460 nm).

To measure glycogen concentration, 50 µl of alkali extract were added to 500 µl of glycogen reagent (50 mM sodium acetate (pH 4.6) and 0.02% BSA; with and without 5 µg/ml amyloglucosidase 14 U/mg). The mixture was incubated for 30 min at 25°C. 500 µl of glucose reagent (100 mM Tris/HCl (pH 8.1), 2 mM $MgCl_2$, 1 mM DTT, 1 mM ATP, 0.2 mM $NADP^+$, and mixture of hexokinase (7 U) and glucose-6-phosphate dehydrogenase (8 U)) were added, and the mixture was incubated for 30 min at 25°C. The NADPH generated from NADP+ was measured fluorimetrically (excitation at 365 nm, emission monitored at 460 nm).

3.2.7 Lipid extraction from yeast cells [191]

Yeast cells were harvested by centrifugation in a Centra CL2 clinical centrifuge at 3,000 × g for 5 min at room temperature. The cell pellet was resuspended in ice-cold 155 mM ammonium bicarbonate (pH 8.0), and the cells were subjected to centrifugation at 16,000 × g for 1 min at 4°C. The cell pellet was stored at -80°C until lipid extraction. For lipid extraction, the pelleted cells kept at -80°C were thawed on ice before being resuspended in 1 ml of ice-cold nanopure water. The volume that contained 5×10^7 cells was transferred to a 15-ml high-strength glass screw top centrifuge tube with a Teflon lined cap (#0556912; Fisher Scientific). The volume of each sample was topped off to 1 ml with ice-cold nanopure water. To each tube the following was added: 20 µl of the internal standard mix prepared in Chromasolv HPLC (>99.9%) chloroform (Sigma-Aldrich)

(Table 3.1), 800 µl of 425-600 µM acid-washed glass beads to break open the cells (#G8772; Sigma-Aldrich) and 3 ml of a Chromasolv HPLC (>99.9%) chloroform-methanol mixture (both from Sigma-Aldrich) at a 17:1 ratio. The samples were then vortexed vigorously for 2 h at 4^{O}C and subjected to centrifugation in a Centra CL2 clinical centrifuge at 3,000 × g for 5 min at room temperature; this centrifugation allowed to separate the upper aqueous phase from the lower organic phase, which contained nonpolar lipids TAG, PC, PE and PG. The lower organic phase was then transferred to another 15-ml high-strength glass screw top centrifuge tube using a glass Pasteur pipette with careful attention not to disrupt the glass beads or upper aqueous phase. 1.5 ml of chloroform-methanol (2:1) solution was added to the remaining upper aqueous phase to allow the separation of polar lipids PA, PS, PI and CL. The samples were again vortexed vigorously at 4^{o}C for 1 h. The initial separated organic band was kept at 4^{o}C for the duration of the second vortexing. At the end of 1 h, the samples were again centrifuged for 5 min at 3,000 × rpm at room temperature; the lower organic phase was then separated and added to the corresponding initial organic phase with a glass Pasteur pipette. With both lower organic phases combined, the solvent was evaporated off by nitrogen gas flow. Once all solvent was evaporated, the remaining lipid film was dissolved in 100 µl of chloroform-methanol (1:2) and immediately transferred into 2-ml glass vials with Teflon screw tops to avoid evaporation until samples were analyzed by mass spectrometry. Samples were then stored at -80^{o}C and ran on the LTQ Orbitrap Mass Spectrometer within one week of the extraction.

Table 3.1. Internal standard mix composition (modified from [191])

Detection mode	Class of lipid standard	Lipid chain composition (number carbons: number double bonds on fatty acid chain)	Exact mass molecular weight (g/mol)	M/Z (mass/ion charge)	Concentration in mix (mg/µL)
Negative	CL	14:0 / 14:0 / 14:0 /14:0	1274.9000	619.4157	0.10
	FFA	19:0	298.2872	297.2711	0.02
	PA	14:0 / 14:0	614.3920	591.4026	0.10
	PE	14:0 / 14:0	635.4526	634.4448	0.10
	PG	14:0 / 14:0	688.4290	665.4394	0.10
	PS	14:0 / 14:0	701.4240	678.4271	0.02
Positive	TAG	13:0 / 13:0 / 13:0	680.5955	698.6299	0.10
	PC	13:0 / 13:0	649.4683	650.4761	0.10

Internal standards CL, PA, PE, PG, PS and PC were all from Avanti Polar Lipid, Alabaster, AL, USA. TAG internal standard originates from Larodan, Malmo, Sweden.

3.2.8 Lipid identification and quantitation using mass spectrometry

Samples were diluted (1:1) with 1:2 chloroform-methanol supplemented with 0.1% ammonium hydroxide for improved ionization efficiency. Samples were injected one at a time using a Thermo Orbitrap Velos Mass Spectrometer equipped with HESI-II ion source (Thermo Scientific) at a flow rate of 5 µl/ min. The instrument settings for the Orbitrap used the optimized settings, as described in reference 191 (Table 3.2).

Table 3.2. Thermo Orbitrap Velos mass spectrometer's tune file instrument settings (from [191])

Instrument polarity	Positive	Negative
Source voltage (kV)	3.9	4
Capillary temperature (^{O}C)	275	275
Sheath gas flow	5	5
Aux gas flow	1	1
FT-MS injection time (ms)	100	500
FT-MS microscans	3	1

Data were acquired according to the Instrument Method for data-dependent acquisition for 5 min in both positive and negative modes by the FT-MS analyzer at a resolution of 100,000 for both MS and MS/MS data (Table 3.3).

Table 3.3. Instrument method for data-dependent acquisition (from [191])

Acquisition time	5 min (with a 0.25-min delay)	
Instrument polarity	Positive	Negative
MS (Segment I)		
Analyzer	FTMS	FTMS
Mass range	Normal	Normal
Resolution	100,000	100,000
Data type	Centroid	Centroid
Scan range	400-1,200	400-1,200
Data-dependent MS/MS (segments 2-10)		
Analyzer	FTMS	FTMS
Resolution	30,000	30,000
Data type	Centroid	Centroid
Activation	HCD	HCD
Activation time (ms)	0.1	0.1
Isolation width	1	1
Collision energy	35	65
Mass range	Normal	Normal
Data type	Centroid	Centroid
Scan range	-	-

Between each sample, the line was flushed with chloroform-methanol (1:2) mixture until the ion detection steadied and returned into the baseline level. Diluted internal standard mix was injected multiple times throughout the acquisition to ensure no sensitivity loss throughout the run.

Once all data was acquired, raw files were converted to open format mzXML using ProteoWizard MSConvert software (http://proteowizard.sourceforge.net/), the file format used by the Lipid Identification Software LipidXplorer (https://wiki.mpi-cbg.de/lipidx/Main_Page). Data files were then imported into this software using settings described in Table 3.4; all lipids in the PA, PC, PE, PI, PS, CL and TAG lipid classes were identified with the help of Molecular Fragmentation Query Language (MFQL) files. MFQL files were obtained from the LipidXplorer page listed above and aided in the identification of lipids by their m/z ratio as well as their fragmentation patterns.

LipidXplorer's output data was then opened under a Microsoft Excel file and all detected lipids were quantified by comparison with the intensity of the corresponding lipid class' internal standard's known concentration in the sample. Each quantified lipid had a corresponding internal standard from the same lipid class, allowing the calculation of molar percentage of each identified lipid species and, therefore, of each lipid class.

Table 3.4. Lipid identification by LipidXplorer import settings for data acquired under positive and negative mode (from [191])

	Positive mode	Negative mode
Selection Window (Da)	1	1
Time range (sec.)	0-350	0-350
Calibration masses		
MS	0	0
MS/MS	0	0
m/z range (m/z-m/z)		
MS	140-1,200	100-400
MS/MS	200-1,400	200-1200
Resolution (FMHW)		
MS	100,000	100,000
MS/MS	30,000	30,000
Tolerance (ppm)		
MS	10	10
MS/MS	10	10
Resolution Gradient (res/(m/z))		
MS	0	-55
MS/MS	0	0
Minimum Occupation (0<1)		
MS	0.5	0.5
MS/MS	0	0
MS1 offset (Da)	0	0

3.2.9 Oxygen consumption assay (cellular respiration measurement)

A sample of cells was taken from a culture at a certain time-point. Cells were pelleted by centrifugation and resuspended in 1 ml of fresh YP medium containing 0.05% glucose. Oxygen uptake by cells was measured continuously in a 2-ml stirred chamber using a custom-designed biological oxygen monitor (Science Technical Center of Concordia University) equipped with a Clark-type oxygen electrode.

3.2.10 Mitochondrial membrane potential measurement

The mitochondrial membrane potential ($\Delta\Psi$) was measured in live yeast by fluorescence microscopy of Rhodamine 123 (R123) staining. For R123 staining, 5×10^6 cells were harvested by centrifugation for 1 min at 21,000 × g at room temperature and then resuspended in 100 µl of 50 mM sodium citrate buffer (pH 5.0) containing 2% glucose. R123 (Invitrogen) was added to a final concentration of 10 µM. Following incubation in the dark for 30 min at room temperature, the cells were washed twice in 50 mM sodium citrate buffer (pH 5.0) containing 2% glucose and then analyzed by fluorescence microscopy. Images were collected with a Zeiss Axioplan fluorescence microscope (Zeiss) mounted with a SPOT Insight 2-megapixel color mosaic digital camera (Spot Diagnostic Instruments). For evaluating the percentage R123-positive cells, the UTHSCSA Image Tool (Version 3.0) software was used to calculate both the total number of cells and the number of stained cells. Fluorescence of individual R123-positive cells in arbitrary units was determined by using the UTHSCSA Image Tool software (Version 3.0). In each of 3 independent experiments, the value of median fluorescence was calculated by analyzing at least 800-1000 cells that were collected at each time-point. The median fluorescence values were plotted as a function of the number of days cells were cultured.

3.2.11 Monitoring the formation of ROS

ROS production in wild-type and mutant cells grown in YEPD (0.2% glucose) with LCA was tested microscopically by incubation with Dihydrorhodamine 123 (DHR). In the cell, this non-fluorescent compound can be oxidized to the fluorescent chromophore rhodamine 123 by ROS. Cells were also probed with a fluorescent counterstain Calcofluor White M2R (CW), which stains the yeast cell walls fluorescent blue. CW was added to each sample to label all cells for their proper

visualization. DHR was stored in the dark at –20°C as 50 µl aliquots of a 1 mg/ml solution in ethanol. CW was stored in the dark at –20°C as the 5-mM stock solution in anhydrous DMSO (dimethyl sulfoxide). The concurrent staining of cells with DHR and CW was carried out as follows. The required amounts of the 50 µl DHR aliquots (1 mg/ml) and of the 5-mM stock solution of CW were taken out of the freezer and warmed to room temperature. The solutions of DHR and CW were then centrifuged at 21,000 × g for 5 min to clear them of any aggregates of fluorophores. For cell cultures with a titer of ~ 10^7 cells/ml, 100 µl was taken out of the culture to be treated. If the cell titer was lower, proportionally larger volumes were used. 6 µl of the 1 mg/ml DHR and 1 µl of the 5-mM CW solutions were added to each 100 µl aliquot of culture. After a 2-h incubation in the dark at room temperature, the samples were centrifuged at 21,000 × g for 5 min. Pellets were resuspended in 10 µl of PBS buffer (20 mM KH_2PO_4/KOH, pH 7.5, and 150 mM NaCl). Each sample was then supplemented with 5 µl of mounting medium, added to a microscope slide, covered with a coverslip, and sealed using nail polish. Once the slides were prepared, they were visualized under the Zeiss Axioplan fluorescence microscope mounted with a SPOT Insight 2-megapixel color mosaic digital camera. Several pictures of the cells on each slide were taken, with two pictures taken of each frame. One of the two pictures was of the cells seen through a rhodamine filter to detect cells dyed with DHR. The second picture was of the cells seen through a DAPI filter to visualize CW, and therefore all the cells present in the frame. For evaluating the percentage of DHR-positive cells, the UTHSCSA Image Tool (Version 3.0) software was used to calculate both the total number of cells and the number of stained cells. Fluorescence of individual DHR-positive cells in arbitrary units was determined by using the UTHSCSA Image Tool software (Version 3.0). In each of 3-5 independent experiments, the value of median fluorescence was calculated by analyzing at least 800-1000 cells that were collected at each time point. The median fluorescence values were plotted as a function of the number of days cells were cultured.

3.2.12 Measurement of oxidative damage to cellular proteins

10^7 yeast cells were harvested by centrifugation for 1 min at 21,000 × g at room temperature. The cell pellet was resuspended in 1 ml of ice-cold 50 mM KH_2PO_4/KOH buffer (pH 7.5) + 1 mM EDTA. The cells were sonicated on ice, harvested by centrifugation for 5 min at 21,000 × g at 4°C and then resuspended in 200 µl of ice-cold 50 mM KH_2PO_4/KOH buffer (pH

7.5) + 1 mM EDTA. The Protein Carbonyl Assay Kit assay kit (#10005020; Cayman Chemical) was used to measure protein carbonylation (i.e. protein oxidative damage) as the amount of protein-hydrozone produced in the DNPH (2,4-dinitrophenylhydrazine) reaction at an absorbance of 360 nm.

3.2.13 Measurement of oxidative damage to cellular membrane lipids

10^7 yeast cells were harvested by centrifugation for 3 min at 16,000 × g at room temperature. The cell pellet was washed with ice-cold ABC buffer (155 mM ammonium bicarbonate, pH 8.0) by centrifugation for 3 min at 16,000 × g at 4°C, and then resuspended in 1 ml of ice-cold ABC buffer. 200 µl of glass beads were added, and the sample was vortexed for 5 min. 1 ml of ice-cold nanopore water was added, and the sample was transferred to a 15-ml glass centrifuge tube. 3 ml of chloroform/methanol (17:1) mixture was added, and the sample was vortexed at 4°C for 2 h. The sample was subjected to centrifugation at 3000 × g for 5 min at room temperature to form two phases. The lower organic phase was transferred to a new 15-ml glass tube. The solvent was evaporated off under nitrogen flow or in a vacuum evaporator. The lipid film was dissolved in 100 µl of methanol/chloroform (2:1) mixture. The PeroXOquant Quantitative Peroxide Assay Kit (#23285; Thermo Scientific Pierce) was used to measure lipid hydroperoxides as the Fe^{3+} complexes with the xylenol orange dye at an absorbance of 595 nm.

3.2.14 Measurement of the frequency of nuclear mutations

The frequency of spontaneous point mutations in the *CAN1* gene of nuclear DNA was evaluated by measuring the frequency of mutations that caused resistance to the antibiotic canavanine. A sample of cells was removed from each culture at various time-points. Cells were plated in triplicate onto YNB (0.67% Yeast Nitrogen Base without amino acids [#DF0919153; Fisher Scientific]) plates containing 2% glucose and supplemented with L-canavanine (50 mg/l), histidine, leucine, lysine and uracil (#C1625, #H8125, #L8912, #L5751 and #U0750, respectively; all from Sigma). In addition, serial dilutions of each sample were plated in triplicate onto YP plates containing 2% glucose for measuring the number of viable cells. The number of CFU was counted after 4 d of incubation at 30°C. For each culture, the frequency of mutations that caused resistance to canavanine was calculated as follows: number of CFU per ml on YNB plates containing 2%

glucose, L-canavanine (50 mg/l), histidine, leucine, lysine and uracil/number of CFU per ml on YP plates containing 2% glucose.

3.2.15 Measurement of the frequency of mitochondrial mutations affecting mitochondrial components

The frequency of spontaneous single-gene (*mit*$^-$ and *syn*$^-$) and deletion (*rho*$^-$ and *rho*^{o}) mutations in mtDNA affecting essential mitochondrial components was evaluated by measuring the fraction of respiratory-competent (*rho*$^+$) yeast cells remaining in their aging population. *rho*$^+$ cells maintained intact their mtDNA and their nuclear genes encoding essential mitochondrial components. Therefore, *rho*$^+$ cells could grow on glycerol, a non-fermentable carbon source. In contrast, mutant cells deficient in mitochondrial respiration were unable to grow on glycerol. These mutant cells carried mutations in mtDNA (including single-gene *mit*$^-$ and *syn*$^-$ mutations or large deletions *rho*$^-$) or completely lacked this DNA (*rho*^{o} mutants). Serial dilutions of cell samples removed from different phases of growth were plated in triplicate onto YP plates containing either 2% glucose or 3% glycerol (#BP229-4; Fisher Scientific) as carbon source. Plates were incubated at 30ºC. The number of CFU on YP plates containing 2% glucose was counted after 2 d of incubation, whereas the number of CFU on YP plates containing 3% glycerol was counted after 6 d of incubation. For each culture, the percentage of respiratory-deficient (*mit*$^-$, *syn*$^-$, *rho*$^-$, *rho*^{o} and *pet*$^-$) cells was calculated as follows: 100 - [(number of CFU per ml on YP plates containing 3% glycerol/number of CFU per ml on YP plates containing 2% glucose) × 100].

The frequency of spontaneous point mutations in the *rib2* and *rib3* loci of mtDNA was evaluated by measuring the frequency of mtDNA mutations that caused resistance to the antibiotic erythromycin. These mutations impair only mtDNA. A sample of cells was removed from each culture at various time-points. Cells were plated in triplicate onto YP plates containing 3% glycerol and erythromycin (1 mg/ml) [#227330050; Acros Organics]. In addition, serial dilutions of each sample were plated in triplicate onto YP plates containing 3% glycerol as carbon source for measuring the number of respiratory-competent (*rho*$^+$) cells. The number of CFU was counted after 6 d of incubation at 30ºC. For each culture, the frequency of mutations that caused resistance to erythromycin was calculated as follows: number of CFU per ml on YP plates containing 3% glycerol and erythromycin/number of CFU per ml on YP plates containing 3% glycerol.

3.2.16 Plating assays for the analysis of resistance to oxidative and thermal stresses

For the analysis of hydrogen peroxide (oxidative stress) resistance, serial dilutions ($1:10^0$ to $1:10^5$) of cells removed from each culture at various time-points were spotted onto two sets of plates. One set of plates contained YP medium with 2% glucose alone, whereas the other set contained YP medium with 2% glucose supplemented with 5 mM hydrogen peroxide. Pictures were taken after a 3-day incubation at 30°C.

For the analysis of thermal stress resistance, serial dilutions ($1:10^0$ to $1:10^5$) of wild-type and mutant cells removed from each culture at various time-points were spotted onto two sets of plates containing YP medium with 2% glucose. One set of plates was incubated at 30°C. The other set of plates was initially incubated at 55°C for 30 min, and was then transferred to 30°C. Pictures were taken after a 3-day incubation at 30°C.

3.2.17 Cell viability assay for monitoring the susceptibility of yeast to a mode of cell death induced by hydrogen peroxide

A sample of cells was taken from a culture on a certain day of culturing. A fraction of the sample was diluted to determine the total number of cells using a hemocytometer. 8×10^7 cells were harvested by centrifugation for 1 min at 21,000 × g at room temperature and resuspended in 8 ml of YP medium containing 0.2% glucose as carbon source. Each cell suspension was divided into 8 equal aliquots. Three pairs of aliquots were supplemented with hydrogen peroxide (#H325-500; Fisher Scientific) to the final concentration of 0.5 mM, 1.5 mM or 2.5 mM for each pair. One pair of aliquots remained untreated. All aliquots were then incubated for 2 h at 30°C on a Labquake rotator (#400110; Thermolyne/Barnstead International) set for 360° rotation. Serial dilutions of cells were plated in duplicate onto plates containing YP medium with 2% glucose as carbon source. After 2 d of incubation at 30°C, the number of CFU per plate was counted. The number of CFU was defined as the number of viable cells in a sample. For each aliquot of cells exposed to hydrogen peroxide, the % of viable cells was calculated as follows: (number of viable cells per ml in the aliquot exposed to hydrogen peroxide/number of viable cells per ml in the control aliquot that was not exposed to hydrogen peroxide) × 100.

3.2.18 Cell viability assay for monitoring the susceptibility of yeast to a mode of cell death induced by palmitoleic acid (POA)

A sample of cells was taken from a culture on a certain day of culturing. A fraction of the sample was diluted to determine the total number of cells using a hemocytometer. 8×10^7 cells were harvested by centrifugation for 1 min at 21,000 × g at room temperature and resuspended in 8 ml of YP medium containing 0.2% glucose as carbon source. Each cell suspension was divided into 8 equal aliquots. Three pairs of aliquots were supplemented with POA (#P9417; Sigma) from a 50-mM stock solution (in 10% chloroform, 45% hexane and 45% ethanol; #650498, #248878 and #34852, respectively; all from Sigma). The final concentration of POA was 0.05 mM, 0.1 mM or 0.15 mM for each pair of aliquots; in all these aliquots, the final concentrations of chloroform, hexane and ethanol were 0.03%, 0.135% and 0.135%, respectively. One pair of aliquots was supplemented only with chloroform, hexane and ethanol added to the final concentrations of 0.03%, 0.135% and 0.135%, respectively. All aliquots were then incubated for 2 h at 30ºC on a Labquake rotator (#400110; Thermolyne/Barnstead International) set for 360º rotation. Serial dilutions of cells were plated in duplicate onto plates containing YP medium with 2% glucose as carbon source. After 2 d of incubation at 30ºC, the number of colony forming units (CFU) per plate was counted. The number of CFU was defined as the number of viable cells in a sample. For each aliquot of cells exposed to POA, the % of viable cells was calculated as follows: (number of viable cells per ml in the aliquot exposed to POA/number of viable cells per ml in the control aliquot that was not exposed to POA) × 100.

3.2.19 Statistical analysis

Statistical analysis was performed using Microsoft Excel's (2010) Analysis ToolPak - VBA. All data on cell survival are presented as mean ± SEM. The *p* values for comparing the means of two groups using an unpaired two-tailed *t* test were calculated with the help of the GraphPad Prism 7 statistics software. The logrank test for comparing each pair of survival curves was performed with GraphPad Prism 7. Two survival curves were considered statistically different if the *p* value was less than 0.05.

3.3 Results

3.3.1 CR accelerates an age-related accumulation of low-density cells in chronologically aging yeast cultures

Chronologically aging yeast cultured under CR conditions in the nutrient-rich YP medium initially containing 0.2% glucose lived significantly longer than yeast undergoing chronological aging under non-CR conditions in YP medium initially supplemented with 2% glucose (Figure 3.1A). Even before glucose is depleted from the medium at the diauxic shift, a yeast culture undergoing chronological aging under non-CR conditions is known to differentiate into cell populations with different buoyant densities [212, 213]. Each of these cell populations can be purified to homogeneity by centrifugation in Percoll density gradient [214].

Using centrifugation in Percoll density gradient for separating cell populations exhibiting different densities, I investigated how CR influences the differentiation of a chronologically aging yeast culture into these distinct cell populations. Samples of cells cultured in YP medium initially containing 0.2% glucose (CR conditions) or 2% glucose (non-CR conditions) were recovered at different time-points following glucose exhaustion from the medium, which occurs 16 or 22 h after cell inoculation, respectively (Figure 3.1B). I found that chronologically aging cultures of CR and non-CR yeast 1) contain both low-density (LD) and high-density (HD) cell populations during logarithmic (L), diauxic (D), post-diauxic (PD) and stationary (ST) growth phases, i.e. through the entire chronological lifespan; and 2) exhibit an age-related increase in the percentage of LD cells (Figures 3.1C and 3.1D). I also noticed that the percentage of LD cells in CR yeast cultures significantly exceeds that in non-CR yeast cultures during any of the four growth phases, i.e. at any stage of the chronological aging process (Figures 3.1C and 3.1D). Moreover, I showed that the percentage of LD cells in CR yeast cultures reaches a plateau on day 5 of culturing (in PD growth phase), whereas the percentage of LD cells in non-CR yeast cultures attains a steady-state level only on day 10 of culturing (in ST growth phase) (Figures 3.1C and 3.1D).

Collectively, these findings indicate that CR accelerates an age-related accumulation of LD cell population in chronologically aging yeast cultures.

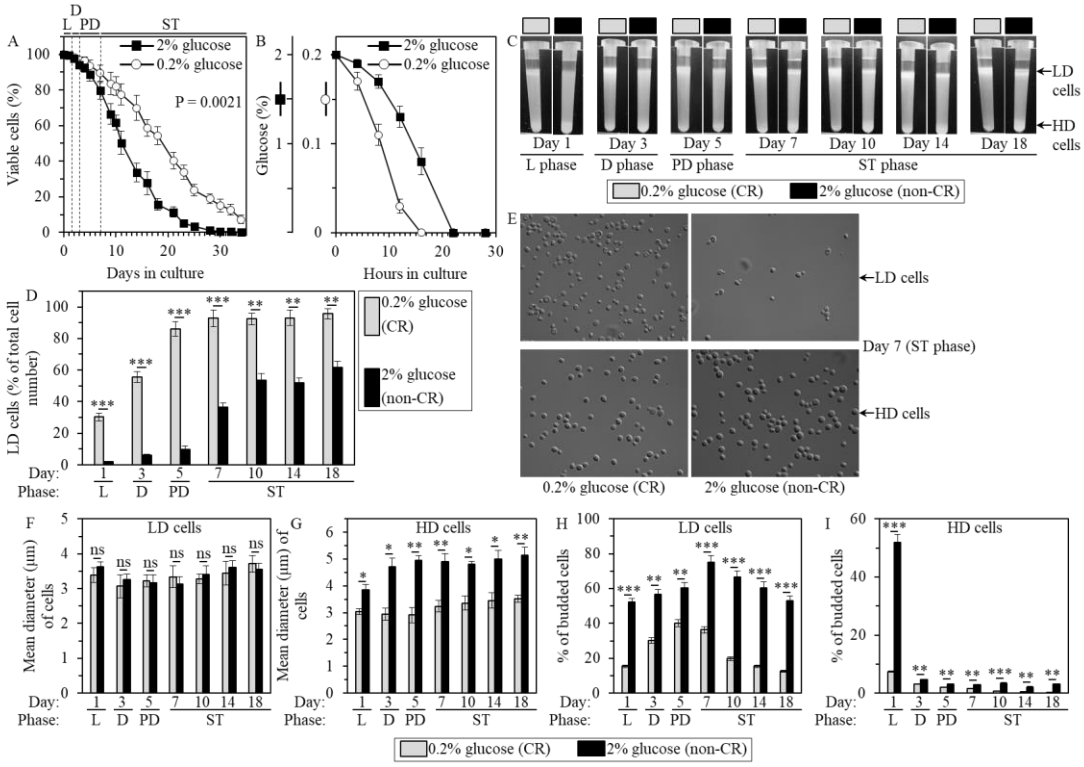

Figure 3.1. Caloric restriction (CR) accelerates an age-related accumulation of low-density (LD) cells, decreases the size of high-density (HD) cells, and lowers the abundance of budded cells in LD and HD populations of chronologically aging yeast cultures. (**A**) Survival of chronologically aging wild-type (WT) yeast cultured in the nutrient-rich YP medium initially containing 0.2% glucose (CR conditions) or 2% glucose (non-CR conditions). The logrank test for comparing each pair of survival curves was performed as described in Materials and Methods. Two survival curves were considered statistically different if the P value was less than 0.05. (**B**) Kinetics of glucose consumption for WT yeast cultured in YP medium initially containing 0.2% glucose (CR conditions) or 2% glucose (non-CR conditions). (**C** to **I**) Samples of WT yeast cultured in YP medium initially containing 0.2% glucose (CR conditions) or 2% glucose (non-CR conditions) were recovered from logarithmic (L), diauxic (D), post-diauxic (PD) or stationary (ST) growth phase and subjected to centrifugation in Percoll density gradient as described in Materials and Methods. Percoll density gradients (**C**), the percentage of LD cells (**D**), differential interference contrast micrographs of LD and HD cells recovered from ST growth phase on day 7 (**E**), mean diameters of LD (**F**) or HD (**G**) cells, and the percentages of budded cells present in LD (**H**) or HD (**I**) populations are shown. Data in **A**, **B**, **D**, **F** - **I** are presented as means ± SEM (n = 3; *P < 0.05; **P < 0.01; ***P < 0.001; ns, not significant).

3.3.2 CR alters cell size and the abundance of budded cells in LD and HD populations

I then assessed how CR influences the morphology of cells present in LD and HD populations. These cell populations were first recovered from yeast cultures of different chronological ages and then separated from each other by centrifugation in Percoll density

gradient. My differential interference contrast (DIC) microscopical examination and subsequent morphometric analysis of these LD and HD cell populations have revealed that through the entire chronological lifespan: 1) LD cells in CR cultures have sizes similar to those of LD cells in non-CR cultures (Figures 3.1E, 3.1F and 3.2); 2) HD cells in CR cultures remain significantly smaller than HD cells in non-CR cultures (Figures 3.1E, 3.1G and 3.2); and 3) although LD cells in CR and non-CR cultures contain both budded and unbudded cells, the percentage of budded LD cells in CR cultures is significantly lower than that in non-CR cultures (Figures 3.1E, 3.1H and 3.2). I also found that, except for HD cells recovered from non-CR cultures in L growth phase, most of HD cells recovered from CR and non-CR cultures were unbudded (Figures 3.1E, 3.1 and 3.2). Moreover, I showed that the percentage of budded HD cells in CR cultures is significantly lower than that in non-CR cultures (Figures 3.1E, 3.1I and 3.2).

In sum, these findings indicate that CR decreases the size of HD cells and lowers the percentage of budded cells in both LD and HD populations through the entire process of chronological aging.

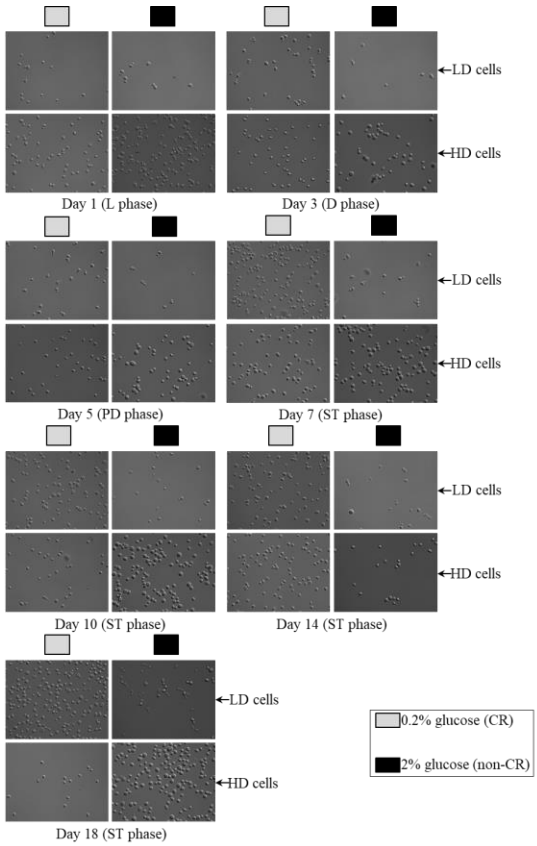

Figure 3.2. Differential interference contrast micrographs of purified LD and HD cells. Samples of wild-type yeast cultured in YP medium initially containing 0.2% glucose (CR conditions) or 2% glucose (non-CR conditions)

were recovered from logarithmic (L), diauxic (D), post-diauxic (PD) or stationary (ST) growth phase and subjected to centrifugation in Percoll density gradient to purify LD and HD cell populations.

3.3.3 CR delays an age-related decline in the reproductive proficiencies of LD and HD cell populations and in their abilities to synchronously re-enter mitosis

My observation that nearly all HD cells in CR and non-CR cultures were unbudded (except of HD cells purified from non-CR cultures in L growth phase, see Figure 3.1I) suggests a hypothesis that HD population contains predominantly Q cells. Q cells are known to be mainly unbudded [214]. Moreover, because LD population recovered from CR and non-CR cultures contained both budded and unbudded cells (Figure 3.1H), I hypothesized that LD population consists mainly of NQ cells. NQ cells are known to represent a mixture of budded and unbudded cells [214].

To test this hypothesis, I compared the following two features of LD and HD populations: 1) the reproductive competence, i.e. the ability of a yeast cell to form a colony when plated on fresh solid medium; and 2) the ability of a yeast cell population to synchronously re-enter the mitotic cell cycle if returned to growth-promoting conditions. Both these abilities are known to be characteristic of Q cells; these fundamental characteristics of Q cells distinguish them from NQ cells [215]. I recovered LD and HD cell populations from CR or non-CR yeast cultures of different chronological ages and then separated them from each other by centrifugation in Percoll density gradient.

My comparative analyses of the reproductive (colony-forming) capacities of LD and HD cells purified from differently aged CR and non-CR yeast cultures have revealed the following: 1) LD cells in CR cultures maintain reproductive (colony-forming) capacity for a long period of time in the course of chronological aging, whereas LD cells in non-CR cultures exhibit a very rapid age-related deterioration in reproductive competence (Figure 3.3A), and 2) HD cells in CR cultures sustain reproductive (colony-forming) ability through the entire process of chronological aging, whereas HD cells in non-CR cultures display an age-related gradual decline in reproductive capability (Figure 3.3B).

My comparison of the abilities of LD and HD cells purified from differently aged CR and non-CR yeast cultures to synchronously re-enter the mitotic cell cycle after cell transfer into fresh medium and incubation for 1 to 4 h has revealed the following: 1) LD cells in CR cultures remain

Q cells (i.e. maintain the ability to synchronously re-enter mitosis following cell transfer) for a long period of time in the course of chronological aging, whereas LD cells in non-CR cultures become NQ cells (i.e. senescent) soon after being formed in the process of differentiation (Figure 3.3C); and 2) HD cells in CR cultures continue to be Q cells through most of the chronological aging process, whereas HD cells in non-CR cultures progressively become NQ cells (Figure 3.3D).

Taken together, these findings provide evidence that 1) HD population contains predominantly Q cells, whereas LD population consists mainly of NQ cells; and 2) CR slows an age-related deterioration in the reproductive competences of Q and NQ cells and in their capabilities to synchronously re-enter the mitotic cell cycle when nutrients become available.

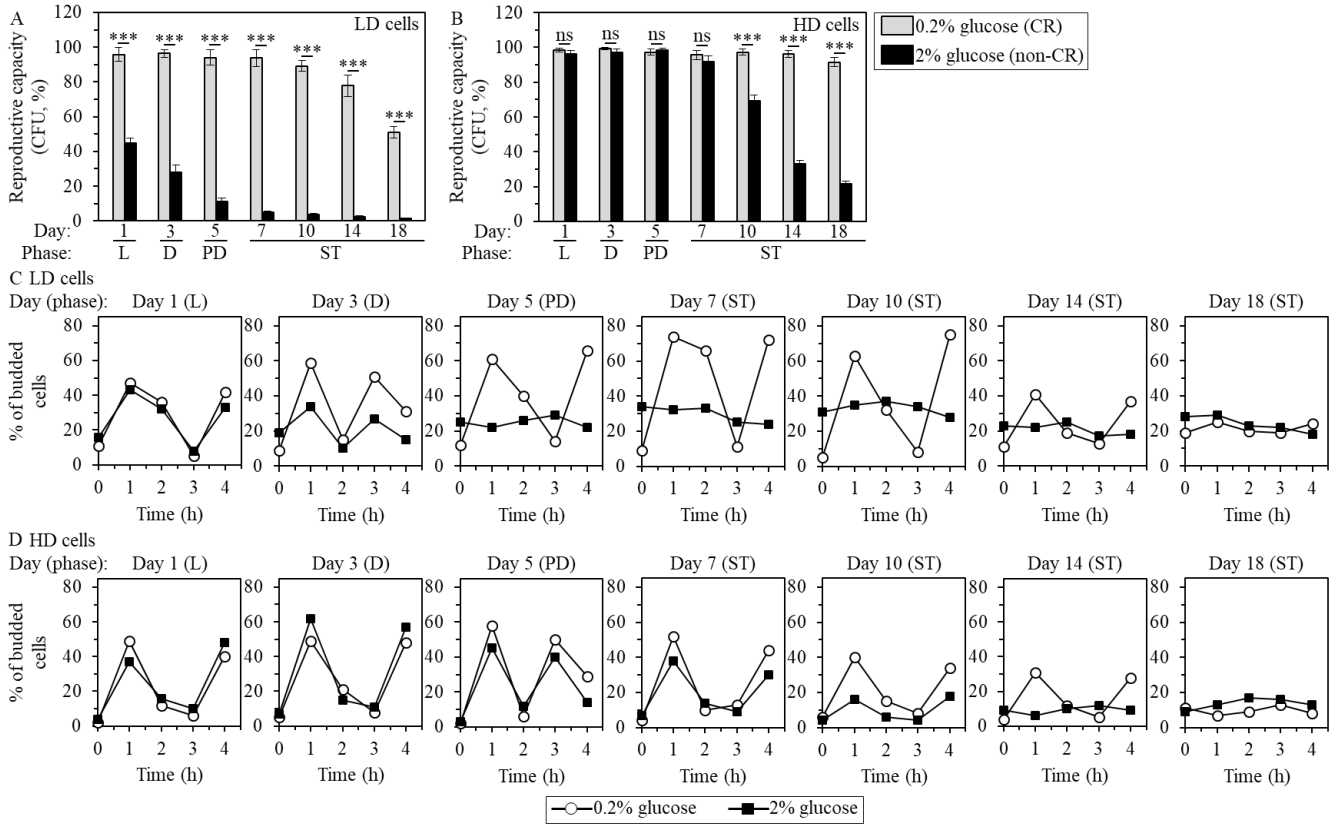

Figure 3.3. CR delays an age-related decline of the reproductive competences of LD and HD cells and of their capabilities to synchronously re-enter the mitotic cell cycle when nutrients become available. (**A** to **D**) Samples of WT yeast cultured in YP medium initially containing 0.2% glucose (CR conditions) or 2% glucose (non-CR conditions) were recovered from L, D, PD or ST growth phase and subjected to centrifugation in Percoll density gradient to purify LD and HD cell populations, as described in Materials and Methods. The reproductive (colony forming) efficiencies of LD (**A**) or HD (**B**) cells, and the efficiencies with which LD (**C**) or HD (**D**) cells can synchronously re-enter the mitotic cell cycle after cell transfer into fresh medium and incubation for 1 to 4 h are

shown. These efficiencies were measured as described in Materials and Methods. Data in **A** and **B** are presented as means ± SEM (n = 3; ***P < 0.001; ns, not significant). Data in **C** and **D** are presented as means (n = 3 - 4).

3.3.4 CR increases the abundance of daughter cells in Q and NQ populations

A culture of the budding yeast *S. cerevisiae* is known to contain first- and higher-generation daughter cells without bud scars and first- and higher-generation mother cells with one or more bud scars on the cell surface [216-218]. Each bud scar marks a division site on the surface of a mother cell and, thus, the number of bud scars accumulating on the mother cell surface is a measure of its replicative age [219-221].

I assessed the relative abundance of first- and higher-generation daughters and replicatively aged mothers present in Q and NQ cell populations. These cell populations were first recovered from CR or non-CR yeast cultures of different chronological ages and then separated from each other by centrifugation in Percoll density gradient. Bud scars were microscopically visualized by staining with Calcofluor White M2R. My comparative analysis of Q and NQ cell populations purified from differently aged CR and non-CR cultures has revealed the following: 1) CR increases the abundance of first- and higher-generation daughters and decreases the percentage of first- and higher-generation mothers present in NQ cell populations through the entire chronological lifespan (Figures 3.4A and 3.5); 2) the abundance of daughter cells decreases and the abundance of mother cells increases in NQ cell populations from non-CR cultures recovered on days 10, 14 and 18 of culturing (Figures 3.4B and 3.5); 3) the percentages of daughter and mother cells remain unchanged through the entire chronological lifespan in NQ cell populations from CR cultures (Figures 3.4C and 3.5); 4) through the entire chronological lifespan, Q cell population in CR cultures is predominantly composed of daughter cells whereas Q cell population in non-CR cultures is a mixture of daughter and mother cells (Figures 3.4D and 3.5); 5) the abundance of daughter cells decreases and the abundance of mother cells increases in the Q cell population that was purified from non-CR cultures recovered very late in chronological lifespan, namely on day 18 of culturing (Figures 3.4E and 3.5); and 6) the percentages of daughter and mother cells remain unaltered through the entire chronological lifespan in Q cell populations purified from CR cultures (Figures 3.4F and 3.5).

Collectively, these findings indicate that 1) through the entire chronological lifespan, CR rises the fraction of daughter cells in Q and NQ populations; and 2) late in chronological lifespan, CR prevents budding of daughter cells in NQ population and, to a lesser extent, in Q population.

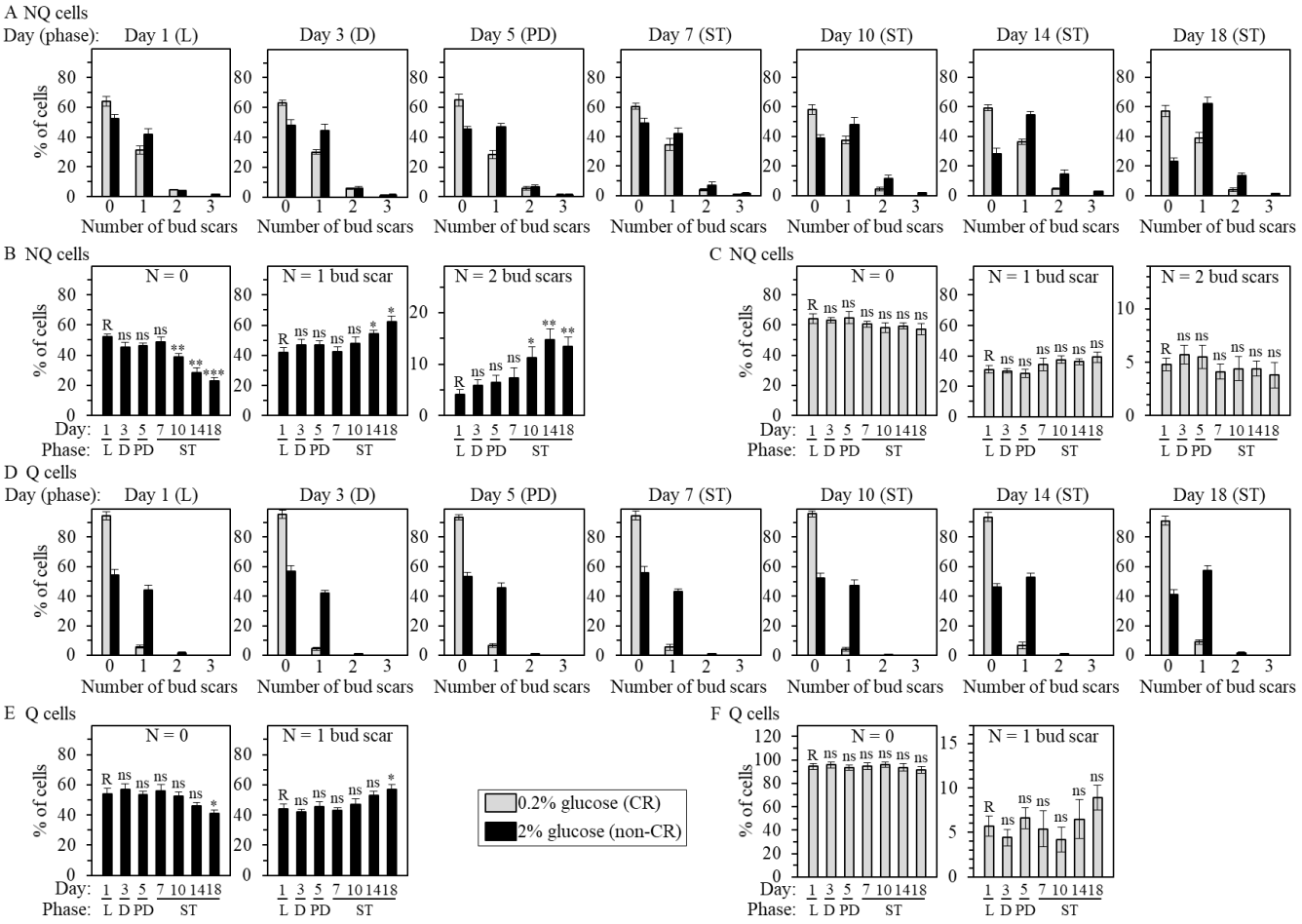

Figure 3.4. CR increases the abundance of daughters in Q and NQ cell populations through the entire chronological lifespan and prevents budding of daughters in these cell populations late in life. (**A** to **F**) Samples of WT yeast cultured in YP medium initially containing 0.2% glucose (CR conditions) or 2% glucose (non-CR conditions) were recovered from L, D, PD or ST growth phase and subjected to centrifugation in Percoll density gradient to purify Q and NQ cell populations, as described in Materials and Methods. Bud scars were microscopically visualized by staining with Calcofluor White M2R, as described in Materials and Methods. The percentages of cells with 0, 1, 2 or 3 bud scars in NQ (**A** to **C**) or Q (**D** to **F**) populations of different chronological ages are shown. Data in **B, C**, **E** and **F** are presented as means ± SEM (n = 3; *P < 0.05; **P < 0.01; ***P < 0.001; ns, not significant; R, reference). Data in **A** and **D** are presented as means (n = 3 - 5).

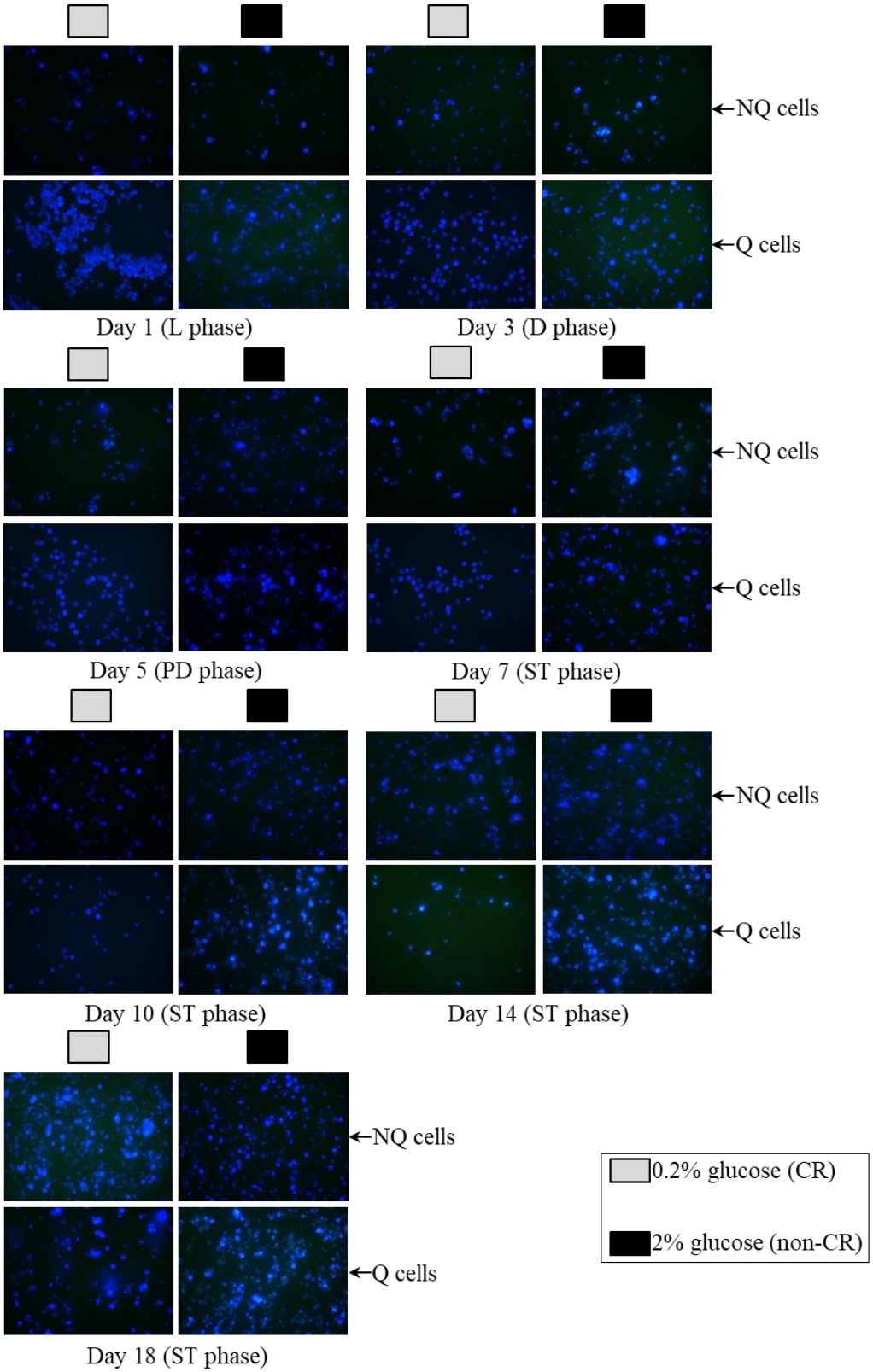

Figure 3.5. CR rises the fraction of daughter cells in Q and NQ populations and, late in chronological lifespan, prevents budding of daughter cells present in both populations. Samples of WT yeast cultured in YP medium

initially containing 0.2% glucose (CR conditions) or 2% glucose (non-CR conditions) were recovered from L, D, PD or ST growth phase and subjected to centrifugation in Percoll density gradient to purify Q and NQ cell populations, as described in Materials and Methods. Bud scars were microscopically visualized by staining with Calcofluor White M2R, as described in Materials and Methods.

3.3.5 CR increases the concentrations of glycogen and trehalose in Q and NQ cell populations

One of the metabolic hallmarks of Q cells that distinguish them from NQ cells is an accumulation of glycogen and trehalose, the two major glucose stores in yeast [214, 222]. In addition to being reserve carbohydrate, trehalose has also been implicated in protecting yeast cells and cellular proteins from oxidative and other stresses [223-226], modulating cellular proteostasis [227-229], and allowing Q cells to re-enter the mitotic cell cycle when nutrients become available [222].

I investigated how CR influences the intracellular concentrations of glycogen and trehalose in Q and NQ cell populations. These cell populations were first recovered from CR or non-CR yeast cultures of different chronological ages and then separated from each other by centrifugation in Percoll density gradient. My comparative analysis of Q and NQ cell populations purified from differently aged CR and non-CR cultures has revealed the following: 1) through most of the chronological lifespan (i.e. since day 3 of culturing), the concentrations of glycogen in NQ and Q cells from CR cultures significantly exceed those in NQ and Q cells from age-matched non-CR cultures (Figures 3.6A and 3.6B, respectively); 2) through the entire chronological lifespan, the concentrations of glycogen in Q cells from CR cultures were higher than those in NQ cells from CR cultures of the same chronological age (compare Figures 3.6A and 3.6B); 3) for the most part (i.e. since day 5 of culturing), the concentrations of trehalose in NQ and Q cells from CR cultures considerably surpass those in NQ and Q cells from age-matched non-CR cultures (Figures 3.6C and 3.6D, respectively); and 4) through the entire chronological lifespan, the concentrations of trehalose in Q cells from CR cultures exceed those in NQ cells from CR cultures of the same chronological age (compare Figures 3.6C and 3.6D).

In sum, these findings indicate that through most of the chronological aging process CR elicits significant rises in the concentrations of glycogen and trehalose in both Q and NQ cell populations.

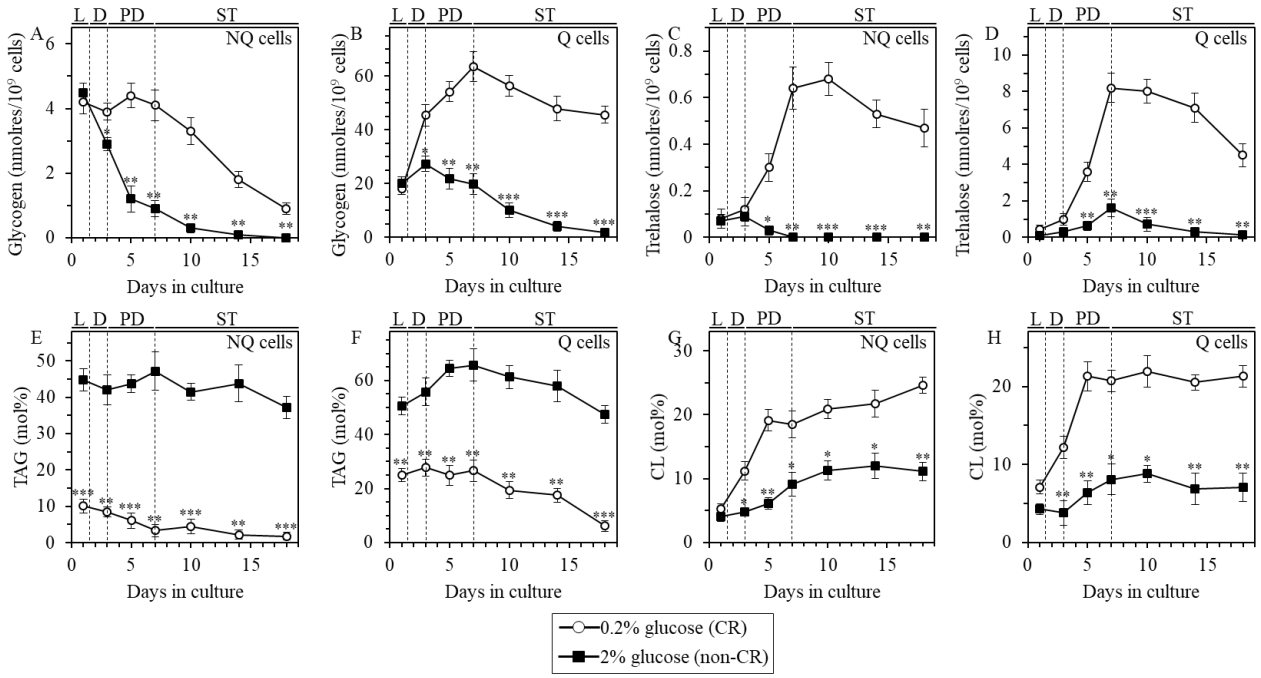

Figure 3.6. CR alters the abundance of glycogen, trehalose, triacylglycerols (TAG) and cardiolipins (CL) in Q and NQ cell populations through most of the chronological lifespan. Samples of WT yeast cultured in YP medium initially containing 0.2% glucose (CR conditions) or 2% glucose (non-CR conditions) were recovered from L, D, PD or ST growth phase and subjected to centrifugation in Percoll density gradient to purify Q and NQ cell populations, as described in Materials and Methods. The concentrations of glycogen (**A** and **B**), trehalose (**C** and **D**), TAG (**E** and **F**) and CL (**G** and **H**) were measured as described in Materials and Methods. Data are presented as means ± SEM (n = 3; *P < 0.05; **P < 0.01; ***P < 0.001).

3.3.6 CR alters the abundance of two lipid classes in Q and NQ cell populations

Recent studies have revealed that the longevity-extending effect of CR in chronologically aging yeast depends on the cellular homeostasis of two classes of lipids, namely triacylglycerols (TAG) and cardiolipins (CL) [85, 87, 230-243]. TAG are so-called neutral lipids that in yeast are synthesized in the endoplasmic reticulum and then deposited in lipid droplets to serve as the main storage molecules for maintaining energy homeostasis and supplying free fatty acids [244-247], whereas CL are signature lipids of the inner mitochondrial membrane implicated in oxidative phosphorylation and several other vital processes confined to mitochondria [248-251].

I examined the effect of CR on the abundance of TAG and CL in Q and NQ cell populations that were first recovered from CR or non-CR yeast cultures of different chronological ages and then purified by centrifugation in Percoll density gradient. My comparison of these Q and NQ cell populations has revealed the following: 1) through the entire chronological lifespan, the

concentrations of TAG in NQ and Q cells from CR cultures are significantly lower than those in NQ and Q cells from age-matched non-CR cultures (Figures 3.6E and 3.6F, respectively); 2) for the most part (i.e. since day 3 of culturing), the concentrations of CL in NQ and Q cells from CR cultures significantly exceed those in NQ and Q cells from non-CR cultures of the same chronological age (Figures 3.6G and 3.6H, respectively); 3) through the entire chronological lifespan, the concentrations of TAG in Q and NQ cells from age-matched CR and non-CR cultures are similar (compare Figures 3.6E and 3.6F); and 4) for the most part (i.e. since day 3 of culturing), the concentrations of CL in Q and NQ cells from CR and non-CR cultures of the same chronological age are also similar (compare Figures 3.6G and 3.6H).

I therefore concluded that through the entire chronological aging process CR induces a significant decline in the concentrations of TAG in Q and NQ cell populations. In contrast, through most of the chronological lifespan CR elicits a substantial rise in the abundance of CL in both these cell populations.

3.3.7 CR alters the dynamics of age-related changes in mitochondrial functionality in Q and NQ cells

Mitochondrial electron transport chain, electrochemical potential across the inner mitochondrial membrane ($\Delta\Psi m$) and mitochondrial ROS play essential roles in defining longevity of chronologically aging yeast [84, 85, 87, 233, 243, 252-261]. Q cells purified from non-CR yeast cultures have been shown to exhibit high rates of mitochondrial respiration and low ROS, whereas NQ cells present in these cultures are known to have low rates of mitochondrial respiration and high ROS [88-90, 262].

I therefore investigated the effect of CR on some longevity-defining traits of mitochondrial functionality in Q and NQ cell populations recovered from CR or non-CR yeast cultures of different chronological ages and purified by centrifugation in Percoll density gradient. These traits included the rate of mitochondrial respiration, $\Delta\Psi m$ and cellular ROS, which in yeast are known to be produced primarily as by-products of mitochondrial respiration [263, 264].

My comparative analyses of these traits of mitochondrial functionality in Q and NQ cells purified from differently aged CR and non-CR yeast cultures have revealed the following: 1) through the entire chronological lifespan, the rate of mitochondrial respiration in NQ cells from CR cultures is significantly higher than that in NQ cells from age-matched non-CR cultures (Figure

3.7A); 2) for the most part (i.e. since day 3 of culturing), the rate of mitochondrial respiration in Q cells from CR cultures substantially exceeds that in Q cells from age-matched non-CR cultures (Figure 3.7B); 3) through most of the chronological lifespan (i.e. since day 3 of culturing), the rates of mitochondrial respiration in NQ and Q cells from CR cultures are considerably higher than those in NQ and Q cells from non-CR cultures of the same chronological age (Figures 3.7C and 3.7D, respectively); 4) early in chronological lifespan (i.e. until day 7 for NQ cells or day 5 for Q cells) the concentrations of ROS in NQ and Q cells from CR cultures are notably lower than those in NQ and Q cells from age-matched non-CR cultures (Figures 3.7E and 3.7F, respectively); and 5) late in chronological lifespan (i.e. after day 10 for NQ cells or day 7 for Q cells) the concentrations of ROS in NQ and Q cells from CR cultures considerably exceed those in NQ and Q cells from non-CR cultures of the same chronological age (Figures 3.7E and 3.7F, respectively).

Taken together, these findings show that CR creates distinct patterns of mitochondrial functionality in Q and NQ cells by altering the chronology of age-related changes in mitochondrial respiration, ΔΨm and ROS.

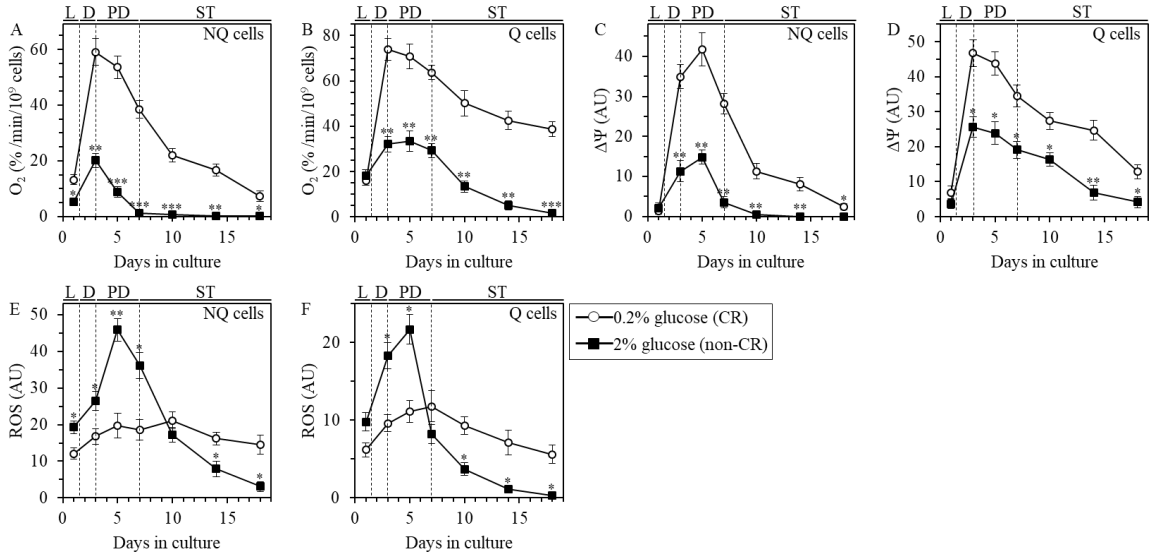

Figure 3.7. CR alters the patterns of age-related changes in certain traits of mitochondrial functionality in Q and NQ cells. Samples of WT yeast cultured in YP medium initially containing 0.2% glucose (CR conditions) or 2% glucose (non-CR conditions) were recovered from L, D, PD or ST growth phase and subjected to centrifugation in Percoll density gradient to purify Q and NQ cell populations, as described in Materials and Methods. The rate of mitochondrial respiration (**A** and **B**), $\Delta\Psi_m$ (**C** and **D**) and ROS (**E** and **F**) were measured as described in Materials and Methods. Data are presented as means ± SEM (n = 3; *P < 0.05; **P < 0.01; ***P < 0.001). Rachel Feldman, Amanda Piano, Anthony Arlia-Ciommo, Vicky Lutchman, Masoumeh Ahmadi, Sarah Elsaser, Hana Fakim, Mahdi Heshmati-

Moghaddam, Asimah Hussain, Sandra Orfali, Harshvardhan Rajen, Negar Roofigari-Esfahani and Leana Rosanelli conducted the experiments.

3.3.8 CR decreases the extent of age-related oxidative damage to proteins, lipids and DNA in Q and NQ cells

An age-related buildup of ROS-inflicted oxidative damage to various cellular macromolecules impairs their stability and is one of the major causes of aging in yeast and other eukaryotes [233, 265-272]. Q cells purified from non-CR yeast cultures are known to be genomically stable, whereas nuclear and mitochondrial DNA (nDNA and mtDNA, respectively) in NQ cells are likely instable because these cells exhibit an age-related excessive production of petite colonies [88, 90, 93]. Moreover, Q cells purified from non-CR yeast cultures do not accumulate SDS-insoluble protein aggregates, whereas NQ cells present in these cultures have been shown to amass such aggregates of irreversibly denatured/damaged proteins [189].

I therefore analyzed how CR influences the extent of age-related oxidative damage to cellular proteins, membrane lipids, nDNA and mtDNA in Q and NQ cell populations that were recovered from differently aged CR or non-CR yeast cultures and purified by centrifugation in Percoll density gradient. My analyses have revealed the following: 1) through most of the chronological lifespan (i.e. since day 3 of culturing), the extent of oxidative damage to proteins in NQ cells from CR cultures is considerably lower than that in NQ cells from age-matched non-CR cultures (Figure 3.8A); 2) late in chronological lifespan (i.e. since day 10) proteins in Q cells from CR cultures are oxidatively damaged to a lesser degree than proteins in Q cells from non-CR cultures of the same chronological age (Figure 3.8B); 3) late in chronological lifespan (i.e. after day 7 for NQ cells or after day 10 for Q cells), the extent of oxidative damage to membrane lipids in Q and NQ cells from CR cultures is significantly decreased as compared to that in NQ cells from age-matched non-CR cultures (Figures 3.8C and 3.8D, respectfully); 4) late in chronological lifespan (i.e. after day 10 for NQ cells or on day 18 for Q cells), the frequencies of spontaneous point mutations in the *CAN1* gene of nDNA in Q and NQ cells from CR cultures are substantially lower than those in Q and NQ cells from age-matched non-CR cultures – probably due to a decreased degree of oxidative damage to nDNA in Q and NQ cells from CR cultures (Figures 3.8E and 3.8F); and 5) late in chronological lifespan (i.e. after day 10 for NQ cells or on day 18 for Q cells), the frequencies of spontaneous point mutations in the *RIB2* and *RIB3* genes of mtDNA in

Q and NQ cells from CR cultures are markedly decreased as compared to those in Q and NQ cells from age-matched non-CR cultures – perhaps due to a decline in the extent of oxidative damage to mtDNA in Q and NQ cells from CR cultures (Figures 3.8G and 3.8H).

In sum, these data imply that CR lessens the degree of age-related oxidative damage to proteins, lipids, nDNA and mtDNA in Q and NQ cells.

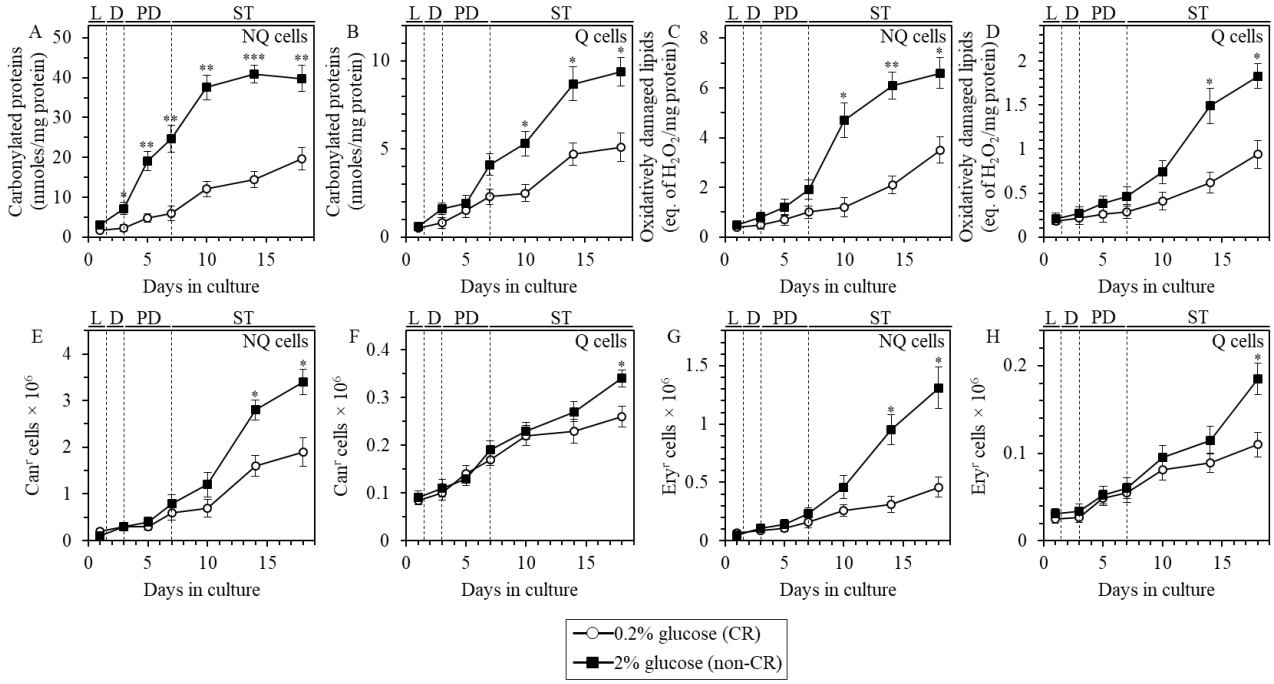

Figure 3.8. CR lessens the extent of age-related oxidative damage to proteins, lipids, nDNA and mtDNA in Q and NQ cells. Samples of WT yeast cultured in YP medium initially containing 0.2% glucose (CR conditions) or 2% glucose (non-CR conditions) were recovered from L, D, PD or ST growth phase and subjected to centrifugation in Percoll density gradient to purify Q and NQ cell populations, as described in Materials and Methods. Carbonylated cellular proteins (**A** and **B**), oxidatively damaged membrane lipids (**C** and **D**), the frequencies of spontaneous point mutations in the *CAN1* gene of nDNA (**E** and **F**), and the frequencies of spontaneous point mutations in the *RIB2* and *RIB3* genes of mtDNA (**G** and **H**) were measured as described in Materials and Methods. Data are presented as means ± SEM (n = 3; *P < 0.05; **P < 0.01; ***P < 0.001). Rachel Feldman, Amanda Piano, Anthony Arlia-Ciommo, Vicky Lutchman, Masoumeh Ahmadi, Sarah Elsaser, Hana Fakim, Mahdi Heshmati-Moghaddam, Asimah Hussain, Sandra Orfali, Harshvardhan Rajen, Negar Roofigari-Esfahani and Leana Rosanelli conducted experiments.

3.3.9 CR increases the resistance of Q and NQ cells to long-term thermal and oxidative stresses

Thermotolerance is one of the characteristic features of Q cells that distinguish them from NQ cells [88, 90]. Moreover, a development of the enhanced resistance to chronic (long-term)

thermal and/or oxidative stresses is known to delay aging in yeast and other eukaryotes [84, 85, 87, 186, 263, 267-279].

I assessed the effects of CR on the abilities of Q and NQ cell populations to resist chronic oxidative and thermal stresses. Q and NQ cell populations were recovered from differently aged CR or non-CR yeast cultures and purified by centrifugation in Percoll density gradient. Chronic thermal stress was administered by spotting pure Q and NQ cells on plates with solid YEPD medium containing 2% glucose, incubating these plates at 55°C for 60 min, and then transferring them to 30°C and incubating for 3 days. Chronic oxidative stress was applied by spotting pure Q and NQ cells on plates with solid YEPD medium containing 2% glucose and 5 mM hydroxide peroxide, and incubating them at 30°C for 3 days. My analyses have revealed the following: 1) early in chronological lifespan (i.e. on day 5 for thermal stress or on day 3 for oxidative stress), NQ cells from CR cultures become more resistant to both these kinds of chronic stresses as compared to NQ cells from age-matched non-CR cultures (Figure 3.9A); and 2) late in chronological lifespan (i.e. since day 10), Q cells from CR cultures exhibit higher resistance to both oxidative and thermal stresses then Q cells from non-CR cultures of the same chronological age (Figure 3.9B).

Collectively, these findings indicate that CR elicits a significant rise in the resistance of Q and NQ cells to long-term thermal and oxidative stresses. Q cells display the stimulatory effect of CR on the tolerance to both kinds of stresses only late in chronological lifespan, whereas in NQ cells such effect can be seen already early in life.

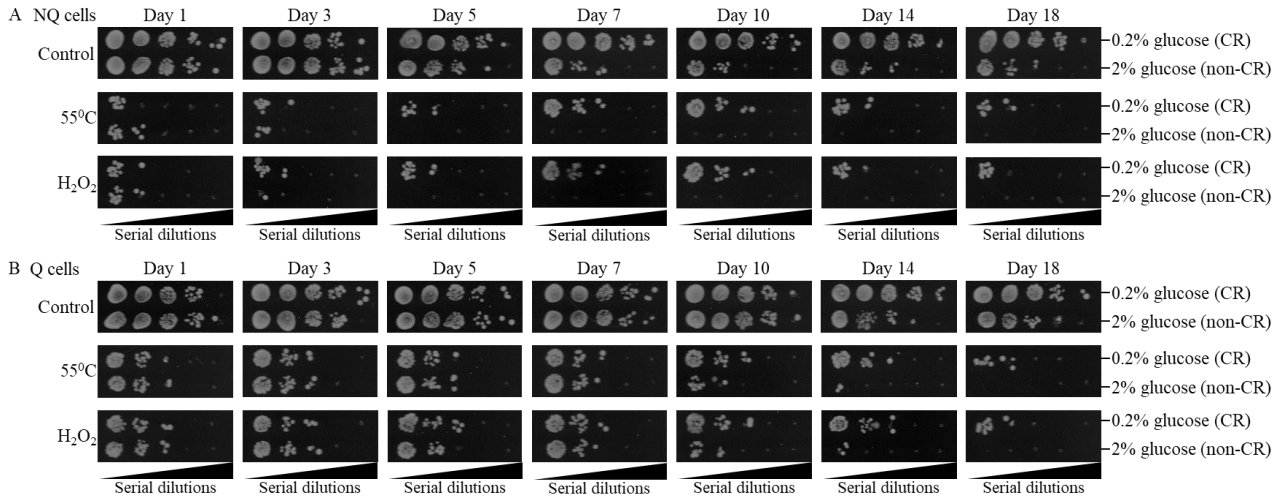

Figure 3.9. CR increases the resistance of Q and NQ cells to long-term thermal and oxidative stresses. Samples of WT yeast cultured in YP medium initially containing 0.2% glucose (CR conditions) or 2% glucose (non-CR

conditions) were recovered from L, D, PD or ST growth phase and subjected to centrifugation in Percoll density gradient to purify Q and NQ cell populations, as described in Materials and Methods. Spot assays for monitoring thermal or oxidative stress resistance were performed as described in Materials and Methods. For chronic thermal stress, serial 10-fold dilutions of pure NQ (**A**) and Q (**B**) cells were spotted on plates with solid YEPD medium containing 2% glucose; these plates were initially exposed to 55^{o}C for 60 min, and then transferred to 30^{o}C and incubated for 3 days. For chronic oxidative stress, serial 10-fold dilutions of pure NQ (**A**) and Q (**B**) cells were spotted on plates with solid YEPD medium containing 2% glucose and 5 mM hydroxide peroxide; these plates were then incubated at 30^{o}C for 3 days. Rachel Feldman, Amanda Piano, Anthony Arlia-Ciommo, Vicky Lutchman, Masoumeh Ahmadi, Sarah Elsaser, Hana Fakim, Mahdi Heshmati-Moghaddam, Asimah Hussain, Sandra Orfali, Harshvardhan Rajen, Negar Roofigari-Esfahani and Leana Rosanelli conducted experiments.

3.3.10 CR delays the onsets of the age-related apoptotic and necrotic modes of PCD in Q and NQ populations

In NQ cells from non-CR yeast cultures, the onsets of the age-related apoptotic and necrotic modes of PCD are known to occur much earlier in chronological lifespan than in Q cells from these cultures [88, 90]. Furthermore, chronologically aging yeast cells in non-CR cultures have been shown to die exhibiting characteristic markers of the apoptotic and/or necrotic subroutines of PCD [85, 280-291].

I therefore investigated how CR influences the onsets of age-related the apoptotic and necrotic modes of PCD in Q and NQ cell populations. Q and NQ cell populations were recovered from differently aged CR or non-CR yeast cultures and purified by centrifugation in Percoll density gradient. Apoptotic PCD was microscopically visualized by Annexin V staining for monitoring phosphatidylserine (PS) translocation from the inner to the outer leaflet of the plasma membrane, a characteristic marker of this PCD subroutine. Propidium iodide (PI) staining for measuring the extent of plasma membrane permeability for small molecules, a hallmark of necrotic PCD, was used to microscopically visualize programmed necrosis. My analyses have revealed the following: 1) through most of the chronological lifespan (i.e. since day 3 of culturing), the percentage of cells undergoing an apoptotic or necrotic mode of PCD in NQ cells from CR cultures is significantly lower than that in NQ cells from age-matched non-CR cultures (Figures 3.10A and 3.10C, respectively); and 2) late in chronological lifespan (i.e. since day 14 for apoptotic PCD or day 10 for necrotic PCD), the percentage of cells committed to any of these two PCD modes in Q cells from CR cultures is considerably decreased as compared to that in Q cells from non-CR cultures of the same chronological age (Figures 3.10B and 3.10D, respectively).

I therefore concluded that CR decelerates the onsets of age-related apoptotic and necrotic PCD in Q and NQ cell populations. In Q cells these effects of CR take place only late in chronological lifespan, whereas NQ cells exhibit them already early in life.

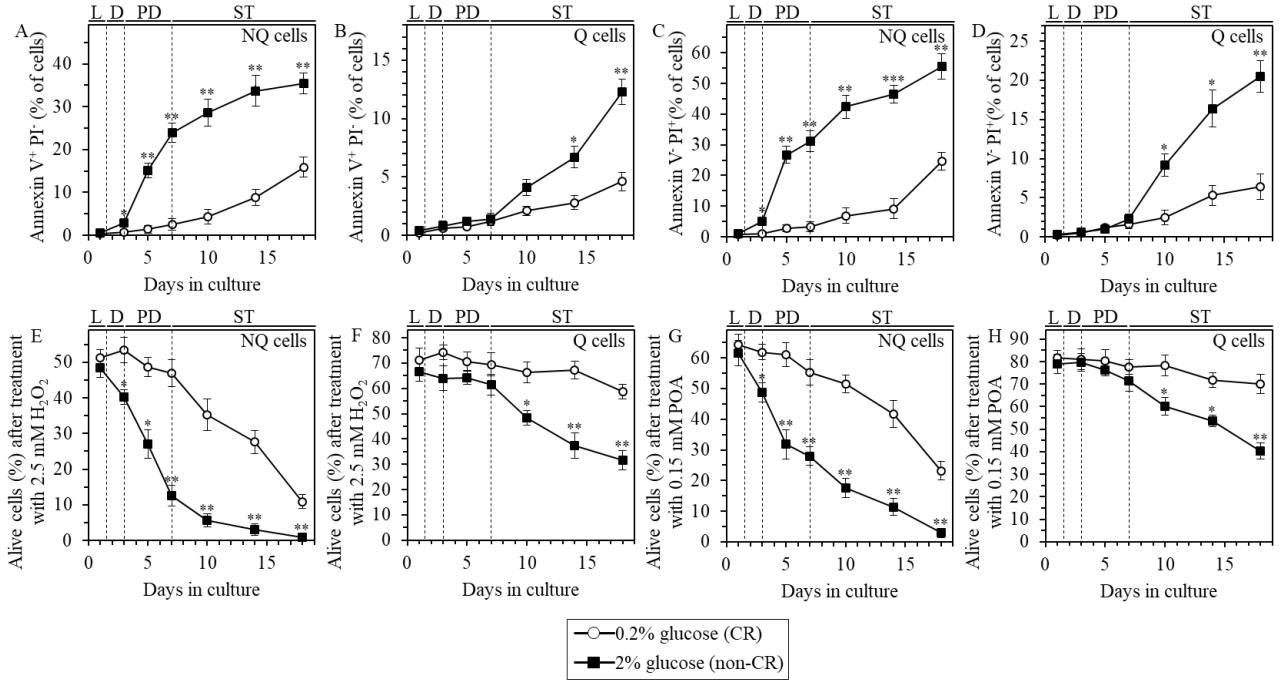

Figure 3.10. CR causes a decline in the susceptibilities of Q and NQ cells to the exogenously induced apoptotic and liponecrotic modes of PCD. Samples of WT yeast cultured in YP medium initially containing 0.2% glucose (CR conditions) or 2% glucose (non-CR conditions) were recovered from L, D, PD or ST growth phase and subjected to centrifugation in Percoll density gradient to purify Q and NQ cell populations, as described in Materials and Methods. Clonogenic assays for monitoring the susceptibilities of NQ (**E** and **G**) and Q (**F** and **H**) cells to the apoptotic (**E** and **F**) or liponecrotic (**G** and **H**) mode of PCD induced in response to a short-term (for 2 h) exposure to exogenous 2.5 mM hydrogen peroxide (**E** and **F**) or 0.15 mM POA (**G** and **H**), respectively, were performed as described in Materials and Methods. Data are presented as means ± SEM (n = 3; *P < 0.05; **P < 0.01; ***P < 0.001). Rachel Feldman, Amanda Piano, Anthony Arlia-Ciommo, Vicky Lutchman, Masoumeh Ahmadi, Sarah Elsaser, Hana Fakim, Mahdi Heshmati-Moghaddam, Asimah Hussain, Sandra Orfali, Harshvardhan Rajen, Negar Roofigari-Esfahani and Leana Rosanelli conducted experiments.

3.3.11 CR decreases the susceptibilities of Q and NQ cells to the exogenously induced apoptotic and liponecrotic modes of PCD

Because CR delays the onsets of age-related the apoptotic and necrotic modes of PCD in Q and NQ populations of chronologically aging yeast, I examined how CR influences the susceptibilities of Q and NQ cells to each of these PCD subroutines that were elicited in response to certain exogenous stimuli. A brief exposure of yeast to exogenous hydrogen peroxide is known to decrease clonogenic survival of cells by causing mitochondria-controlled apoptotic PCD [281, 284, 289, 292, 293], whereas a short-term treatment of yeast with exogenous palmitoleic acid (POA) has been shown to reduce clonogenic survival of cells by eliciting a liponecrotic mode of PCD [288-291].

My comparative analyses have revealed the following: 1) through most of the chronological lifespan (i.e. since day 3 of culturing), clonogenic survival of NQ cells from CR cultures briefly exposed to exogenous hydrogen peroxide (to elicit apoptotic PCD) or POA (to trigger liponecrotic PCD) significantly exceeds that of NQ cells from age-matched non-CR cultures (Figures 3.10E and 3.10G, respectively); and 2) late in chronological lifespan (i.e. since day 10), clonogenic survival of Q cells from CR cultures subjected to a short-term treatment with exogenous hydrogen peroxide (to initiate apoptotic PCD) or POA (to induce liponecrotic PCD) is significantly higher than that of Q cells from non-CR cultures of the same chronological age (Figures 3.10F and 3.10H, respectively).

In sum, these data indicate that CR causes a decline in the susceptibilities of Q and NQ cell populations to the apoptotic and liponecrotic modes of PCD induced in response to a short-term exposure to exogenous hydrogen peroxide or POA, respectively. In Q cells, the abilities of CR to cause these effects can be seen only late in chronological lifespan, whereas NQ cells display both effects of CR already early in life.

3.4 Discussion

This study revealed that CR extends yeast chronological lifespan via a mechanism that links cellular aging to cell cycle regulation, maintenance of the Q state, entry into the NQ state and survival in the NQ state. My comparative analyses of physical, morphological, reproductive, biochemical and physiological properties of Q and NQ cells from differently aged CR or non-CR yeast cultures suggest a hypothetical model for this mechanism. This model is depicted schematically in Figure 3.11.

The model posits that Q and NQ cell populations exist as several subpopulations related to each other in a chronological age-dependent manner. One of these subpopulations is a subpopulation of non-differentiated Q cells that represents a ″stem″ cell niche (Figure 3.11). I call these stem cells G_Q^{HD} because they are high-density cells that are arrested at the G_1 phase of the cell cycle and exist in a specialized non-proliferative state called G_0. G_Q^{HD} cells constituting the stem cell niche are viable unbudded cells that 1) exhibit high reproductive (colony-forming) capacity; 2) are able to synchronously re-enter the mitotic cell cycle after cell transfer into fresh medium; 3) display high concentrations of glycogen and trehalose, the two major glucose stores; 4) possess low concentrations of TAG and high concentrations of CL; 5) have fully functional mitochondria; 6) exhibit low concentrations of ROS; 7) display low degree of oxidative damage to proteins, lipids and DNA; 8) are resistant to long-term thermal and oxidative stresses; and 9) display low susceptibilities to the mitochondria-controlled apoptotic and fatty acid-induced liponecrotic forms of PCD.

In L (for CR yeast cultures) or SP (for non-CR yeast cultures) phase, G_Q^{HD} cells become committed to entry into a program that we call the differentiation program (Figure 3.11). Such commitment of G_Q^{HD} cells to differentiation is manifested in a significant decrease of their buoyant density, so that they are converted to a subpopulation of Q cells that we call G_Q^{LD} cells because of their low density. The chronological age-related progression of G_Q^{LD} cells through the differentiation program causes a gradual decline in the following features: viability, reproductive (colony-forming) capacity, the ability to synchronously re-enter the mitotic cell cycle after cell transfer into fresh medium, glycogen and trehalose concentrations, TAG concentration, mitochondrial functionality, the ability to maintain low concentration of ROS, the capacity to limit oxidative molecular damage, the tolerance to long-term thermal and oxidative stresses, and the resistance to the apoptotic and liponecrotic modes of PCD. The progression of G_Q^{LD} cells through the differentiation program ultimately leads to their conversion into a subpopulation of NQ cells that we call G_{NQ}^{LD} cells; these cells are committed to the programmed, age-related modes of apoptotic and/or liponecrotic cell death (Figure 3.11).

When a yeast culture enters ST phase, most (for CR yeast cultures) or many (for non-CR yeast cultures) of non-differentiated G_Q^{HD} cells from the stem cell niche have been committed to entry into and progression through the differentiation program and, thus, exist in the G_Q^{LD} and G_{NQ}^{LD} forms. However, a portion of cells within this culture still remains in the G_Q^{HD} form (Figure

3.11). Through the entire chronological lifespan, these non-differentiated stem cells progress through a program which we call the maintenance program. A progression of G_Q^{LD} stem cells through this maintenance program is manifested in a much slower deterioration in the same features as the ones whose relatively fast decline occurs during the differentiation program (Figure 3.11). The advancement of G_Q^{HD} cells through the maintenance program eventually results in their conversion into a subpopulation of NQ cells that we call G_{NQ}^{HD} cells; these cells are susceptible to the chronological age-related subroutines of apoptotic and/or liponecrotic PCD (Figure 3.11).

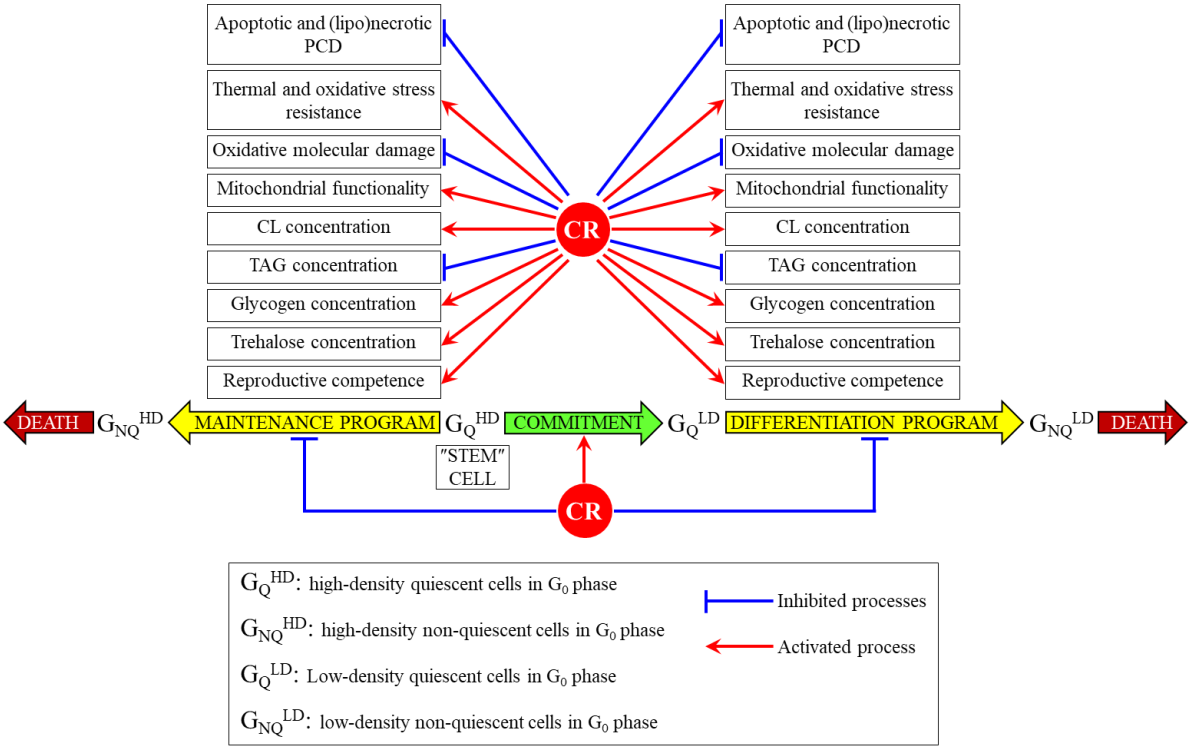

Figure 3.11. A model for how CR extends yeast chronological lifespan via a mechanism that links cellular aging to cell cycle regulation, maintenance of quiescence, entry into the non-quiescent state and survival in the non-quiescent state. CR delays yeast chronological aging by causing specific changes at the G_1 checkpoint for cell cycle arrest and entry into the G_0 state, timing of G_Q^{HD} (high-density, quiescent) cells commitment to conversion into G_Q^{LD} (low-density, quiescent) cells, pace of progression of G_Q^{LD} (low-density, quiescent) cells through a differentiation program yielding G_{NQ}^{LD} (low-density, non-quiescent) cells, and rate of advancement of G_Q^{HD} (high-density, quiescent) cells via a maintenance program leading to their conversion into G_{NQ}^{HD} (high-density, non-quiescent) cells. Please see text for additional details.

My findings suggest that CR delays yeast chronological aging by causing specific changes in a G_1 checkpoint for cell cycle arrest and entry into the G_0 state, a growth phase in which G_Q^{HD} cells undergo the commitment to become G_Q^{LD} cells, the differentiation of G_Q^{LD} cells into G_{NQ}^{LD} cells, and the conversion of G_Q^{HD} cells into G_{NQ}^{HD} cells. These changes are described below.

Judging from the very small size of G_Q^{HD} stem cells seen in CR cultures (Figure 3.1G), CR may arrest the cell cycle at a previously unknown checkpoint in early G_1. This is unlike the large size of G_Q^{HD} stem cells observed in non-CR cultures (Figure 3.1G), whose cell cycle is known to be arrested at the checkpoint START A in late G_1 [97, 294].

Furthermore, CR is likely to accelerate the onset of commitment of G_Q^{HD} stem cells to entry into the differentiation program (Figure 3.11). Indeed, G_Q^{HD} cells in CR cultures become committed to entry into this program already in L growth phase, whereas in CR cultures such commitment occurs only in SP phase (Figure 3.1D).

Moreover, my data indicate that CR can also decrease both the pace of progression of G_Q^{LD} cells through the differentiation program and the rate of advancement of G_Q^{HD} cells via the maintenance program (Figure 3.11). These effects of CR slow down yeast chronological aging because they delay the conversion of these two subpopulations of Q cells into G_{NQ}^{LD} and G_{NQ}^{HD} subpopulations of NQ cells (respectively), both of which are committed to the chronological age-related modes of apoptotic and liponecrotic PCD (Figure 3.11). My findings suggest that the observed abilities of CR to decelerate the differentiation and maintenance programs are due to specific effects of this low-calorie diet on a distinct set of morphological, reproductive, biochemical and physiological processes in G_Q^{LD} and G_Q^{HD} cells (as outlined above, all these processes have been implicated in defining longevity of chronologically aging yeast). These specific effects of CR in G_Q^{LD} and G_Q^{HD} cells include the following: 1) CR slows a chronological age-related deterioration in the reproductive competences of these cells and in their capabilities to synchronously re-enter the mitotic cell cycle when nutrients become available; 2) CR increases glycogen and trehalose concentrations in these cells; 3) CR decreases the concentrations of TAG and raises CL concentrations in these cells; 4) CR improves mitochondrial functionality in these cells; 5) CR reduces ROS concentrations and lessens the degree of oxidative molecular damage in these cells; 6) CR increases the resistance of these cells to long-term thermal and oxidative stresses; and 7) CR decreases the susceptibilities of these cells to the apoptotic and liponecrotic forms of PCD (Figure 3.11).

4 A network of interorganellar communications underlies cellular aging

4.1 Introduction

Aging of multicellular and unicellular eukaryotic organisms is due to dysregulation of many processes within cells; the extent of such dysregulation progresses with cellular and organismal age [301]. The spatiotemporal organization of these numerous cellular processes and their functional states define the replicative and chronological age of a eukaryotic cell [302, 303]. All these cellular processes are governed by an evolutionarily conserved signaling network. The network integrates the insulin/insulin-like growth factor 1 (IGF-1), AMP-activated protein kinase/target of rapamycin (AMPK/TOR) and cAMP/protein kinase A (cAMP/PKA) nutrient- and energy-sensing signaling pathways [301, 302]. By sensing the intracellular and organismal nutrient and energy status, this longevity signaling network coordinates information flow along its convergent, divergent and multiply branched pathways to regulate cellular aging, influence age-related pathologies and define organismal lifespan [301, 303].

A theoretical framework of network biology has been successfully applied to system biological and computational analyses of age-related changes in gene expression, protein-protein interactions and metabolomes; these analyses yielded several models of the so-called biomolecular networks of cellular aging [302, 304, 305]. Recent findings support the notion that such biomolecular networks may progress through a series of lifespan checkpoints, each being monitored by a checkpoint-specific nutrient- and energy-sensing signaling pathway or pathways [302, 304, 305].

Numerous processes that define the replicative and chronological age of a eukaryotic cell are confined to various cellular organelles and take place in the cytosol [306, 307]. The organelles housing these processes communicate with each other by establishing zones of close apposition and being involved in the unidirectional or bidirectional flow of certain soluble metabolites, peptides, proteins, DNA fragments and lipids; the flow of metabolites and proteins also underlies the communication between some of these organelles and the cytosol [306-308]. Emergent evidence supports the view that such directed, coordinated and regulated organelle-organelle and organelle-cytosol communications are essential for the development of a pro- or anti-aging cellular pattern [306-308]. To reflect the essential role of crosstalk between different types of organelles in regulating cellular aging, we coined the term ″an endomembrane system that governs cellular

aging″ [306]. Here, I outline numerous interorganellar communications that institute this endomembrane system. I discuss recent progress in understanding how various interorganellar communications within the system - along with crosstalk between this endomembrane system and the cytosol - influence the development of a pro- or anti-aging cellular pattern. I summarize and integrate into a model the evidence that an intricate network of intercompartmental (i.e., organelle-organelle and organelle-cytosol) communications underlies cellular aging in evolutionarily distant organisms.

4.2 Organelles generate, distribute and process the flow of information that initiates the development of a pro- or anti-aging cellular pattern

The functional state of a cellular organelle depends on the rates and efficiencies of processes confined to it. Growing evidence supports the notion that in response to age-related intracellular stresses and environmental factors some organelles can alter their functional states to become platforms for generating, directing and processing the flow of information that set off a pro- or anti-aging cellular pattern [306-311]. This critical information is generated by an organelle as certain soluble metabolites, lipids, proteins, peptides or DNA fragments. These primary molecular signals are then distributed to other cellular compartments capable of processing them into the secondary molecular signals that ultimately define the long-term viability of the cell [306-311]. In this section, I outline how several cellular organelles respond to age-related alterations in their functional states by generating certain primary molecular signals, how these primary signals are distributed to other compartments within the cell, and how these other cellular compartments process them into some secondary molecular signals that are critical for cell viability.

Mitochondria

Mitochondria compartmentalize numerous processes that regulate cellular aging [303, 307, 308, 312, 313]. Age-related and environment-dependent changes in the rates and efficiencies of these processes modulate the ability of mitochondria to generate and release various molecular signals. Outside mitochondria, these signals initiate cascades of events that alter the rates and efficiencies of pro- and/or anti-aging processes in other cellular locations [303, 307, 308, 312, 313]. Such dynamic communications of mitochondria with other compartments within the cell are essential for establishing the rate of cellular aging.

A progressive decline in mitochondrial respiratory chain activity with the replicative age of a yeast cell causes an age-related gradual reduction of mitochondrial membrane potential ($\Delta\psi_m$) [312]. Such progressive deterioration of $\Delta\psi_m$ in replicatively aging yeast is the primary signal responsible for the activation of the mitochondrial retrograde (RTG) signaling pathway of cellular aging regulation [307, 312] (Figure 4.1; path 1). The decline in $\Delta\psi_m$ activates the Rtg2 protein via a yet-to-be characterized mechanism. Rtg2 then stimulates nuclear import of the Rtg1-Rtg3 heterodimeric transcription factor, which in the nucleus triggers an anti-aging transcriptional program [307, 312]. In addition, the nuclear pool of Rtg2 in replicatively aging yeast plays a vital anti-aging role by enhancing genome stability and suppressing the deleterious accumulation of extrachromosomal rDNA circles [307, 312] (Figure 4.1; path 1). A similar mitochondrial RTG pathway exists in mammalian cells, where functionally compromised mitochondria stimulate the NFκB protein attached to their surface [312] (Figure 4.1; path 8). The ensuing association of NFκB with several other proteins yields heterodimeric transcription factors that are imported into the nucleus to orchestrate a global stress response program affecting several age-related pathologies [312].

In addition to its stimulating effect on the anti-aging RTG pathway, the progressive decline in $\Delta\psi_m$ with the replicative age of yeast cells also causes (via a yet-to-be established mechanism) a reduction of the TOR complex 1 (TORC1) protein kinase activity, thereby attenuating this master regulator of the key pro-aging signaling pathway [307, 312] (Figure 4.1; path 2).

Lack of Afo1, a protein component of the large subunit of the mitochondrial ribosome, delays replicative aging of non-respiring yeast cells in an independent of mitochondrial translation manner [314]. Afo1 regulates replicative aging of yeast cells via the so-called back-signaling pathway; this pathway operates under conditions repressing the RTG pathway and is mediated by Sfp1, a transcription activator of genes encoding cytoplasmic ribosomal proteins [314] (Figure 4.1; path 3). In addition, Afo1 indirectly suppresses the TORC1-governed pro-aging signaling pathway via a mechanism that remains to be defined [314] (Figure 4.1; path 4).

The maintenance of protein homeostasis in mitochondria of mammalian cells and cells of the nematode *Caenorhabditis elegans* plays an important role in regulating cellular aging; mitochondrial proteostasis in these cells is sustained with the help of several anti-aging unfolded protein response (UPR^{mt}) pathways of mitochondria-to-nucleus communications [3013, 315]. If unfolded or misfolded proteins accumulate within the intermembrane space (IMS) of mitochondria

in mammalian cells, a yet-to-be identified molecular signal activates the UPR^{mt} pathway [313]. This anti-aging pathway is mediated by the protein kinase AKT, which initiates a cascade of events stimulating transcription of nuclear genes coding for an IMS quality control protease and a transcription factor essential for mitochondrial biogenesis [313] (Figure 4.1; path 5). Accumulation of unfolded or misfolded proteins within the matrix of mitochondria in mammalian cells triggers the anti-aging UPR^{mt} pathway mediated by the protein kinase JNK2 and the transcription factor CHOP; a similar UPR^{mt} pathway in *C. elegans* cells operates via the transcription factor ATFS-1 [313, 315, 316] (Figure 4.1; path 6). Another UPR^{mt} pathway activated in *C. elegans* cells in response to a build-up of unfolded or misfolded proteins within the mitochondrial matrix involves the ubiquitin-like protein UBL-5 and the transcription factor DVE-1 [313, 315] (Figure 4.1; path 7). The UPR^{mt} pathways maintaining proteostasis within the matrix of mitochondria activate transcription of nuclear genes encoding several mitochondrial quality control proteases and chaperones [313, 315, 316]. Both anti-aging UPR^{mt} pathways operating in *C. elegans* cells are triggered by an HAF-1-driven efflux of peptides formed due to a ClpP-dependent proteolysis of the unfolded and misfolded proteins excessively accumulated within the mitochondrial matrix [317].

An age-related mitochondrial dysfunction and the resulting decline in $\Delta\psi_m$ in mammalian cells reduce mitochondrial uptake of Ca^{2+}, thereby elevating the concentration of free Ca^{2+} in the cytosol [318]. This rise in cytosolic free Ca^{2+} stimulates calcineurin (a protein phosphatase) and several Ca^{2+}-dependent protein kinases that in response activate nuclear import of a distinct set of transcription factors, including ATF2, CHOP, CREB, Egr1, NFAT and NFκB [318] (Figure 4.1; path 8). In the nucleus, these transcription factors cause a remodeling of gene expression patterns to influence several age-related pathologies – such as aging of neuronal cells, age-related degeneration of neurons and brain aging [319].

Certain dietary and pharmacological interventions that slow down cellular and organismal aging have been shown to elevate the cytosolic NAD^+/NADH ratio by activating mitochondrial fatty acid oxidation and stimulating a malate-aspartate shuttle in the mitochondrial membrane [320]. The resulting increase in cytosolic NAD^+ level activates the NAD^+-dependent type III deacetylase SIRT1, which resides predominately in the nucleus [321] (Figure 4.1; path 9). Active SIRT1 then de-acetylates and thus activates such transcription factors as FOXO1, FOXO3a, NFκB, PGC-1α and PPAR-α; in response, these transcription factors stimulate expression of numerous

genes that are required for delaying cellular aging and slowing down the age-related progression of metabolic disorders [303, 320, 321].

Intracellular reactive oxygen species (ROS) are generated mainly as by-products of mitochondrial respiration; in addition, the IMS protein $p66^{shc}$ is involved in mitochondrial ROS formation in mice cells by oxidizing cytochrome *c* [322]. A body of evidence supports the view that ROS play a dual role in regulating cellular aging. If mitochondrially produced ROS are maintained at sub-lethal levels, these potent signaling molecules initiate an anti-aging cellular program by activating protein kinases JNK (in *C. elegans* and fruit flies *Drosophila melanogaster*) and MST-1 (in *C. elegans*) [303, 323-325] (Figure 4.1; path 10). Both JNK and MST-1 then phosphorylate and thus activate the forkhead transcription factor FOXO, known to turn on expression of many genes required for slowing down cellular aging [303, 323-325] (Figure 4.1; path 10). If, as it has been first postulated by the mitochondrial free radical theory of aging [326], mitochondria are unable to maintain ROS concentration below a toxic threshold, ROS promote cellular aging by oxidatively damaging proteins, lipids and nucleic acids in various cellular locations [322, 327] (Figure 4.1; path 16).

After being synthesized within and exported from mitochondria, iron-sulfur clusters (ISC) in the cytosol of yeast and mammalian cells are actively transferred to various apoproteins as essential inorganic cofactors required for their activity [328, 329]. Some of these ISC-containing proteins are then imported into the nucleus, where they play vital roles in slowing down cellular aging by sustaining genome integrity through their involvement in DNA replication, DNA repair and telomere maintenance [329, 330] (Figure 4.1; path 12). In replicatively aging yeast, the cytosolic ISC also attenuate activity and/or nuclear import of Aft1, a transcription factor that activates expression of genes involved in iron uptake by and distribution within cells [328, 330] (Figure 4.1; path 11). The resulting drop in free intracellular iron significantly reduces the extent of oxidative damage to various cellular proteins, thereby mitigating a process that accelerates cellular aging [330]. An age-related mitochondrial dysfunction and the ensuing decline in $\Delta\psi_m$ in replicatively aging yeast hamper ISC synthesis in and/or export from mitochondria and, thus, reduce genome stability and elevate oxidative protein damage [330].

Both, the rate of mitochondrial DNA (mtDNA) fragments migration to the nucleus and the frequency of mtDNA fragments insertion into nuclear DNA, rise with the chronological age of a yeast cell [331, 332]. These progressive mitochondria-originated processes with age make

essential contributions to cellular aging regulation in chronologically aging yeast, likely by influencing nuclear DNA replication, recombination, repair and transcription and ultimately reducing nuclear genome stability in an age-related manner [331, 332] (Figure 4.1; path 13).

Protein components comprising the so-called mitochondrial translation control (MTC) module are known to be involved in the processing, stabilization and translational activation of mtDNA-encoded mRNAs [333]. Lack of any of the eight specific members of this protein module slows down replicative aging of yeast cells 1) independently of the effects of its absence on mitochondrial translation, respiration, ROS production and oxidative damage; and 2) autonomously from the anti-aging RTG and back-signaling pathways (see Figure 4.1; paths 1 and 3, respectively) [334]. The absence of any of these MTC proteins beneficially influences the replicative lifespan of a yeast cell via two different pathways. One pathway delays cellular aging by suppressing the deleterious accumulation of extrachromosomal rDNA circles in the nucleus in a Pnc1- and Sir2-dependent manner [334] (Figure 4.1; path 14); Pnc1 has been shown to deplete the level of nicotinamide, a strong non-competitive inhibitor of the NAD^+-dependent protein deacetylase Sir2 [301, 302]. Another pathway slows down cellular aging by reducing cAMP level and the protein kinase A (PKA) activity [334] (Figure 4.1, path 15), thereby attenuating a global pro-aging PKA signaling network that inhibits vacuole-dependent autophagy, activates protein synthesis in the cytosol and suppresses a stress-response transcriptional program in the nucleus [301, 302]. The identity of the primary mitochondria-generated molecular signal that triggers these two pathways in response to the absence of a critical protein component of the MTC module remains to be established.

An age-related mitochondrial dysfunction and the resulting decline in intracellular ATP levels and rise in intracellular AMP levels increase the AMP-activated protein kinase (AMPK) activity in organisms across phyla [303, 320] (Figure 4.1; path 17). In *C. elegans* and mammals, AMPK, a central regulator of cellular energy homeostasis, can be also activated in response to certain longevity-extending dietary and pharmacological interventions [303, 320]. Activated AMPK delays cellular aging by 1) inhibiting the TORC1 protein kinase activity, thereby attenuating this master regulator of the key pro-aging signaling pathway [303]; 2) turning on an anti-aging process of lysosome-dependent autophagy [335]; 3) promoting a SIRT1-dependent activating de-acetylation of FOXO and PGC-1α transcription factors known to stimulate expression of numerous genes required for slowing down cellular aging and age-related metabolic

disorders [303, 320, 321]; 4) phosphorylating histone H2b to activate transcription of numerous stress-response genes essential for cell survival [336]; and 5) inhibiting lipolysis of the neutral lipids triacylglycerols deposited in lipid droplets (LD) [337].

The m-AAA protease Afg3 with chaperone-like activity in the inner membrane of mitochondria is involved in degradation of unfolded and misfolded membrane proteins, assembly of electron transport chain complexes, and proteolytic maturation of a mitochondrial ribosomal protein of the large subunit [338]. Lack of Afg3 delays replicative aging of yeast cells, reduces the rate of protein synthesis in the cytosol and enhances resistance to the tunicamycin-induced unfolded protein stress in the endoplasmic reticulum (ER) [339]. Thus, the Afg3-assisted protein degradation and/or multi-protein complex assembly in the inner membrane of mitochondria may accelerate replicative aging of yeast cells by generating some yet-to-be identified molecular signals that stimulate the pro-aging processes of protein synthesis in the cytosol and unfolded protein stress build-up in the ER [339] (Figure 4.1; paths 18 and 19, respectively).

Lack of the outer mitochondrial membrane protein Uth1 slows down replicative aging of yeast cells and eliminates the micromitophagic mode of mitophagy, a mechanism of mitochondrial quality and quantity control responsible for the autophagic degradation within vacuoles of aged, dysfunctional, damaged or excessive mitochondria [340]. In the absence of Uth1, another mode of mitophagy, called macromitophagy, remains functional [340]. It has been recently suggested that macromitophagy could be a highly selective process responsible for autophagic degradation of only dysfunctional mitochondria accumulating in replicatively aging yeast cells, whereas a less selective process of micromitophagy could eliminate mitochondria *en masse*, regardless of their functional state [307]. If such a hypothesis is correct, then lack of Uth1 (or perhaps a progressive decline in its level with the replicative age of a yeast cell) could delay cellular aging by reducing the extent of non-selective micromitophagic degradation of functional mitochondria, while preserving (or even increasing) the efficacy with which only dysfunctional mitochondria are eliminated in a selective process of macromitophagy (Figure 4.1; path 20).

Aup1p is a protein phosphatase within the IMS of yeast mitochondria [340]. In chronologically aging yeast cells, Aup1 functions as a longevity assurance protein which 1) stimulates the anti-aging process of selective macromitophagy [340] (Figure 4.1; path 21); and 2) promotes the dephosphorylation and nuclear import of Rtg3, a key transcriptional activator of the anti-aging RTG signaling pathway [341] (Figure 4.1; path 22).

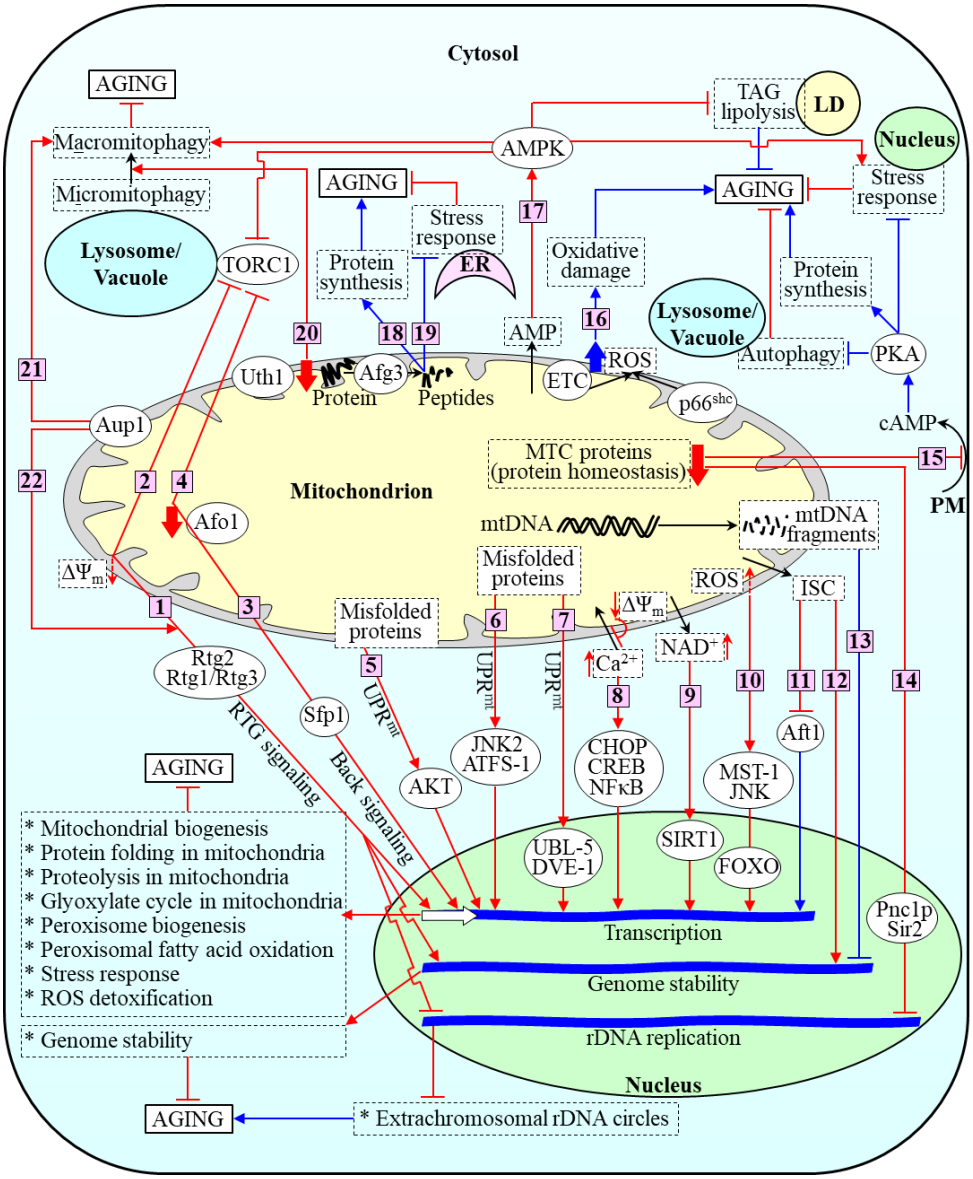

Figure 4.1. Communications of mitochondria with many other compartments within the cell are essential for establishing the rate of cellular aging. Age-related changes in the rates and efficiencies of numerous processes that regulate cellular aging and are confined to mitochondria modulate the ability of these organelles to generate and release diverse molecular signals. After being released from mitochondria, these signals trigger cascades of events that cause the development of a pro- or anti-aging cellular pattern. Activation arrows and inhibition bars denote pro-aging processes (displayed in blue color) or anti-aging processes (displayed in red color). Please see text for additional details. ER, endoplasmic reticulum; ETC, electron transport chain; ISC, iron-sulfur clusters; LD, lipid droplet; MTC, mitochondrial translation control; mtDNA, mitochondrial DNA; PM, plasma membrane; ROS, reactive oxygen species; RTG, retrograde; TAG, triacylglycerols; UPRmt, mitochondrial unfolded protein response pathway; ΔΨm, electrochemical potential across the inner mitochondrial membrane.

Lysosomes and vacuoles

The surface of lysosomes in mammalian cells (vacuoles in yeast cells) provides a platform for the activation of TORC1, a master regulator of the key signaling pathway accelerating cellular aging [310, 311]. Dietary regimens that reduce the intake of amino acids, the most critical intracellular signals for TORC1 activation, are known to delay aging in evolutionarily distant organisms [342]. A rise in the level of amino acids in the cytosol of yeast cells causes an increase in protein kinase activity of TORC1 by stimulating the formation of a complex between permanently bound to the vacuolar surface inactive TORC1 and two Rag family GTPases [343]. In mammalian cells, elevated levels of amino acids in the cytosol trigger the Rag GTPase-dependent recruitment of an enzymatically inactive TORC1 from the cytosol to the surface of lysosomes; TORC1 is activated at the lysosomal surface only after it binds to the small GTPase Rheb in its GTP-bound state acquired in response to active growth factor signaling [310, 343].

Once activated at the surface of lysosomes or vacuoles, TORC1 sets off a pro-aging program in the cell by phosphorylating several target proteins that then activate pro-aging processes or inhibit anti-aging processes confined to various cellular compartments [310, 311, 343]. From the surface of lysosomes or vacuoles, active TORC1 phosphorylates the following proteins essential for cellular aging regulation: 1) the key translational regulators 4E-BP1 and S6K1 in mammalian cells, thereby stimulating the pro-aging process of protein synthesis in the cytosol (Figure 4.2; path 23); 2) the autophagy-initiating proteins ATG13 and ULK1 in mammalian cells (Atg13 in yeast cells), thus inhibiting autophagosome formation in the cytosol to suppress the anti-aging process of autophagy (Figure 4.2; path 24); 3) the nutrient-sensory protein kinase Sch9 in yeast cells, therefore attenuating the anti-aging processes of protein synthesis in mitochondria (Figure 4.2; path 25) and transcription of numerous stress-response genes in the nucleus (Figure 4.2; path 26); 4) the phosphatidic acid phosphatase Lipin-1 in mammalian cells, consequently stimulating the pro-aging process of transcription of many genes involved in *de novo* lipid synthesis and adipogenesis (Figure 4.2; path 27); and 5) the transcription factor TFEB in mammalian cells, thereby suppressing the anti-aging process of transcription of several genes essential for lysosome biogenesis and autophagy (Figure 4.2; path 28) [310, 311, 344].

It needs to be emphasized that in replicatively aging yeast cells cytosolic concentration of neutral amino acids (including glutamine, a potent TORC1 activator), is under the stringent control

of age-related changes in vacuolar pH [345, 346]. In replicatively "young" cells, the high activity of the vacuolar H^+-ATPase maintains high vacuole acidity by efficiently coupling ATP hydrolysis to proton import into the vacuole [345]. The high concentration of protons in the vacuole of replicatively "young" cells drives the proton-dependent import of neutral amino acids from the cytosol into this organelle – thereby sustaining the concentration of neutral amino acids (including glutamine) in the cytosol at a low level [345]. A progressive decline in vacuole acidity with the replicative age of a yeast cell attenuates the proton-dependent import of neutral amino acids into the vacuole and, thus, increases their concentrations in the cytosol [345]. The gradual rise in the levels of neutral amino acids (including the potent TORC1 activator glutamine) in the cytosol of replicatively aging cells may initiate the development of a pro-aging cellular pattern by: 1) intensifying the proton-dependent uptake of amassed in the cytosol neutral amino acids by mitochondria, thereby significantly reducing $\Delta\psi_m$ to ultimately cause mitochondrial fragmentation [345] (Figure 4.2; path 29); and/or 2) activating TORC1 at the vacuolar surface in a glutamine-dependent fashion [346] (Figure 4.2; path 30), thus promoting TORC1-dependent phosphorylation of several target proteins that in respond activate pro-aging processes or inhibit anti-aging processes confined to various cellular compartments (Figure 4.2; paths 23-28).

Peroxisomes

We recently discussed findings supporting the notion that dynamic communications of peroxisomes with other compartments within the cell influence the development of a pro- or anti-aging cellular pattern [306, 309]. Efficient peroxisomal import of the hydrogen peroxide-decomposing enzyme catalase (Cta1) in replicatively and chronologically "young" cells not only minimizes the oxidative macromolecular damage within peroxisomes but also enables these organelles to sustain the extraperoxisomal concentration of hydrogen peroxide at a certain non-toxic and pro-hormetic level [306, 309]. At such a level, this ROS can stimulate a redox signaling network known to elicit "stress-response hormesis" by activating transcription of numerous nuclear stress-response genes essential for cell survival, thereby slowing down cellular aging [303, 306, 309, 322, 325] (Figure 4.3A; path 31). A progressive decline in the efficacy of peroxisomal import of hydrogen peroxide-metabolizing catalase with the replicative and chronological age of a eukaryotic cell not only gradually elevates the oxidative macromolecular damage within peroxisomes but also impairs the ability of these organelles to maintain the extraperoxisomal

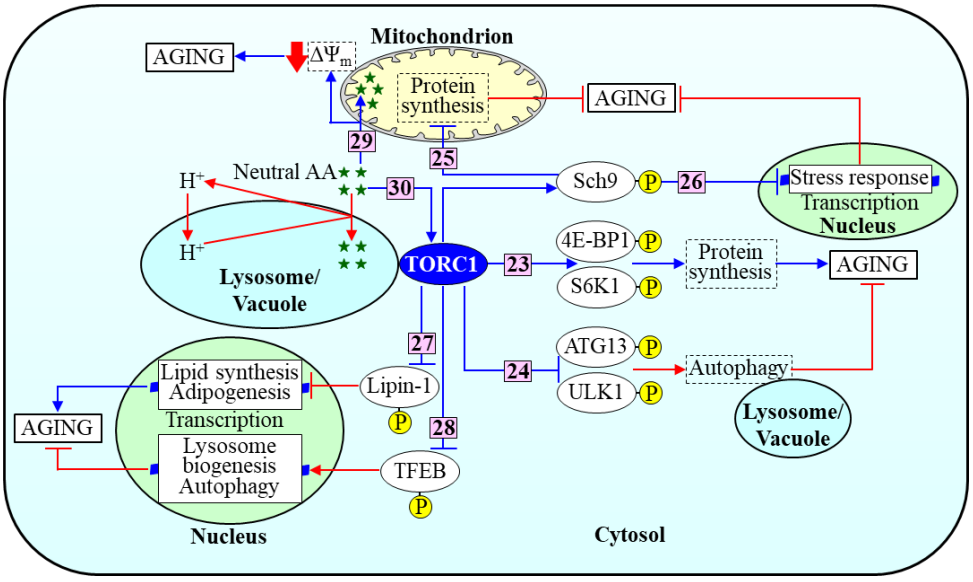

Figure 4.2. Following its activation at the surface of mammalian lysosomes or yeast vacuoles, the target of rapamycin complex 1 (TORC1) initiates a pro-aging program by phosphorylating several target proteins in the cytosol. Once phosphorylated, these proteins activate pro-aging processes or inhibit anti-aging processes in several other cellular compartments. In replicatively aging yeast cells, a progressive reduction of vacuole acidity with cellular age mitigates the proton-dependent transport of neutral amino acids (AA) from the cytosol to the vacuole. The resulting increase in the cytosolic concentration of neutral amino acids (including the potent TORC1 activator glutamine) triggers the development of a pro-aging cellular pattern by impairing mitochondrial function and activating TORC1 at the vacuolar surface. Activation arrows and inhibition bars denote pro-aging processes (displayed in blue color) or anti-aging processes (displayed in red color). Please see text for additional details. ΔΨm, electrochemical potential across the inner mitochondrial membrane.

concentration of hydrogen peroxide below a non-toxic threshold [306, 309]. Following a release of hydrogen peroxide in toxic concentrations from peroxisomes to the cytosol in replicatively and chronologically "old" cells, this ROS accelerates cellular aging by oxidatively damaging proteins, lipids and nucleic acids in various cellular locations [303, 306, 309, 322] (Figure 4.3B; path 32).

Replicatively and chronologically "young" cells are proficient in peroxisomal import of Fox1, Fox2, and Fox3, the core enzymes of fatty acid β-oxidation [306, 309]. Therefore, peroxisomes of these cells efficiently oxidize fatty acids to acetyl-CoA. The subsequent conversion of acetyl-CoA to citrate and acetyl-carnitine in anaplerotic reactions taking place within peroxisomes of "young" cells promotes the replenishment of tricarboxylic acid (TCA) cycle intermediates destined for mitochondria [309] (Figure 4.3A; path 33). The resulting stimulation of the TCA cycle and electron transport chain (ETC) in mitochondria of these cells allows these

organelles to maintain ROS at sub-lethal levels that turn on expression of many nuclear genes required for decelerating cellular aging (Figure 4.1; path 10). A progressive decrease in the efficacy of peroxisomal import of Fox1, Fox2, and Fox3 with the replicative and chronological age of a eukaryotic cell slows down fatty acid oxidation and anaplerotic reactions in peroxisomes, thereby diminishing the TCA cycle and ETC in mitochondria of "old" cells [309] (Figure 4.3B; path 34). This, in turn, leads to an age-related decline in $\Delta\psi_m$ and causes a fragmentation of mitochondria by promoting fission of a mitochondrial network [304]. The resulting release of cytochrome *c* (and, perhaps, of other pro-apoptotic proteins) from fragmented mitochondria in "old" cells triggers an age-related form of apoptotic cell death [304] (Figure 4.3B).

The age-related deterioration of peroxisomal import of Fox1, Fox2, and Fox3 seen in "old" cells ultimately suppresses peroxisomal oxidation of fatty acids that originate from triacylglycerols (TAG) synthesized in the ER and then deposited within lipid droplets (LD) [304, 347] (Figure 4.3B). This initiates several negative feedback loops that reduce lipolysis of TAG in LD and their biosynthesis in the ER, thus causing the excessive accumulation of fatty acids and diacylglycerol both in the ER and LD [304, 347] (Figure 4.3B; path 35). Such remodeling of lipid dynamics promotes cellular aging and accelerates the onset an age-related form of necrotic cell death [304, 344] (Figure 4.3B).

Peroxisomal polyamine oxidase in "young" cells is involved in the synthesis of spermidine, a polyamine whose intracellular level substantially declines with the replicative and chronological age of a eukaryotic cell [348, 349] (Figure 4.3A). Spermidine has been shown to delay cellular aging in evolutionarily distant organisms by stimulating an anti-aging process of lysosome/vacuole-dependent autophagy [348] (Figure 4.3A; path 36).

In addition to its essential roles in yeast peroxisomal protein import, ER-derived pre-peroxisomal vesicle fusion, and cell differentiation [306], the predominantly peroxisomal protein Pex6 is also involved in sequestering dysfunctional mitochondria in replicatively "old" mother cells and/or segregating only functional mitochondria to their replicatively "young" budding progeny [350]. The ability of Pex6 to regulate replicative aging of yeast cells by ensuring the age-related asymmetrical segregation of functional mitochondria between mother and daughter cells is likely due to its involvement in mitochondrial import of Atp2, a β-subunit of the F_1 sector of mitochondrial F_0, F_1-ATP synthase [350]. It has been suggested that a mechanism underlying the essential contribution of peroxisome-associated pool of Pex6 to mitochondrial import of Atp2p

and to the maintenance of age asymmetry between the mother and daughter cells with respect to segregation of functional mitochondria may involve a recently discovered mitochondria-to-peroxisome vesicular traffic [306] (Figure 4.3A; path 37).

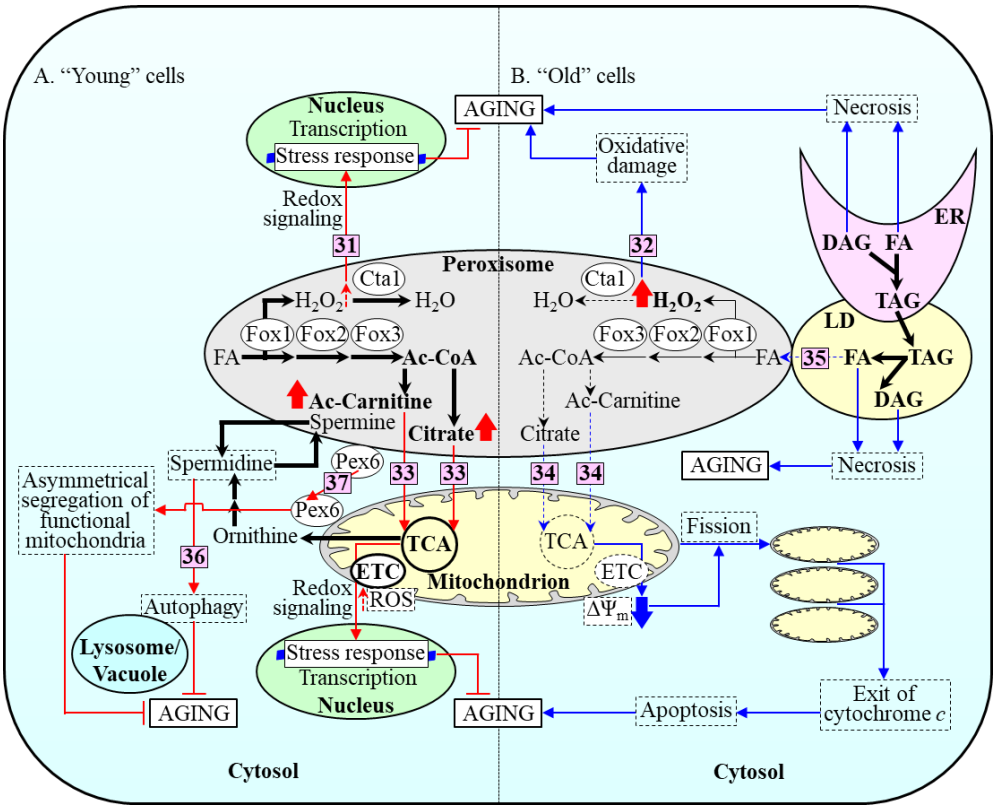

Figure 4.3. Age-related changes in the rates and efficiencies of several processes taking place in peroxisomes modulate the rates and efficiencies with which these organelles generate and/or release certain molecular signals. (A) In replicatively and chronologically "young" cells, these signals activate anti-aging processes in several other cellular compartments. (B) In replicatively and chronologically "old" cells, such signals activate pro-aging processes in other cellular locations. Activation arrows and inhibition bars denote pro-aging processes (displayed in blue color) or anti-aging processes (displayed in red color). Please see text for additional details. Ac-Carnitine, acetyl-carnitine; DAG, diacylglycerol; ER, endoplasmic reticulum; ETC, electron transport chain; FA, fatty acids; LD, lipid droplet; ROS, reactive oxygen species; TAG, triacylglycerols; TCA, tricarboxylic acid cycle; ΔΨm, electrochemical potential across the inner mitochondrial membrane.

4.3 A model of an intricate network of intercompartmental communications underlying cellular aging

A body of evidence summarized here and elsewhere [306, 309] suggests a depicted schematically in Figure 4.4 model for an intricate network of intercompartmental (i.e., organelle-organelle and organelle-cytosol) communications that underlies cellular aging in evolutionarily

distant organisms. The presented in Figure 4.4 model summarizes Figures 4.1 to 4.3, and each path in Figure 4.4 is numbered as in Figures 4.1, 4.2 or 4.3. In my model, the network integrates unidirectional communications between 1) mitochondria and the nucleus (Figure 4.4; paths 1, 3, 5-14 and 22); 2) peroxisomes and the nucleus (Figure 4.4; path 31); 3) lysosomes/vacuoles and the nucleus (Figure 4.4; paths 27 and 28); 4) mitochondria and lysosomes/vacuoles (Figure 4.4; paths 2, 4, 20 and 21); 5) peroxisomes and mitochondria (Figure 4.4; paths 33, 34 and 37); 6) mitochondria and the ER (Figure 4.4; path 19); 7) mitochondria and the plasma membrane (Figure 4.4; path 15); 8) the cytosol and the nucleus (Figure 4.4; path 26); and 9) peroxisomes and the cytosol (Figure 4.4; path 32). Mitochondria and the cytosol (Figure 4.4; paths 16-18, 25 and 29) as well as lysosomes/vacuoles and the cytosol (Figure 4.4; paths 23, 24, 27, 28, 30 and 36) are also involved in bidirectional communications within the network underlying cellular aging. As outlined in the previous section, these unidirectional and bidirectional communications between different cellular compartments integrated into the network operate as a flow of certain soluble metabolites, peptides, proteins and DNA fragments. Moreover, the ER, LD and peroxisomes establish zones of close apposition. Within the network underlying cellular aging, these three organelles communicate via unidirectional flow of several lipid species; this lipid flow is under the stringent control of several negative feedback loops [304, 344, 347] (Figure 4.4; path 35).

The central tenet of the depicted in Figure 4.4 model is that the numerous directed, coordinated and regulated organelle-organelle and organelle-cytosol communications integrated into the network are essential for the development of a pro- or anti-aging cellular pattern. Thus, this network of intercompartmental communications plays a critical role in regulating cellular aging by programming the long-term viability of a eukaryotic cell.

4.4 Conclusions and future perspectives

Emergent evidence supports the view that numerous directed, coordinated and regulated organelle-organelle and organelle-cytosol communications within a eukaryotic cell are integrated into an intricate network critical for regulating cellular aging. The challenge remains to define molecular mechanisms underlying the various pathways of intercompartmental communications constituting this network. Future work will aim at understanding how age-related intracellular stresses and environmental factors influence the spatiotemporal dynamics of the entire network and how the network defines the long-term viability of a eukaryotic cell. This knowledge may

reveal novel targets for anti-aging dietary and pharmacological interventions that can slow down cellular and organismal aging by modulating information flow along the pathways of multidirectional intercompartmental communications within the network.

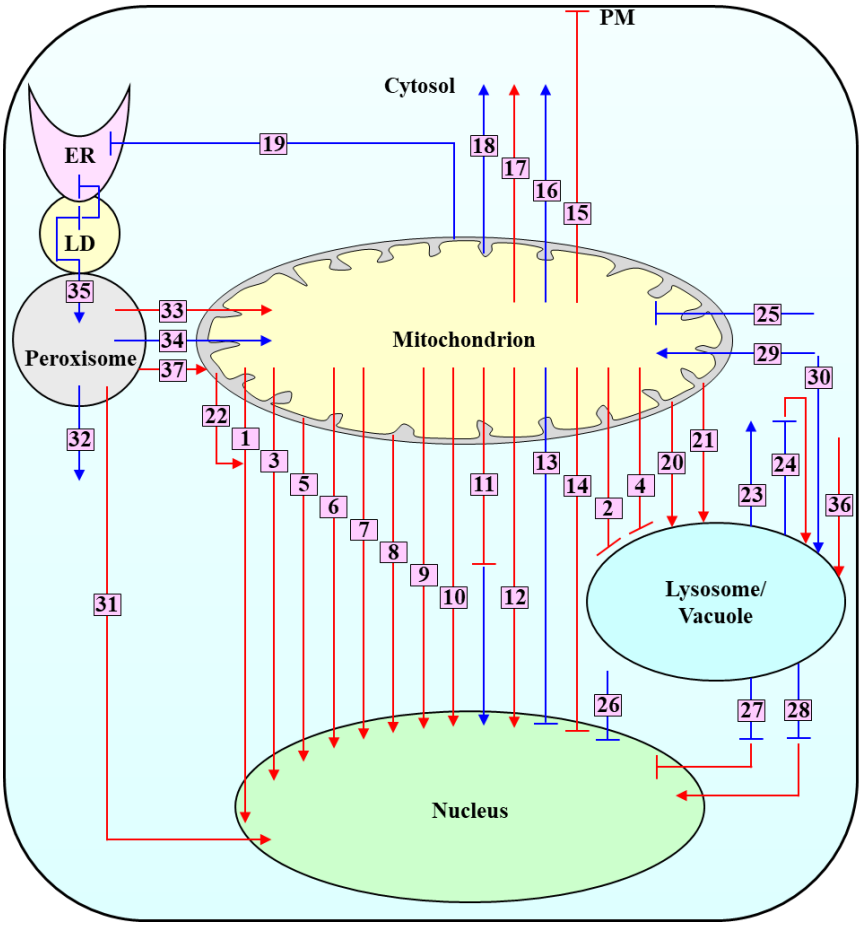

Figure 4.4. A model of an intricate network of organelle-organelle and organelle-cytosol communications underlying cellular aging. The model summarizes Figures 4.1 to 4.3, and each path is numbered as in Figures 4.1, 4.2 or 4.3. By defining the long-term viability of a eukaryotic cell, this network of intercompartmental communications plays an essential role in regulating cellular aging. Activation arrows and inhibition bars denote pro-aging processes (displayed in blue color) or anti-aging processes (displayed in red color). Please see text for additional details. ER, endoplasmic reticulum; LD, lipid droplet; PM, plasma membrane.

5 Future Directions

One challenge for the future is to define molecular mechanisms underlying the LCA-driven remodeling of mitochondrial lipidome and proteome. Our previous findings suggested a hypothesis in which LCA may cause such remodeling of mitochondrial lipidome by 1) slowing down the Psd1-dependent reaction of the synthesis of PE from PS in the IMM and/or OMM; 2) decelerating the Crd1-dependent reaction of CL synthesis from PG in the IMM; and 3) attenuating a negative feedback loop that involves a CL-dependent inhibition of PA transport from the OMM across the IMS to the IMM, which is catalyzed by the Ups1/Mdm35 protein complex (Figure 2.1) [81]. Studies aimed at testing this hypothesis are currently in progress in the Titorenko laboratory.

Furthermore, we previously demonstrated that LCA causes major changes not only in mitochondrial membrane lipidome but also in the size, number and morphology of mitochondria [81]. One could envision that these LCA-driven changes in mitochondrial abundance and morphology may affect mitochondrial protein import, folding, assembly and other aspects of mitochondrial proteostasis, thereby altering mitochondrial proteome. The ongoing studies in the Titorenko laboratory address the validity of this assumption.

Moreover, it will be important to test my hypothesis that CR decelerates the differentiation and maintenance programs of G_Q^{LD} and G_Q^{HD} cells (respectively) because this low-calorie diet modulates the above-mentioned set of longevity-defining processes. To test this hypothesis, it will be essential to assess how genetic interventions impairing each of these processes may influence the chronological age-related relative abundance of G_Q^{HD}, G_Q^{LD}, G_{NQ}^{HD} and G_{NQ}^{LD} subpopulations in CR and non-CR yeast cultures. It will be also interesting to examine how these genetic interventions may affect longevity of chronologically aging yeast under CR and non-CR conditions.

Another challenge for the future is to explore how genetic and pharmacological interventions known to delay yeast chronological aging by modulating a network of certain signaling pathways and protein kinases may impinge on the described here mechanism that links cellular aging to cell cycle regulation, maintenance of the Q state, entry into the NQ state and survival in the NQ state. This network integrates the TORC1, PKA, Snf1 and Pho85 core hubs of the signaling network of quiescence, as well as their downstream effector proteins Sch9, Rim15 and others [84, 95, 97, 104, 111, 252, 283, 295-300].

References

1. Fontana L, Partridge L, Longo VD. Extending healthy life span - from yeast to humans. Science 2010; 328:321-6.

2. Kaeberlein M. Lessons on longevity from budding yeast. Nature 2010; 464:513-9.

3. Longo VD, Shadel GS, Kaeberlein M, Kennedy B. Replicative and chronological aging in Saccharomyces cerevisiae. Cell Metab 2012; 16:18-31.

4. Arlia-Ciommo A, Leonov A, Piano A, Svistkova V, Titorenko VI. Cell-autonomous mechanisms of chronological aging in the yeast Saccharomyces cerevisiae. Microbial Cell 2014; 1:164-78.

5. Denoth Lippuner A, Julou T, Barral Y. Budding yeast as a model organism to study the effects of age. FEMS Microbiol Rev 2014; 38:300-25.

6. Eisenberg T, Knauer H, Schauer A, Büttner S, Ruckenstuhl C, Carmona-Gutierrez D, Ring J, Schroeder S, Magnes C, Antonacci L, Fussi H, Deszcz L, Hartl R, Schraml E, Criollo A, Megalou E, Weiskopf D, Laun P, Heeren G, Breitenbach M, Grubeck-Loebenstein B, Herker E, Fahrenkrog B, Fröhlich KU, Sinner F, Tavernarakis N, Minois N, Kroemer G, Madeo F. Induction of autophagy by spermidine promotes longevity. Nat Cell Biol 2009; 11:1305-14.

7. Goldberg AA, Richard VR, Kyryakov P, Bourque SD, Beach A, Burstein MT, Glebov A, Koupaki O, Boukh-Viner T, Gregg C, Juneau M, English AM, Thomas DY, Titorenko VI. Chemical genetic screen identifies lithocholic acid as an anti-aging compound that extends yeast chronological life span in a TOR-independent manner, by modulating housekeeping longevity assurance processes. Aging (Albany NY) 2010; 2:393-414.

8. Minois N, Carmona-Gutierrez D, Madeo F. Polyamines in aging and disease. Aging (Albany NY) 2011; 3:716-32.

9. Titorenko VI, Terlecky SR. Peroxisome metabolism and cellular aging. Traffic 2011; 12:252-9.

10. Beach A, Burstein MT, Richard VR, Leonov A, Levy S, Titorenko VI. Integration of peroxisomes into an endomembrane system that governs cellular aging. Front Physiol 2012; 3:283.

11. Jazwinski SM. The retrograde response and other pathways of interorganelle communication in yeast replicative aging. Subcell Biochem 2012; 57:79-100.

12. Longo VD, Fabrizio P. Chronological aging in Saccharomyces cerevisiae. Subcell Biochem 2012; 57:101-21.

13. Piper PW. Maximising the yeast chronological lifespan. Subcell Biochem 2012; 57:145-59.

14. Sutphin GL, Olsen BA, Kennedy BK, Kaeberlein M. Genome-wide analysis of yeast aging. Subcell Biochem 2012; 57:251-89.

15. Beach A, Titorenko VI. Essential roles of peroxisomally produced and metabolized biomolecules in regulating yeast longevity. Subcell Biochem 2013; 69:153-67.

16. Jazwinski SM. The retrograde response: when mitochondrial quality control is not enough. Biochim Biophys Acta 2013; 1833:400-9.

17. Leonov A, Titorenko VI. (2013). A network of interorganellar communications underlies cellular aging. IUBMB Life; 2013; 65:665-74.

18. de Cabo R, Carmona-Gutierrez D, Bernier M, Hall MN, Madeo F. The search for antiaging interventions: from elixirs to fasting regimens. Cell 2014; 157:1515-26.

19. Hubbard BP, Sinclair DA. Small molecule SIRT1 activators for the treatment of aging and age-related diseases. Trends Pharmacol Sci 2014; 35:146-54.

20. Nyström T, Liu B. Protein quality control in time and space - links to cellular aging. FEMS Yeast Res 2014; 14:40-8.

21. Nyström T, Liu B. The mystery of aging and rejuvenation - a budding topic. Curr Opin Microbiol 2014; 18:61-7.

22. López-Otín C, Blasco MA, Partridge L, Serrano M, Kroemer G. The hallmarks of aging. Cell. 2013; 153:1194-1217.

23. Nunnari J, Suomalainen A. Mitochondria: in sickness and in health. Cell. 2012; 148:1145-1159.

24. Vafai SB, Mootha VK. Mitochondrial disorders as windows into an ancient organelle. Nature. 2012; 491:374-383.

25. Pagliarini DJ, Rutter J. Hallmarks of a new era in mitochondrial biochemistry. Genes Dev. 2013; 27:2615-2627.

26. Chandel NS. Mitochondria as signaling organelles. BMC Biol. 2014; 12:34.

27. Shadel GS, Horvath TL. Mitochondrial ROS signaling in organismal homeostasis. Cell. 2015; 163:560-569.

28. Mishra P, Chan DC. Metabolic regulation of mitochondrial dynamics. J Cell Biol. 2016; 212:379-387.

29. Picard M, Wallace DC, Burelle Y. The rise of mitochondria in medicine. Mitochondrion. 2016; 30:105-116.

30. Schrepfer E, Scorrano L. Mitofusins, from Mitochondria to Metabolism. Mol Cell. 2016; 61:683-694.

31. Vyas S, Zaganjor E, Haigis MC. Mitochondria and Cancer. Cell. 2016; 166:555-566.

32. Longo VD, Shadel GS, Kaeberlein M, Kennedy B. Replicative and chronological aging in *Saccharomyces cerevisiae*. Cell Metab. 2012; 16:18-31.

33. Arlia-Ciommo A, Leonov A, Piano A, Svistkova V, Titorenko VI. Cell-autonomous mechanisms of chronological aging in the yeast *Saccharomyces cerevisiae*. Microbial Cell. 2014; 1:164-178.

34. Beach A, Leonov A, Arlia-Ciommo A, Svistkova V, Lutchman V, Titorenko VI. Mechanisms by which different functional states of mitochondria define yeast longevity. Int J Mol Sci. 2015; 16:5528-5554.

35. Jazwinski SM. Mitochondria to nucleus signaling and the role of ceramide in its integration into the suite of cell quality control processes during aging. Ageing Res Rev. 2015; 23:67-74.

36. Ruetenik A, Barrientos A. Dietary restriction, mitochondrial function and aging: from yeast to humans. Biochim Biophys Acta. 2015; 1847:1434-1447.

37. Bonawitz ND, Chatenay-Lapointe M, Pan Y, Shadel GS. Reduced TOR signaling extends chronological life span via increased respiration and upregulation of mitochondrial gene expression. Cell Metab. 2007; 5:265-277.

38. Goldberg AA, Bourque SD, Kyryakov P, Gregg C, Boukh-Viner T, Beach A, Burstein MT, Machkalyan G, Richard V, Rampersad S, Cyr D, Milijevic S, Titorenko VI. Effect of calorie restriction on the metabolic history of chronologically aging yeast. Exp Gerontol. 2009; 44:555-571.

39. Pan Y, Shadel GS. Extension of chronological life span by reduced TOR signaling requires down-regulation of Sch9p and involves increased mitochondrial OXPHOS complex density. Aging (Albany NY). 2009; 1:131-145.

40. Veatch JR, McMurray MA, Nelson ZW, Gottschling DE. Mitochondrial dysfunction leads to nuclear genome instability via an iron-sulfur cluster defect. Cell. 2009; 137:1247-1258.

41. Goldberg AA, Richard VR, Kyryakov P, Bourque SD, Beach A, Burstein MT, Glebov A, Koupaki O, Boukh-Viner T, Gregg C, Juneau M, English AM, Thomas DY, Titorenko VI. Chemical genetic screen identifies lithocholic acid as an anti-aging compound that extends yeast chronological life span in a TOR-independent manner, by modulating housekeeping longevity assurance processes. Aging (Albany NY). 2010; 2:393-414.

42. Pan Y, Schroeder EA, Ocampo A, Barrientos A, Shadel GS. Regulation of yeast chronological life span by TORC1 via adaptive mitochondrial ROS signaling. Cell Metab. 2011; 13:668-678.

43. Ocampo A, Liu J, Schroeder EA, Shadel GS, Barrientos A. Mitochondrial respiratory thresholds regulate yeast chronological life span and its extension by caloric restriction. Cell Metab. 2012; 16:55-67.

44. McFaline-Figueroa JR, Vevea J, Swayne TC, Zhou C, Liu C, Leung G, Boldogh IR, Pon LA. Mitochondrial quality control during inheritance is associated with lifespan and mother-daughter age asymmetry in budding yeast. Aging Cell. 2011; 10:885-895.

45. Hughes AL, Gottschling DE. An early age increase in vacuolar pH limits mitochondrial function and lifespan in yeast. Nature. 2012; 492:261-265.

46. Fehrmann S, Paoletti C, Goulev Y, Ungureanu A, Aguilaniu H, Charvin G. Aging yeast cells undergo a sharp entry into senescence unrelated to the loss of mitochondrial membrane potential. Cell Rep. 2013; 5:1589-1599.

47. Knorre DA, Popadin KY, Sokolov SS, Severin FF. Roles of mitochondrial dynamics under stressful and normal conditions in yeast cells. Oxid Med Cell Longev. 2013; 2013:139491.

48. Leonov A, Titorenko VI. A network of interorganellar communications underlies cellular aging. IUBMB Life. 2013; 65:665-674.

49. Schroeder EA, Raimundo N, Shadel GS. Epigenetic silencing mediates mitochondria stress-induced longevity. Cell Metab. 2013; 17:954-964.

50. Denoth Lippuner A, Julou T, Barral Y. Budding yeast as a model organism to study the effects of age. FEMS Microbiol Rev. 2014; 38:300-325.

51. Nyström T, Liu B. Protein quality control in time and space - links to cellular aging. FEMS Yeast Res. 2014; 14:40-48.

52. Sorokin MI, Knorre DA, Fedor F, Severin FF. Early manifestations of replicative aging in the yeast *Saccharomyces cerevisiae*. Microbial Cell 2014; 1:37-42.

53. Schroeder EA, Shadel GS. Crosstalk between mitochondrial stress signals regulates yeast chronological lifespan. Mech Ageing Dev. 2014; 135:41-49.

54. da Cunha FM, Torelli NQ, Kowaltowski AJ. Mitochondrial Retrograde Signaling: Triggers, Pathways, and Outcomes. Oxid Med Cell Longev. 2015; 2015:482582.

55. Dakik P, Titorenko VI. Communications between Mitochondria, the Nucleus, Vacuoles, Peroxisomes, the Endoplasmic Reticulum, the Plasma Membrane, Lipid Droplets, and the Cytosol during Yeast Chronological Aging. Front Genet. 2016; 7:177.

56. Perocchi F, Jensen LJ, Gagneur J, Ahting U, von Mering C, Bork P, Prokisch H, Steinmetz LM. Assessing systems properties of yeast mitochondria through an interaction map of the organelle. PLoS Genet. 2006; 2: e170.

57. Koppen M, Langer T. Protein degradation within mitochondria: versatile activities of AAA proteases and other peptidases. Crit Rev Biochem Mol Biol. 2007; 42:221-242.

58. Heeren G, Rinnerthaler M, Laun P, von Seyerl P, Kössler S, Klinger H, Hager M, Bogengruber E, Jarolim S, Simon-Nobbe B, Schüller C, Carmona-Gutierrez D, Breitenbach-Koller L, Mück C, Jansen-Dürr P, Criollo A, Kroemer G, Madeo F, Breitenbach M. The mitochondrial ribosomal protein of the large subunit, Afo1p, determines cellular longevity through mitochondrial back-signaling via TOR1. Aging (Albany NY). 2009; 1:622-636.

59. Merz S, Westermann B. Genome-wide deletion mutant analysis reveals genes required for respiratory growth, mitochondrial genome maintenance and mitochondrial protein synthesis in Saccharomyces cerevisiae. Genome Biol. 2009; 10: R95.

60. Baker MJ, Tatsuta T, Langer T. Quality control of mitochondrial proteostasis. Cold Spring Harb Perspect Biol. 2011; 3: a007559.

61. Caballero A, Ugidos A, Liu B, Öling D, Kvint K, Hao X, Mignat C, Nachin L, Molin M, Nyström T. Absence of mitochondrial translation control proteins extends life span by activating sirtuin-dependent silencing. Mol Cell. 2011; 42:390-400.

62. Chen XJ. The search for nonconventional mitochondrial determinants of aging. Mol Cell. 2011; 42:271-273.

63. Breitenbach M, Laun P, Dickinson JR, Klocker A, Rinnerthaler M, Dawes IW, Aung-Htut MT, Breitenbach-Koller L, Caballero A, Nyström T, Büttner S, Eisenberg T, Madeo F, Ralser M. The role of mitochondria in the aging processes of yeast. Subcell Biochem. 2012; 57:55-78.

64. Delaney JR, Ahmed U, Chou A, Sim S, Carr D, Murakami CJ, Schleit J, Sutphin GL, An EH, Castanza A, Fletcher M, Higgins S, Jelic M, Klum S, Muller B, Peng ZJ, Rai D, Ros V, Singh M, Wende HV, Kennedy BK, Kaeberlein M. Stress profiling of longevity mutants identifies Afg3 as

a mitochondrial determinant of cytoplasmic mRNA translation and aging. Aging Cell. 2013; 12:156-166.

65. Yang JS, Kim J, Park S, Jeon J, Shin YE, Kim S. Spatial and functional organization of mitochondrial protein network. Sci Rep. 2013; 3:1403.

66. Arlia-Ciommo A, Piano A, Leonov A, Svistkova V, Titorenko VI. Quasi-programmed aging of budding yeast: a trade-off between programmed processes of cell proliferation, differentiation, stress response, survival and death defines yeast lifespan. Cell Cycle. 2014; 13:3336-3349.

67. Perić M, Dib PB, Dennerlein S, Musa M, Rudan M, Lovrić A, Nikolić A, Šarić A, Sobočanec S, Mačak Ž, Raimundo N, Kriško A. Crosstalk between cellular compartments protects against proteotoxicity and extends lifespan. Sci Rep. 2016; 6:28751.

68. Suhm T, Ott M. Mitochondrial translation and cellular stress response. Cell Tissue Res. 2017; 367:21-31.

69. Veatch JR, McMurray MA, Nelson ZW, Gottschling DE. Mitochondrial dysfunction leads to nuclear genome instability via an iron-sulfur cluster defect. Cell. 2009; 137:1247-1258.

70. Xu XM, Møller SG. Iron-sulfur clusters: biogenesis, molecular mechanisms, and their functional significance. Antioxid Redox Signal. 2011; 15:271-307.

71. Gottschling DE. Molecular biology. Fragile delivery to the genome. Science. 2012; 337:160-161.

72. Crespo JL, Powers T, Fowler B, Hall MN. The TOR-controlled transcription activators GLN3, RTG1, and RTG3 are regulated in response to intracellular levels of glutamine. Proc Natl Acad Sci USA. 2002; 99:6784-6789.

73. Schmidt M, Kennedy BK. Aging: one thing leads to another. Curr Biol. 2012; 22: R1048-

R1051.

74. Jewell JL, Russell RC, Guan KL. Amino acid signalling upstream of mTOR. Nat Rev Mol Cell Biol. 2013; 14:133-139.

75. Conrad M, Schothorst J, Kankipati HN, Van Zeebroeck G, Rubio-Texeira M, Thevelein JM. Nutrient sensing and signaling in the yeast *Saccharomyces cerevisiae*. FEMS Microbiol Rev. 2014; 38:254-299.

76. Shimobayashi M, Hall MN. Making new contacts: the mTOR network in metabolism and signalling crosstalk. Nat Rev Mol Cell Biol. 2014; 15:155-162.

77. Swinnen E, Ghillebert R, Wilms T, Winderickx J. Molecular mechanisms linking the evolutionary conserved TORC1-Sch9 nutrient signalling branch to lifespan regulation in *Saccharomyces cerevisiae*. FEMS Yeast Res. 2014; 14:17-32.

78. Barral Y. A new answer to old questions. Elife. 2013; 2: e00515.

79. Brandes N, Tienson H, Lindemann A, Vitvitsky V, Reichmann D, Banerjee R, Jakob U. Time line of redox events in aging postmitotic cells. Elife. 2013; 2: e00306.

80. Burstein MT, Kyryakov P, Beach A, Richard VR, Koupaki O, Gomez-Perez A, Leonov A, Levy S, Noohi F, Titorenko VI. Lithocholic acid extends longevity of chronologically aging yeast only if added at certain critical periods of their lifespan. Cell Cycle. 2012; 11:3443-3462.

81. Beach A, Richard VR, Leonov A, Burstein MT, Bourque SD, Koupaki O, Juneau M, Feldman R, Iouk T, Titorenko VI. Mitochondrial membrane lipidome defines yeast longevity. Aging (Albany NY). 2013; 5:551-574.

82. Beach A, Richard VR, Bourque S, Boukh-Viner T, Kyryakov P, Gomez-Perez A, Arlia-Ciommo A, Feldman R, Leonov A, Piano A, Svistkova V, Titorenko VI. Lithocholic bile acid

accumulated in yeast mitochondria orchestrates a development of an anti-aging cellular pattern by causing age-related changes in cellular proteome. Cell Cycle. 2015; 14:1643-1656.

83. Medkour Y, Titorenko VI. Mitochondria operate as signaling platforms in yeast aging. Aging (Albany NY). 2016; 8:212-213.

84. Longo VD, Shadel GS, Kaeberlein M, Kennedy B. Replicative and chronological aging in Saccharomyces cerevisiae. Cell Metab. 2012; 16:18-31.

85. Arlia-Ciommo A, Leonov A, Piano A, Svistkova V, Titorenko VI. Cell-autonomous mechanisms of chronological aging in the yeast Saccharomyces cerevisiae. Microb Cell. 2014; 1:163-178.

86. Sinclair DA. Toward a unified theory of caloric restriction and longevity regulation. Mech Ageing Dev. 2005; 126:987-1002.

87. Goldberg AA, Bourque SD, Kyryakov P, Gregg C, Boukh-Viner T, Beach A, Burstein MT, Machkalyan G, Richard V, Rampersad S, Cyr D, Milijevic S, Titorenko VI. Effect of calorie restriction on the metabolic history of chronologically aging yeast. Exp Gerontol. 2009; 44:555-71.

88. Allen C, Büttner S, Aragon AD, Thomas JA, Meirelles O, Jaetao JE, Benn D, Ruby SW, Veenhuis M, Madeo F, Werner-Washburne M. Isolation of quiescent and nonquiescent cells from yeast stationary-phase cultures. J Cell Biol. 2006; 174:89-100.

89. Davidson GS, Joe RM, Roy S, Meirelles O, Allen CP, Wilson MR, Tapia PH, Manzanilla EE, Dodson AE, Chakraborty S, Carter M, Young S, Edwards B, et al. The proteomics of quiescent and nonquiescent cell differentiation in yeast stationary-phase cultures. Mol Biol Cell. 2011; 22:988-98.

90. Werner-Washburne M, Roy S, Davidson GS. Aging and the survival of quiescent and non-quiescent cells in yeast stationary-phase cultures. Subcell Biochem. 2012; 57:123-43.

91. Miles S, Li L, Davison J, Breeden LL. Xbp1 directs global repression of budding yeast transcription during the transition to quiescence and is important for the longevity and reversibility of the quiescent state. PLoS Genet. 2013; 9:e1003854.

92. Gray JV, Petsko GA, Johnston GC, Ringe D, Singer RA, Werner-Washburne M. "Sleeping beauty": quiescence in Saccharomyces cerevisiae. Microbiol Mol Biol Rev. 2004; 68:187-206.

93. Aragon AD, Rodriguez AL, Meirelles O, Roy S, Davidson GS, Tapia PH, Allen C, Joe R, Benn D, Werner-Washburne M. Characterization of differentiated quiescent and nonquiescent cells in yeast stationary-phase cultures. Mol Biol Cell. 2008; 19:1271-80.

94. Li L, Miles S, Melville Z, Prasad A, Bradley G, Breeden LL. Key events during the transition from rapid growth to quiescence in budding yeast require posttranscriptional regulators. Mol Biol Cell. 2013; 24:3697-709.

95. Smets B, Ghillebert R, De Snijder P, Binda M, Swinnen E, De Virgilio C, Winderickx J. Life in the midst of scarcity: adaptations to nutrient availability in Saccharomyces cerevisiae. Curr Genet. 2010; 56:1-32.

96. Broach JR. Nutritional control of growth and development in yeast. Genetics. 2012; 192:73-105.

97. De Virgilio C. The essence of yeast quiescence. FEMS Microbiol Rev. 2012; 36:306-39.

98. Conrad M, Schothorst J, Kankipati HN, Van Zeebroeck G, Rubio-Texeira M, Thevelein JM. Nutrient sensing and signaling in the yeast Saccharomyces cerevisiae. FEMS Microbiol Rev. 2014; 38:254-99.

99. Swinnen E, Ghillebert R, Wilms T, Winderickx J. Molecular mechanisms linking the evolutionary conserved TORC1-Sch9 nutrient signalling branch to lifespan regulation in Saccharomyces cerevisiae. FEMS Yeast Res. 2014; 14:17-32.

100. Honigberg SM. Similar environments but diverse fates: Responses of budding yeast to nutrient deprivation. Microb Cell. 2016; 3:302-328.

101. Wanke V, Pedruzzi I, Cameroni E, Dubouloz F, De Virgilio C. Regulation of G0 entry by the Pho80-Pho85 cyclin-CDK complex. EMBO J. 2005; 24:4271-8.

102. Cai L, Tu BP. Driving the cell cycle through metabolism. Annu Rev Cell Dev Biol. 2012; 28:59-87.

103. Reinders A, Bürckert N, Boller T, Wiemken A, De Virgilio C. Saccharomyces cerevisiae cAMP-dependent protein kinase controls entry into stationary phase through the Rim15p protein kinase. Genes Dev. 1998; 12:2943-55.

104. Fabrizio P, Pozza F, Pletcher SD, Gendron CM, Longo VD. Regulation of longevity and stress resistance by Sch9 in yeast. Science. 2001; 292:288-90.

105. Lenssen E, Oberholzer U, Labarre J, De Virgilio C, Collart MA. Saccharomyces cerevisiae Ccr4-Not complex contributes to the control of Msn2p-dependent transcription by the Ras/cAMP pathway. Mol Microbiol. 2002; 43:1023-37.

106. Pedruzzi I, Dubouloz F, Cameroni E, Wanke V, Roosen J, Winderickx J, De Virgilio C. TOR and PKA signaling pathways converge on the protein kinase Rim15 to control entry into G0. Mol Cell. 2003; 12:1607-13.

107. Lenssen E, James N, Pedruzzi I, Dubouloz F, Cameroni E, Bisig R, Maillet L, Werner M, Roosen J, Petrovic K, Winderickx J, Collart MA, De Virgilio C. The Ccr4-Not complex independently controls both Msn2-dependent transcriptional activation - via a newly identified

Glc7/Bud14 type I protein phosphatase module - and TFIID promoter distribution. Mol Cell Biol. 2005; 25:488-98.

108. Roosen J, Engelen K, Marchal K, Mathys J, Griffioen G, Cameroni E, Thevelein JM, De Virgilio C, De Moor B, Winderickx J. PKA and Sch9 control a molecular switch important for the proper adaptation to nutrient availability. Mol Microbiol. 2005; 55:862-80.

109. Cameroni E, Hulo N, Roosen J, Winderickx J, De Virgilio C. The novel yeast PAS kinase Rim 15 orchestrates G0-associated antioxidant defense mechanisms. Cell Cycle. 2004; 3:462-8.

110. Wanke V, Cameroni E, Uotila A, Piccolis M, Urban J, Loewith R, De Virgilio C. Caffeine extends yeast lifespan by targeting TORC1. Mol Microbiol. 2008; 69:277-85.

111. Wei M, Fabrizio P, Hu J, Ge H, Cheng C, Li L, Longo VD. Life span extension by calorie restriction depends on Rim15 and transcription factors downstream of Ras/PKA, Tor, and Sch9. PLoS Genet. 2008; 4: e13.

112. Zhang N, Wu J, Oliver SG. Gis1 is required for transcriptional reprogramming of carbon metabolism and the stress response during transition into stationary phase in yeast. Microbiology. 2009; 155:1690-8.

113. Talarek N, Cameroni E, Jaquenoud M, Luo X, Bontron S, Lippman S, Devgan G, Snyder M, Broach JR, De Virgilio C. Initiation of the TORC1-regulated G0 program requires Igo1/2, which license specific mRNAs to evade degradation via the 5'-3' mRNA decay pathway. Mol Cell. 2010; 38:345-55.

114. Luo X, Talarek N, De Virgilio C. Initiation of the yeast G0 program requires Igo1 and Igo2, which antagonize activation of decapping of specific nutrient-regulated mRNAs. RNA Biol. 2011; 8:14-7.

115. Urban J, Soulard A, Huber A, Lippman S, Mukhopadhyay D, Deloche O, Wanke V, Anrather D, Ammerer G, Riezman H, Broach JR, De Virgilio C, Hall MN, Loewith R. Sch9 is a major target of TORC1 in Saccharomyces cerevisiae. Mol Cell. 2007; 26:663-74.

116. Huber A, Bodenmiller B, Uotila A, Stahl M, Wanka S, Gerrits B, Aebersold R, Loewith R. Characterization of the rapamycin-sensitive phosphoproteome reveals that Sch9 is a central coordinator of protein synthesis. Genes Dev. 2009; 23:1929-43.

117. Lee J, Moir RD, Willis IM. Regulation of RNA polymerase III transcription involves SCH9-dependent and SCH9-independent branches of the target of rapamycin (TOR) pathway. J Biol Chem. 2009; 284:12604-8.

118. Wei Y, Zheng XF. Sch9 partially mediates TORC1 signaling to control ribosomal RNA synthesis. Cell Cycle. 2009; 8:4085-90.

119. Huber A, French SL, Tekotte H, Yerlikaya S, Stahl M, Perepelkina MP, Tyers M, Rougemont J, Beyer AL, Loewith R. Sch9 regulates ribosome biogenesis via Stb3, Dot6 and Tod6 and the histone deacetylase complex RPD3L. EMBO J. 2011; 30:3052-64.

120. Garrett S, Menold MM, Broach JR. The Saccharomyces cerevisiae YAK1 gene encodes a protein kinase that is induced by arrest early in the cell cycle. Mol Cell Biol. 1991; 11:4045-52.

121. Moriya H, Shimizu-Yoshida Y, Omori A, Iwashita S, Katoh M, Sakai A. Yak1p, a DYRK family kinase, translocates to the nucleus and phosphorylates yeast Pop2p in response to a glucose signal. Genes Dev. 2001; 15:1217-28.

122. Martin DE, Soulard A, Hall MN. TOR regulates ribosomal protein gene expression via PKA and the Forkhead transcription factor FHL1. Cell. 2004; 119:969-79.

123. Lee P, Cho BR, Joo HS, Hahn JS. Yeast Yak1 kinase, a bridge between PKA and stress-responsive transcription factors, Hsf1 and Msn2/Msn4. Mol Microbiol. 2008; 70:882-95.

124. Lee P, Paik SM, Shin CS, Huh WK, Hahn JS. Regulation of yeast Yak1 kinase by PKA and autophosphorylation-dependent 14-3-3 binding. Mol Microbiol. 2011; 79:633-46.

125. Lim MY, Dailey D, Martin GS, Thorner J. Yeast MCK1 protein kinase autophosphorylates at tyrosine and serine but phosphorylates exogenous substrates at serine and threonine. J Biol Chem. 1993; 268:21155-64.

126. Quan Z, Cao L, Tang Y, Yan Y, Oliver SG, Zhang N. The yeast GSK-3 homologue Mck1 is a key controller of quiescence entry and chronological lifespan. PloS Genet. 2015; 11: e1005282.

127. Cao L, Tang Y, Quan Z, Zhang Z, Oliver SG, Zhang N. Chronological lifespan in yeast is dependent on the accumulation of storage carbohydrates mediated by Yak1, Mck1 and Rim15 kinases. PLoS Genet. 2016; 12: e1006458.

128. Martínez-Pastor MT, Marchler G, Schüller C, Marchler-Bauer A, Ruis H, Estruch F. The Saccharomyces cerevisiae zinc finger proteins Msn2p and Msn4p are required for transcriptional induction through the stress response element (STRE). EMBO J. 1996; 15:2227-35.

129. Görner W, Durchschlag E, Martinez-Pastor MT, Estruch F, Ammerer G, Hamilton B, Ruis H, Schüller C. Nuclear localization of the C2H2 zinc finger protein Msn2p is regulated by stress and protein kinase A activity. Genes Dev. 1998; 12:586-97.

130. Beck T, Hall MN. The TOR signalling pathway controls nuclear localization of nutrient-regulated transcription factors. Nature. 1999; 402:689-92.

131. Estruch F. Stress-controlled transcription factors, stress-induced genes and stress tolerance in budding yeast. FEMS Microbiol Rev. 2000; 24:469-86.

132. Gasch AP, Spellman PT, Kao CM, Carmel-Harel O, Eisen MB, Storz G, Botstein D, Brown PO. Genomic expression programs in the response of yeast cells to environmental changes. Mol Biol Cell. 2000; 11:4241-57.

133. Pedruzzi I, Bürckert N, Egger P, De Virgilio C. Saccharomyces cerevisiae Ras / cAMP pathway controls post-diauxic shift element-dependent transcription through the zinc finger protein Gis1. EMBO J. 2000; 19:2569-79.

134. Görner W, Durchschlag E, Wolf J, Brown EL, Ammerer G, Ruis H, Schüller C. Acute glucose starvation activates the nuclear localization signal of a stress-specific yeast transcription factor. EMBO J. 2002; 21:135-44.

135. Mayordomo I, Estruch F, Sanz P. Convergence of the target of rapamycin and the Snf1 protein kinase pathways in the regulation of the subcellular localization of Msn2, a transcriptional activator of STRE (Stress Response Element)-regulated genes. J Biol Chem. 2002; 277:35650-6.

136. Jacquet M, Renault G, Lallet S, De Mey J, Goldbeter A. Oscillatory nucleocytoplasmic shuttling of the general stress response transcriptional activators Msn2 and Msn4 in Saccharomyces cerevisiae. J Cell Biol. 2003; 161:497-505.

137. De Wever V, Reiter W, Ballarini A, Ammerer G, Brocard C. A dual role for PP1 in shaping the Msn2-dependent transcriptional response to glucose starvation. EMBO J. 2005; 24:4115-23.

138. Galdieri L, Mehrotra S, Yu S, Vancura A. Transcriptional regulation in yeast during diauxic shift and stationary phase. OMICS. 2010; 14:629-38.

139. De Wever, Hahn JS, Hu Z, Thiele DJ, Iyer VR. Genome-wide analysis of the biology of stress responses through heat shock transcription factor. Mol Cell Biol. 2004; 24:5249-56.

140. Hahn JS, Thiele DJ. Activation of the Saccharomyces cerevisiae heat shock transcription factor under glucose starvation conditions by Snf1 protein kinase. J Biol Chem. 2004; 279:5169-76.

141. Burnie JP, Carter TL, Hodgetts SJ, Matthews RC. Fungal heat-shock proteins in human disease. FEMS Microbiol Rev. 2006; 30:53-88.

142. Eastmond DL, Nelson HC. Genome-wide analysis reveals new roles for the activation domains of the Saccharomyces cerevisiae heat shock transcription factor (Hsf1) during the transient heat shock response. J Biol Chem. 2006; 281:32909-21.

143. Bysani N, Daugherty JR, Cooper TG. Saturation mutagenesis of the UASNTR (GATAA) responsible for nitrogen catabolite repression-sensitive transcriptional activation of the allantoin pathway genes in Saccharomyces cerevisiae. J Bacteriol. 1991; 173:4977-82.

144. Blinder D, Magasanik B. Recognition of nitrogen-responsive upstream activation sequences of Saccharomyces cerevisiae by the product of the GLN3 gene. J Bacteriol. 1995; 177:4190-3.

145. Bertram PG, Choi JH, Carvalho J, Ai W, Zeng C, Chan TF, Zheng XF. Tripartite regulation of Gln3p by TOR, Ure2p, and phosphatases. J Biol Chem. 2000; 275:35727-33.

146. Bertram PG, Choi JH, Carvalho J, Chan TF, Ai W, Zheng XF. Convergence of TOR-nitrogen and Snf1-glucose signaling pathways onto Gln3. Mol Cell Biol. 2002; 22:1246-52.

147. Cox KH, Tate JJ, Cooper TG. Cytoplasmic compartmentation of Gln3 during nitrogen catabolite repression and the mechanism of its nuclear localization during carbon starvation in Saccharomyces cerevisiae. J Biol Chem. 2002; 277:37559-66.

148. Hardy TA, Roach PJ. Control of yeast glycogen synthase-2 by COOH-terminal phosphorylation. J Biol Chem. 1993; 268:23799-805.

149. Hardy TA, Huang D, Roach PJ. Interactions between cAMP-dependent and SNF1 protein kinases in the control of glycogen accumulation in Saccharomyces cerevisiae. J Biol Chem. 1994; 269:27907-13.

150. Ni HT, LaPorte DC. Response of a yeast glycogen synthase gene to stress. Mol Microbiol. 1995; 16:1197-205.

151. Huang D, Farkas I, Roach PJ. Pho85p, a cyclin-dependent protein kinase, and the Snf1p protein kinase act antagonistically to control glycogen accumulation in Saccharomyces cerevisiae. Mol Cell Biol. 1996; 16:4357-65.

152. Huang D, Moffat J, Wilson WA, Moore L, Cheng C, Roach PJ, Andrews B. Cyclin partners determine Pho85 protein kinase substrate specificity in vitro and in vivo: control of glycogen biosynthesis by Pcl8 and Pcl10. Mol Cell Biol. 1998; 18:3289-99.

153. Parrou JL, Enjalbert B, Plourde L, Bauche A, Gonzalez B, François J. Dynamic responses of reserve carbohydrate metabolism under carbon and nitrogen limitations in Saccharomyces cerevisiae. Yeast. 1999; 15:191-203.

154. Wilson WA, Mahrenholz AM, Roach PJ. Substrate targeting of the yeast cyclin-dependent kinase Pho85p by the cyclin Pcl10p. Mol Cell Biol. 1999; 19:7020-30.

155. Enjalbert B, Parrou JL, Teste MA, François J. Combinatorial control by the protein kinases PKA, PHO85 and SNF1 of transcriptional induction of the Saccharomyces cerevisiae GSY2 gene at the diauxic shift. Mol Genet Genomics. 2004; 271:697-708.

156. Kamada Y, Funakoshi T, Shintani T, Nagano K, Ohsumi M, Ohsumi Y. Tor-mediated induction of autophagy via an Apg1 protein kinase complex. J Cell Biol. 2000; 150:1507-13.

157. Wang Z, Wilson WA, Fujino MA, Roach PJ. Antagonistic controls of autophagy and glycogen accumulation by Snf1p, the yeast homolog of AMP-activated protein kinase, and the cyclin-dependent kinase Pho85p. Mol Cell Biol. 2001; 21:5742-52.

158. Budovskaya YV, Stephan JS, Reggiori F, Klionsky DJ, Herman PK. The Ras/cAMP-dependent protein kinase signaling pathway regulates an early step of the autophagy process in Saccharomyces cerevisiae. J Biol Chem. 2004; 279:20663-71.

159. Budovskaya YV, Stephan JS, Deminoff SJ, Herman PK. An evolutionary proteomics approach identifies substrates of the cAMP-dependent protein kinase. Proc Natl Acad Sci USA. 2005; 102:13933-8.

160. Kabeya Y, Kamada Y, Baba M, Takikawa H, Sasaki M, Ohsumi Y. Atg17 functions in cooperation with Atg1 and Atg13 in yeast autophagy. Mol Biol Cell. 2005; 16:2544-53.

161. Yorimitsu T, Zaman S, Broach JR, Klionsky DJ. Protein kinase A and Sch9 cooperatively regulate induction of autophagy in Saccharomyces cerevisiae. Mol Biol Cell. 2007; 18:4180-9.

162. Stephan JS, Yeh YY, Ramachandran V, Deminoff SJ, Herman PK. The Tor and PKA signaling pathways independently target the Atg1/Atg13 protein kinase complex to control autophagy. Proc Natl Acad Sci USA. 2009; 106:17049-54.

163. Kamada Y, Yoshino K, Kondo C, Kawamata T, Oshiro N, Yonezawa K, Ohsumi Y. Tor directly controls the Atg1 kinase complex to regulate autophagy. Mol Cell Biol. 2010; 30:1049-58.

164. Jorgensen P, Rupes I, Sharom JR, Schneper L, Broach JR, Tyers M. A dynamic transcriptional network communicates growth potential to ribosome synthesis and critical cell size. Genes Dev. 2004; 18:2491-505.

165. Marion RM, Regev A, Segal E, Barash Y, Koller D, Friedman N, O'Shea EK. Sfp1 is a stress- and nutrient-sensitive regulator of ribosomal protein gene expression. Proc Natl Acad Sci USA. 2004; 101:14315-22.

166. Cipollina C, van den Brink J, Daran-Lapujade P, Pronk JT, Porro D, de Winde JH. Saccharomyces cerevisiae SFP1: at the crossroads of central metabolism and ribosome biogenesis. Microbiology. 2008; 154:1686-99.

167. Cipollina C, van den Brink J, Daran-Lapujade P, Pronk JT, Vai M, de Winde JH. Revisiting the role of yeast Sfp1 in ribosome biogenesis and cell size control: a chemostat study. Microbiology. 2008; 154:337-46.

168. Lempiäinen H, Shore D. Growth control and ribosome biogenesis. Curr Opin Cell Biol. 2009; 21:855-63.

169. Lempiäinen H, Uotila A, Urban J, Dohnal I, Ammerer G, Loewith R, Shore D. Sfp1 interaction with TORC1 and Mrs6 reveals feedback regulation on TOR signaling. Mol Cell. 2009; 33:704-16.

170. Wei Y, Tsang CK, Zheng XF. Mechanisms of regulation of RNA polymerase III-dependent transcription by TORC1. EMBO J. 2009; 28:2220-30.

171. Cherkasova VA, Hinnebusch AG. Translational control by TOR and TAP42 through dephosphorylation of eIF2alpha kinase GCN2. Genes Dev. 2003; 17:859-72.

172. Cherkasova V, Qiu H, Hinnebusch AG. Snf1 promotes phosphorylation of the alpha subunit of eukaryotic translation initiation factor 2 by activating Gcn2 and inhibiting phosphatases Glc7 and Sit4. Mol Cell Biol. 2010; 30:2862-73.

173. Matheos DP, Kingsbury TJ, Ahsan US, Cunningham KW. Tcn1p/Crz1p, a calcineurin-dependent transcription factor that differentially regulates gene expression in Saccharomyces cerevisiae. Genes Dev. 1997; 11:3445-58.

174. Stathopoulos AM, Cyert MS. Calcineurin acts through the CRZ1/TCN1-encoded transcription factor to regulate gene expression in yeast. Genes Dev. 1997; 11:3432-44.

175. Yoshimoto H, Saltsman K, Gasch AP, Li HX, Ogawa N, Botstein D, Brown PO, Cyert MS. Genome-wide analysis of gene expression regulated by the calcineurin/Crz1p signaling pathway in Saccharomyces cerevisiae. J Biol Chem. 2002; 277:31079-88.

176. Kafadar KA, Cyert MS. Integration of stress responses: modulation of calcineurin signaling in Saccharomyces cerevisiae by protein kinase A. Eukaryot Cell. 2004; 3:1147-53.

177. Sopko R, Huang D, Preston N, Chua G, Papp B, Kafadar K, Snyder M, Oliver SG, Cyert M, Hughes TR, Boone C, Andrews B. Mapping pathways and phenotypes by systematic gene overexpression. Mol Cell. 2006; 21:319-30.

178. Mai B, Breeden L. Xbp1, a stress-induced transcriptional repressor of the Saccharomyces cerevisiae Swi4/Mbp1 family. Mol Cell Biol. 1997; 17:6491-501.

179. Weinberger M, Feng L, Paul A, Smith DL Jr, Hontz RD, Smith JS, Vujcic M, Singh KK, Huberman JA, Burhans WC. DNA replication stress is a determinant of chronological lifespan in budding yeast. PLoS One. 2007; 2: e748.

180. Bontron S, Jaquenoud M, Vaga S, Talarek N, Bodenmiller B, Aebersold R, De Virgilio C. Yeast endosulfines control entry into quiescence and chronological life span by inhibiting protein phosphatase 2A. Cell Rep. 2013; 3:16-22.

181. Juanes MA, Khoueiry R, Kupka T, Castro A, Mudrak I, Ogris E, Lorca T, Piatti S. Budding yeast greatwall and endosulfines control activity and spatial regulation of PP2A(Cdc55) for timely mitotic progression. PLoS Genet. 2013; 9:e1003575.

182. Sarkar S, Dalgaard JZ, Millar JB, Arumugam P. The Rim15-endosulfine-PP2ACdc55 signalling module regulates entry into gametogenesis and quiescence via distinct mechanisms in budding yeast. PLoS Genet. 2014; 10: e1004456.

183. Moreno-Torres M, Jaquenoud M, De Virgilio C. TORC1 controls G1-S cell cycle transition in yeast via Mpk1 and the greatwall kinase pathway. Nat Commun. 2015; 6:8256.

184. Moreno-Torres M, Jaquenoud M, Péli-Gulli MP, Nicastro R, De Virgilio C. TORC1 coordinates the conversion of Sic1 from a target to an inhibitor of cyclin-CDK-Cks1. Cell Discov. 2017; 3:17012.

185. Colman RJ, Anderson RM, Johnson SC, Kastman EK, Kosmatka KJ, Beasley TM, Allison DB, Cruzen C, Simmons HA, Kemnitz JW, Weindruch R. Caloric restriction delays disease onset and mortality in rhesus monkeys. Science. 2009; 325:201-4.

186. Fontana L, Partridge L, Longo VD. Extending healthy life span - from yeast to humans. Science. 2010; 328:321-6.

187. Colman RJ, Beasley TM, Kemnitz JW, Johnson SC, Weindruch R, Anderson RM. Caloric restriction reduces age-related and all-cause mortality in rhesus monkeys. Nat Commun. 2014; 5:3557.

188. de Cabo R, Carmona-Gutierrez D, Bernier M, Hall MN, Madeo F. The search for antiaging interventions: from elixirs to fasting regimens. Cell. 2014; 157:1515-26.

189. Lee C, Longo V. Dietary restriction with and without caloric restriction for healthy aging. F1000Res. 2016; 5: F1000 Faculty Rev-117.

190. Peters TW, Rardin MJ, Czerwieniec G, Evani US, Reis-Rodrigues P, Lithgow GJ, Mooney SD, Gibson BW, Hughes RE. Tor1 regulates protein solubility in Saccharomyces cerevisiae. Mol Biol Cell. 2012; 23:4679-88.

191. Richard VR, Bourque SD, Titorenko VI. Metabolomic and lipidomic analyses of chronologically aging yeast. Methods Mol Biol. 2014; 1205:359-373.

192. Connerth M, Tatsuta T, Haag M, Klecker T, Westermann B, Langer T. Intramitochondrial transport of phosphatidic acid in yeast by a lipid transfer protein. Science. 2012; 338:815-818.

193. Horvath SE, Daum G. Lipids of mitochondria. Prog Lipid Res. 2013; 52:590-614.

194. Baile MG, Lu YW, Claypool SM. The topology and regulation of cardiolipin biosynthesis and remodeling in yeast. Chem Phys Lipids. 2014; 179:25-31.

195. Aaltonen MJ, Friedman JR, Osman C, Salin B, di Rago JP, Nunnari J, Langer T, Tatsuta T. MICOS and phospholipid transfer by Ups2-Mdm35 organize membrane lipid synthesis in mitochondria. J Cell Biol. 2016; 213:525-534.

196. Miyata N, Watanabe Y, Tamura Y, Endo T, Kuge O. Phosphatidylserine transport by Ups2-Mdm35 in respiration-active mitochondria. J Cell Biol. 2016; 214:77-88.

197. Dimmer KS, Rapaport D. Mitochondrial contact sites as platforms for phospholipid exchange. Biochim Biophys Acta. 2017; 1862:69-80.

198. Mårtensson CU, Doan KN, Becker T. Effects of lipids on mitochondrial functions. Biochim Biophys Acta. 2017; 1862:102-113.

199. Tatsuta T, Langer T. Intramitochondrial phospholipid trafficking. Biochim Biophys Acta. 2017; 1862:81-89.

200. Watanabe Y, Tamura Y, Kawano S, Endo T. Structural and mechanistic insights into phospholipid transfer by Ups1-Mdm35 in mitochondria. Nat Commun. 2015; 6:7922.

201. Yu F, He F, Yao H, Wang C, Wang J, Li J, Qi X, Xue H, Ding J, Zhang P. Structural basis of intramitochondrial phosphatidic acid transport mediated by Ups1-Mdm35 complex. EMBO Rep. 2015; 16:813-823.

202. McMahon HT, Gallop JL. Membrane curvature and mechanisms of dynamic cell membrane remodelling. Nature. 2005; 438:590-596.

203. Zimmerberg J. Membrane biophysics. Curr Biol. 2006; 16: R272- R276.

204. van Meer G, Voelker DR, Feigenson GW. Membrane lipids: where they are and how they behave. Nat Rev Mol Cell Biol. 2008; 9:112-124.

205. Shibata Y, Hu J, Kozlov MM, Rapoport TA. Mechanisms shaping the membranes of cellular organelles. Annu Rev Cell Dev Biol. 2009; 25:329-354.

206. McMahon HT, Boucrot E. Membrane curvature at a glance. J Cell Sci. 2015; 128:1065-1070.

207. Jarsch IK, Daste F, Gallop JL. Membrane curvature in cell biology: An integration of molecular mechanisms. J Cell Biol. 2016; 214:375-387.

208. Clancey CJ, Chang SC, Dowhan W. Cloning of a gene (PSD1) encoding phosphatidylserine decarboxylase from Saccharomyces cerevisiae by complementation of an Escherichia coli mutant. J Biol Chem. 1993; 268:24580-24590.

209. Trotter PJ, Pedretti J, Voelker DR. Phosphatidylserine decarboxylase from Saccharomyces cerevisiae. Isolation of mutants, cloning of the gene, and creation of a null allele. J Biol Chem. 1993; 268:21416-21424.

210. Giorgio M, Trinei M, Migliaccio E, Pelicci PG. Hydrogen peroxide: a metabolic by-product or a common mediator of ageing signals? Nat Rev Mol Cell Biol. 2007; 8:722-728.

211. Fraenkel DG. Respiration. In: Fraenkel DG. Yeast intermediary metabolism. Cold Spring Harbor, NY: Cold Spring Harbor Laboratory Press, 2011:135-171.

212. Davidson GS, Joe RM, Roy S, Meirelles O, Allen CP, Wilson MR, Tapia PH, Manzanilla EE, Dodson AE, Chakraborty S, Carter M, Young S, Edwards B, et al. The proteomics of quiescent and nonquiescent cell differentiation in yeast stationary-phase cultures. Mol Biol Cell. 2011; 22:988-98.

213. Miles S, Li L, Davison J, Breeden LL. Xbp1 directs global repression of budding yeast transcription during the transition to quiescence and is important for the longevity and reversibility of the quiescent state. PLoS Genet. 2013; 9: e1003854.

214. Allen C, Büttner S, Aragon AD, Thomas JA, Meirelles O, Jaetao JE, Benn D, Ruby SW, Veenhuis M, Madeo F, Werner-Washburne M. Isolation of quiescent and nonquiescent cells from yeast stationary-phase cultures. J Cell Biol. 2006; 174:89-100.

215. Werner-Washburne M, Roy S, Davidson GS. Aging and the survival of quiescent and non-quiescent cells in yeast stationary-phase cultures. Subcell Biochem. 2012; 57:123-43.

216. Hartwell LH, Unger MW. Unequal division in Saccharomyces cerevisiae and its implications for the control of cell division. J Cell Biol. 1977; 75:422-35.

217. Powell CD, Quain DE, Smart KA. Chitin scar breaks in aged Saccharomyces cerevisiae. Microbiology. 2003; 149:3129-37.

218. Cabib E, Arroyo J. How carbohydrates sculpt cells: chemical control of morphogenesis in the yeast cell wall. Nat Rev Microbiol. 2013; 11:648-55.

219. Barton AA. Some aspects of cell division in Saccharomyces cerevisiae. J Gen Microbiol. 1950; 4:84-6.

220. Egilmez NK, Chen JB, Jazwinski SM. Preparation and partial characterization of old yeast cells. J Gerontol. 1990; 45: B9-17.

221. Sinclair D, Mills K, Guarente L. Aging in Saccharomyces cerevisiae. Annu Rev Microbiol. 1998; 52:533-60.

222. Shi L, Sutter BM, Ye X, Tu BP. Trehalose is a key determinant of the quiescent metabolic state that fuels cell cycle progression upon return to growth. Mol Biol Cell. 2010; 21:1982-90.

223. Benaroudj N, Lee DH, Goldberg AL. Trehalose accumulation during cellular stress protects cells and cellular proteins from damage by oxygen radicals. J Biol Chem. 2001; 276:24261-7.

224. Trevisol ET, Panek AD, Mannarino SC, Eleutherio EC. The effect of trehalose on the fermentation performance of aged cells of Saccharomyces cerevisiae. Appl Microbiol Biotechnol. 2011; 90:697-704.

225. Eleutherio E, Panek A, De Mesquita JF, Trevisol E, Magalhães R. Revisiting yeast trehalose metabolism. Curr Genet. 2015; 61:263-74.

226. Babazadeh R, Lahtvee PJ, Adiels CB, Goksör M, Nielsen JB, Hohmann S. The yeast osmostress response is carbon source dependent. Sci Rep. 2017; 7:990.

227. Singer MA, Lindquist S. Multiple effects of trehalose on protein folding in vitro and in vivo. Mol Cell. 1998; 1:639-48.

228. Singer MA, Lindquist S. Thermotolerance in Saccharomyces cerevisiae: the Yin and Yang of trehalose. Trends Biotechnol. 1998; 16:460-8.

229. Kyryakov P, Beach A, Richard VR, Burstein MT, Leonov A, Levy S, Titorenko VI. Caloric restriction extends yeast chronological lifespan by altering a pattern of age-related changes in trehalose concentration. Front Physiol. 2012; 3:256.

230. Goldberg AA, Bourque SD, Kyryakov P, Boukh-Viner T, Gregg C, Beach A, Burstein MT, Machkalyan G, Richard V, Rampersad S, Titorenko VI. A novel function of lipid droplets in regulating longevity. Biochem Soc Trans. 2009; 37:1050-5.

231. Goldberg AA, Richard VR, Kyryakov P, Bourque SD, Beach A, Burstein MT, Glebov A, Koupaki O, Boukh-Viner T, Gregg C, Juneau M, English AM, Thomas DY, et al. Chemical genetic screen identifies lithocholic acid as an anti-aging compound that extends yeast chronological life span in a TOR-independent manner, by modulating housekeeping longevity assurance processes. Aging (Albany NY). 2010; 2:393-414.

232. Beach A, Titorenko VI. In search of housekeeping pathways that regulate longevity. Cell Cycle. 2011; 10:3042-4.

233. Beach A, Burstein MT, Richard VR, Leonov A, Levy S, Titorenko VI. Integration of peroxisomes into an endomembrane system that governs cellular aging. Front Physiol. 2012; 3:283.

234. Beach A, Richard VR, Leonov A, Burstein MT, Bourque SD, Koupaki O, Juneau M, Feldman R, Iouk T, Titorenko VI. Mitochondrial membrane lipidome defines yeast longevity. Aging (Albany NY). 2013; 5:551-74.

235. Leonov A, Titorenko VI. A network of interorganellar communications underlies cellular aging. IUBMB Life. 2013; 65:665-74.

236. Burstein MT, Titorenko VI. A mitochondrially targeted compound delays aging in yeast through a mechanism linking mitochondrial membrane lipid metabolism to mitochondrial redox biology. Redox Biol. 2014; 2:305-7.

237. Beach A, Richard VR, Bourque S, Boukh-Viner T, Kyryakov P, Gomez-Perez A, Arlia-Ciommo A, Feldman R, Leonov A, Piano A, Svistkova V, Titorenko VI. Lithocholic bile acid accumulated in yeast mitochondria orchestrates a development of an anti-aging cellular pattern by causing age-related changes in cellular proteome. Cell Cycle. 2015; 14:1643-56.

238. Dakik P, Titorenko VI. Communications between mitochondria, the nucleus, vacuoles, peroxisomes, the endoplasmic reticulum, the plasma membrane, lipid droplets, and the cytosol during yeast chronological aging. Front Genet. 2016; 7:177.

239. Handee W, Li X, Hall KW, Deng X, Li P, Benning C, Williams BL, Kuo MH. An energy-independent pro-longevity function of triacylglycerol in yeast. PloS Genet. 2016; 12:e1005878.

240. Medkour Y, Titorenko VI. Mitochondria operate as signaling platforms in yeast aging. Aging (Albany NY). 2016; 8:212-3.

241. Leonov A, Arlia-Ciommo A, Bourque SD, Koupaki O, Kyryakov P, Dakik P, McAuley M, Medkour Y, Mohammad K, Di Maulo T, Titorenko VI. Specific changes in mitochondrial lipidome alter mitochondrial proteome and increase the geroprotective efficiency of lithocholic acid in chronologically aging yeast. Oncotarget. 2017; 8:30672-30691.

242. Li X, Handee W, Kuo MH. The slim, the fat, and the obese: guess who lives the longest? Curr Genet. 2017; 63:43-49.

243. Medkour Y, Dakik P, McAuley M, Mohammad K, Mitrofanova D, Titorenko VI. Mechanisms underlying the essential role of mitochondrial membrane lipids in yeast chronological aging. Oxid Med Cell Longev. 2017; 2017:2916985.

244. Walther TC, Farese RV Jr. Lipid droplets and cellular lipid metabolism. Annu Rev Biochem. 2012; 81:687-714.

245. Kohlwein SD, Veenhuis M, van der Klei IJ. Lipid droplets and peroxisomes: key players in cellular lipid homeostasis or a matter of fat--store 'em up or burn 'em down. Genetics. 2013; 193:1-50.

246. Pol A, Gross SP, Parton RG. Review: biogenesis of the multifunctional lipid droplet: lipids, proteins, and sites. J Cell Biol. 2014; 204:635-46.

247. Gao Q, Goodman JM. The lipid droplet-a well-connected organelle. Front Cell Dev Biol. 2015; 3:49.

248. Horvath SE, Daum G. Lipids of mitochondria. Prog Lipid Res. 2013; 52:590-614.

249. Baile MG, Lu YW, Claypool SM. The topology and regulation of cardiolipin biosynthesis and remodeling in yeast. Chem Phys Lipids. 2014; 179:25-31.

250. Mårtensson CU, Doan KN, Becker T. Effects of lipids on mitochondrial functions. Biochim Biophys Acta. 2017; 1862:102-113.

251. Tatsuta T, Langer T. Intramitochondrial phospholipid trafficking. Biochim Biophys Acta. 2017; 1862:81-89.

252. Bonawitz ND, Chatenay-Lapointe M, Pan Y, Shadel GS. Reduced TOR signaling extends chronological life span via increased respiration and upregulation of mitochondrial gene expression. Cell Metab. 2007; 5:265-77.

253. Pan Y, Shadel GS. Extension of chronological life span by reduced TOR signaling requires down-regulation of Sch9p and involves increased mitochondrial OXPHOS complex density. Aging (Albany NY). 2009; 1:131-45.

254. Pan Y, Schroeder EA, Ocampo A, Barrientos A, Shadel GS. Regulation of yeast chronological life span by TORC1 via adaptive mitochondrial ROS signaling. Cell Metab. 2011; 13:668-78.

255. Titorenko VI, Terlecky SR. Peroxisome metabolism and cellular aging. Traffic. 2011; 12:252-9.

256. Ocampo A, Liu J, Schroeder EA, Shadel GS, Barrientos A. Mitochondrial respiratory thresholds regulate yeast chronological life span and its extension by caloric restriction. Cell Metab. 2012; 16:55-67.

257. Beach A, Titorenko VI. Essential roles of peroxisomally produced and metabolized biomolecules in regulating yeast longevity. Subcell Biochem. 2013; 69:153-67.

258. Beach A, Leonov A, Arlia-Ciommo A, Svistkova V, Lutchman V, Titorenko VI. Mechanisms by which different functional states of mitochondria define yeast longevity. Int J Mol Sci. 2015; 16:5528-54.

259. da Cunha FM, Torelli NQ, Kowaltowski AJ. Mitochondrial retrograde signaling: triggers, pathways, and outcomes. Oxid Med Cell Longev. 2015; 2015:482582.

260. Jazwinski SM. Mitochondria to nucleus signaling and the role of ceramide in its integration into the suite of cell quality control processes during aging. Ageing Res Rev. 2015; 23:67-74.

261. Ruetenik A, Barrientos A. Dietary restriction, mitochondrial function and aging: from yeast to humans. Biochim Biophys Acta. 2015; 1847:1434-47.

262. Arlia-Ciommo A, Piano A, Leonov A, Svistkova V, Titorenko VI. Quasi-programmed aging of budding yeast: a trade-off between programmed processes of cell proliferation, differentiation, stress response, survival and death defines yeast lifespan. Cell Cycle. 2014; 13:3336-49.

263. Giorgio M, Trinei M, Migliaccio E, Pelicci PG. Hydrogen peroxide: a metabolic by-product or a common mediator of ageing signals? Nat Rev Mol Cell Biol. 2007; 8:722-728.

264. Fraenkel DG. Respiration. In: Fraenkel DG. Yeast intermediary metabolism. Cold Spring Harbor, NY: Cold Spring Harbor Laboratory Press, 2011:135-171.

265. Cui H, Kong Y and Zhang H. Oxidative stress, mitochondrial dysfunction, and aging. J Signal Transduct. 2012; 2012:646354.

266. Ray PD, Huang BW and Tsuji Y. Reactive oxygen species (ROS) homeostasis and redox regulation in cellular signaling. Cell Signal. 2012; 24:981-90.

267. Gladyshev VN. The origin of aging: imperfectness-driven non-random damage defines the aging process and control of lifespan. Trends Genet. 2013; 29:506-12.

268. Gladyshev VN. The free radical theory of aging is dead. Long live the damage theory! Antioxid Redox Signal. 2014; 20:727-31.

269. Ristow M and Schmeisser K. Mitohormesis: Promoting health and lifespan by increased levels of reactive oxygen species (ROS). Dose Response. 2014; 12:288-341.

270. Schieber M and Chandel NS. ROS function in redox signaling and oxidative stress. Curr Biol. 2014; 24: R453-62.

271. Shadel GS and Horvath TL. Mitochondrial ROS signaling in organismal homeostasis. Cell. 2015; 163:560-9.

272. Wang Y, Hekimi S. Mitochondrial dysfunction and longevity in animals: Untangling the knot. Science. 2015; 350:1204-7.

273. Gems D and Partridge L. Stress-response hormesis and aging: "that which does not kill us makes us stronger". Cell Metab. 2008; 7:200-3.

274. Calabrese V, Cornelius C, Cuzzocrea S, Iavicoli I, Rizzarelli E and Calabrese EJ. Hormesis, cellular stress response and vitagenes as critical determinants in aging and longevity. Mol Aspects Med. 2011; 32:279-304.

275. Calabrese EJ and Mattson MP. Hormesis provides a generalized quantitative estimate of biological plasticity. J Cell Commun Signal. 2011; 5:25-38.

276. Veal E and Day A. Hydrogen peroxide as a signaling molecule. Antioxid Redox Signal. 2011; 15:147-51.

277. Calabrese V, Cornelius C, Dinkova-Kostova AT, Iavicoli I, Di Paola R, Koverech A, Cuzzocrea S, Rizzarelli E and Calabrese EJ. Cellular stress responses, hormetic phytochemicals and vitagenes in aging and longevity. Biochim Biophys Acta. 2012; 1822:753-83.

278. Gomez-Perez A, Kyryakov P, Burstein MT, Asbah N, Noohi F, Iouk T, Titorenko VI. Empirical validation of a hypothesis of the hormetic selective forces driving the evolution of longevity regulation mechanisms. Front Genet. 2016; 7:216.

279. Medkour Y, Svistkova V, Titorenko VI. Cell-nonautonomous mechanisms underlying cellular and organismal aging. Int Rev Cell Mol Biol. 2016; 321:259-97.

280. Herker E, Jungwirth H, Lehmann KA, Maldener C, Fröhlich KU, Wissing S, Büttner S, Fehr M, Sigrist S, Madeo F. Chronological aging leads to apoptosis in yeast. J Cell Biol. 2004; 164:501-7.

281. Büttner S, Eisenberg T, Herker E, Carmona-Gutierrez D, Kroemer G, Madeo F. Why yeast cells can undergo apoptosis: death in times of peace, love, and war. J Cell Biol. 2006; 175:521-5.

282. Fabrizio P, Longo VD. Chronological aging-induced apoptosis in yeast. Biochim Biophys Acta. 2008; 1783:1280-5.

283. Eisenberg T, Knauer H, Schauer A, Büttner S, Ruckenstuhl C, Carmona-Gutierrez D, Ring J, Schroeder S, Magnes C, Antonacci L, Fussi H, Deszcz L, Hartl R, et al. Induction of autophagy by spermidine promotes longevity. Nat Cell Biol. 2009; 11:1305-14.

284. Carmona-Gutierrez D, Eisenberg T, Büttner S, Meisinger C, Kroemer G, Madeo F. Apoptosis in yeast: triggers, pathways, subroutines. Cell Death Differ. 2010; 17:763-73.

285. Eisenberg T, Carmona-Gutierrez D, Büttner S, Tavernarakis N, Madeo F. Necrosis in yeast. Apoptosis. 2010; 15:257-68.

286. Laun P, Büttner S, Rinnerthaler M, Burhans WC, Breitenbach M. Yeast aging and apoptosis. Subcell Biochem. 2012; 57:207-32.

287. Eisenberg T, Büttner S. Lipids and cell death in yeast. FEMS Yeast Res. 2014; 14:179-97.

288. Richard VR, Beach A, Piano A, Leonov A, Feldman R, Burstein MT, Kyryakov P, Gomez-Perez A, Arlia-Ciommo A, Baptista S, Campbell C, Goncharov D, Pannu S, et al. Mechanism of liponecrosis, a distinct mode of programmed cell death. Cell Cycle. 2014; 13:3707-26.

289. Sheibani S, Richard VR, Beach A, Leonov A, Feldman R, Mattie S, Khelghatybana L, Piano A, Greenwood M, Vali H, Titorenko VI. Macromitophagy, neutral lipids synthesis, and peroxisomal fatty acid oxidation protect yeast from "liponecrosis", a previously unknown form of programmed cell death. Cell Cycle. 2014; 13:138-47.

290. Arlia-Ciommo A, Svistkova V, Mohtashami S, Titorenko VI. A novel approach to the discovery of anti-tumor pharmaceuticals: searching for activators of liponecrosis. Oncotarget. 2016; 7:5204-25.

291. Falcone C, Mazzoni C. External and internal triggers of cell death in yeast. Cell Mol Life Sci. 2016; 73:2237-50.

292. Fannjiang Y, Cheng WC, Lee SJ, Qi B, Pevsner J, McCaffery JM, Hill RB, Basañez G, Hardwick JM. Mitochondrial fission proteins regulate programmed cell death in yeast. Genes Dev. 2004; 18:2785-97.

293. Pereira C, Silva RD, Saraiva L, Johansson B, Sousa MJ, Côrte-Real M. Mitochondria-dependent apoptosis in yeast. Biochim Biophys Acta. 2008; 1783:1286-302.

294. Daignan-Fornier B, Sagot I. Proliferation/Quiescence: When to start? Where to stop? What to stock? Cell Div. 2011; 6:20.

295. Powers RW 3rd, Kaeberlein M, Caldwell SD, Kennedy BK, and Fields S. Extension of chronological life span in yeast by decreased TOR pathway signaling. Genes Dev. 2006; 20:174-84.

296. Alvers AL, Fishwick LK, Wood MS, Hu D, Chung HS, Dunn WA Jr, Aris JP. Autophagy and amino acid homeostasis are required for chronological longevity in Saccharomyces cerevisiae. Aging Cell. 2009; 8:353-69.

297. Alvers AL, Wood MS, Hu D, Kaywell AC, Dunn WA Jr, Aris JP. Autophagy is required for extension of yeast chronological life span by rapamycin. Autophagy. 2009; 5:847-849.

298. Huang X, Withers BR, Dickson RC. Sphingolipids and lifespan regulation. Biochim Biophys Acta. 2014; 1841: 657-64.

299. Jiao R, Postnikoff S, Harkness TA, Arnason TG. The SNF1 kinase ubiquitin-associated domain restrains its activation, activity, and the yeast life span. J Biol Chem. 2015; 290:15393-404.

300. Teixeira V, Costa V. Unraveling the role of the target of rapamycin signaling in sphingolipid metabolism. Prog Lipid Res. 2016; 61:109-33.

301. Fontana L, Partridge L, Longo VD. Extending healthy life span - from yeast to humans. Science. 2010; 328:321-326.

302. Longo VD, Shadel GS, Kaeberlein M, Kennedy B. Replicative and chronological aging in Saccharomyces cerevisiae. Cell Metab. 2012; 16:18-31.

303. Greer EL, Brunet A. Signaling networks in aging. J Cell Sci. 2008; 121:407-412.

304. Goldberg AA, Bourque SD, Kyryakov P, Gregg C, Boukh-Viner T, Beach A, Burstein MT, Machkalyan G, Richard V, Rampersad S, Cyr D, Milijevic S, Titorenko VI. Effect of calorie restriction on the metabolic history of chronologically aging yeast. Exp Gerontol. 2009; 44:555-571.

305. Burstein MT, Kyryakov P, Beach A, Richard VR, Koupaki O, Gomez-Perez A, Leonov A, Levy S, Noohi F, Titorenko VI. Lithocholic acid extends longevity of chronologically aging yeast only if added at certain critical periods of their lifespan. Cell Cycle. 2012; 11:3443-3462.

306. Beach A, Burstein MT, Richard VR, Leonov A, Levy S, Titorenko VI. Integration of peroxisomes into an endomembrane system that governs cellular aging. Front Physiol. 2012; 3:283.

307. Jazwinski SM. The retrograde response retrograde response and other pathways of interorganelle communication interorganelle communication in yeast replicative aging. Subcell Biochem. 2012; 57:79-100.

308. Nunnari J, Suomalainen A. Mitochondria: in sickness and in health. Cell. 2012; 148:1145-1159.

309. Titorenko VI, Terlecky SR. Peroxisome metabolism and cellular aging. Traffic. 2011; 12:252-259.

310. Zoncu R, Efeyan A, Sabatini DM. mTOR: from growth signal integration to cancer, diabetes and ageing. Nat Rev Mol Cell Biol. 2011; 12:21-35.

311. Laplante M, Sabatini DM. mTOR signaling in growth control and disease. Cell. 2012; 149:274-293.

312. Jazwinski SM, Kriete A. The yeast retrograde response as a model of intracellular signaling of mitochondrial dysfunction. Front Physiol. 2012; 3:139.

313. Pellegrino MW, Nargund AM, Haynes CM. Signaling the mitochondrial unfolded protein response. Biochim Biophys Acta. 2013; 1833:410-416.

314. Heeren G, Rinnerthaler M, Laun P, von Seyerl P, Kössler S, Klinger H, Hager M, Bogengruber E, Jarolim S, Simon-Nobbe B, Schüller C, Carmona-Gutierrez D, Breitenbach-Koller L, Mück C, Jansen-Dürr P, Criollo A, Kroemer G, Madeo F, Breitenbach M. The mitochondrial ribosomal protein of the large subunit, Afo1p, determines cellular longevity through mitochondrial back-signaling via TOR1. Aging (Albany NY). 2009; 1:622-636.

315. Baker BM, Haynes CM. Mitochondrial protein quality control during biogenesis and aging. Trends Biochem Sci. 2011; 36:254-261.

316. Nargund AM, Pellegrino MW, Fiorese CJ, Baker BM, Haynes CM. Mitochondrial import efficiency of ATFS-1 regulates mitochondrial UPR activation. Science. 2012; 337:587-590.

317. Haynes CM, Yang Y, Blais SP, Neubert TA, Ron D. The matrix peptide exporter HAF-1 signals a mitochondrial UPR by activating the transcription factor ZC376.7 in C. elegans. Mol Cell. 2010; 37:529-540.

318. Butow RA, Avadhani NG. Mitochondrial signaling: the retrograde response. Mol Cell. 2004; 14:1-15.

319. Buchholz JN, Behringer EJ, Pottorf WJ, Pearce WJ, Vanterpool CK. Age-dependent changes in Ca2+ homeostasis in peripheral neurones: implications for changes in function. Aging Cell. 2007; 6:285-296.

320. Cantó C, Gerhart-Hines Z, Feige JN, Lagouge M, Noriega L, Milne JC, Elliott PJ, Puigserver P, Auwerx J. AMPK regulates energy expenditure by modulating NAD+ metabolism and SIRT1 activity. Nature. 2009; 458:1056-1060.

321. Libert S, Guarente L. Metabolic and neuropsychiatric effects of calorie restriction and sirtuins. Annu Rev Physiol. 2013; 75:669-684.

322. Giorgio M, Trinei M, Migliaccio E, Pelicci PG. Hydrogen peroxide: a metabolic by-product or a common mediator of ageing signals? Nat Rev Mol Cell Biol. 2007; 8:722-728.

323. Oh SW, Mukhopadhyay A, Svrzikapa N, Jiang F, Davis RJ, Tissenbaum HA. JNK regulates lifespan in Caenorhabditis elegans by modulating nuclear translocation of forkhead transcription factor/DAF-16. Proc Natl Acad Sci U S A. 2005; 102:4494-4499.

324. Wang MC, Bohmann D, Jasper H. JNK extends life span and limits growth by antagonizing cellular and organism-wide responses to insulin signaling. Cell. 2005; 121:115-125.

325. Lehtinen MK, Yuan Z, Boag PR, Yang Y, Villén J, Becker EB, DiBacco S, de la Iglesia N, Gygi S, Blackwell TK, Bonni A. A conserved MST-FOXO signaling pathway mediates oxidative-stress responses and extends life span. Cell. 2006; 125:987-1001.

326. Harman D. The biologic clock: the mitochondria? J Am Geriatr Soc. 1972; 20:145-147.

327. Vendelbo MH, Nair KS. Mitochondrial longevity pathways. Biochim Biophys Acta. 2011; 1813:634-644.

328. Xu XM, Møller SG. Iron-sulfur clusters: biogenesis, molecular mechanisms, and their functional significance. Antioxid Redox Signal. 2011; 15:271-307.

329. Gottschling DE. Molecular biology. Fragile delivery to the genome. Science. 2012; 337:160-161.

330. Veatch JR, McMurray MA, Nelson ZW, Gottschling DE. Mitochondrial dysfunction leads to nuclear genome instability via an iron-sulfur cluster defect. Cell. 2009; 137:1247-1258.

331. Cheng X, Ivessa AS. The migration of mitochondrial DNA fragments to the nucleus affects the chronological aging process of Saccharomyces cerevisiae. Aging Cell. 2010; 9:919-923.

332. Cheng X, Ivessa AS. Accumulation of linear mitochondrial DNA fragments in the nucleus shortens the chronological life span of yeast. Eur J Cell Biol. 2012; 91:782-788.

333. Perocchi F, Jensen LJ, Gagneur J, Ahting U, von Mering C, Bork P, Prokisch H, Steinmetz LM. Assessing systems properties of yeast mitochondria through an interaction map of the organelle. PLoS Genet. 2006; 2:e170.

334. Caballero A, Ugidos A, Liu B, Öling D, Kvint K, Hao X, Mignat C, Nachin L, Molin M, Nyström T. Absence of mitochondrial translation control proteins extends life span by activating sirtuin-dependent silencing. Mol Cell. 2011; 42:390-400.

335. Kim J, Kundu M, Viollet B, Guan KL. AMPK and mTOR regulate autophagy through direct phosphorylation of Ulk1. Nat Cell Biol. 2011; 13:132-141.

336. Bungard D, Fuerth BJ, Zeng PY, Faubert B, Maas NL, Viollet B, Carling D, Thompson CB, Jones RG, Berger SL. Signaling kinase AMPK activates stress-promoted transcription via histone H2B phosphorylation. Science. 2010; 329:1201-1205.

337. Narbonne P, Roy R. Caenorhabditis elegans dauers need LKB1/AMPK to ration lipid reserves and ensure long-term survival. Nature. 2009; 457:210-214.

338. Koppen M, Langer T. Protein degradation within mitochondria: versatile activities of AAA proteases and other peptidases. Crit Rev Biochem Mol Biol. 2007; 42:221-242.

339. Delaney JR, Ahmed U, Chou A, Sim S, Carr D, Murakami CJ, Schleit J, Sutphin GL, An EH, Castanza A, Fletcher M, Higgins S, Jelic M, Klum S, Muller B, Peng ZJ, Rai D, Ros V, Singh M, Wende HV, Kennedy BK, Kaeberlein M. Stress profiling of longevity mutants identifies Afg3 as a mitochondrial determinant of cytoplasmic mRNA translation and aging. Aging Cell. 2013; 12:156-166.

340. Bhatia-Kiššová I, Camougrand N. Mitophagy in yeast: actors and physiological roles. FEMS Yeast Res. 2010; 10:1023-1034.

341. Journo D, Mor A, Abeliovich H. Aup1-mediated regulation of Rtg3 during mitophagy. J Biol Chem. 2009; 284:35885-35895.

342. Piper MD, Partridge L, Raubenheimer D, Simpson SJ. Dietary restriction and aging: a unifying perspective. Cell Metab. 2011; 14:154-160.

343. Jewell JL, Russell RC, Guan KL. Amino acid signalling upstream of mTOR. Nat Rev Mol Cell Biol. 2013; 14:133-139.

344. Goldberg AA, Richard VR, Kyryakov P, Bourque SD, Beach A, Burstein MT, Glebov A, Koupaki O, Boukh-Viner T, Gregg C, Juneau M, English AM, Thomas DY, Titorenko VI. Chemical genetic screen identifies lithocholic acid as an anti-aging compound that extends yeast

chronological life span in a TOR-independent manner, by modulating housekeeping longevity assurance processes. Aging (Albany NY). 2010; 2:393-414.

345. Hughes AL, Gottschling DE. An early age increase in vacuolar pH limits mitochondrial function and lifespan in yeast. Nature. 2012; 492:261-265.

346. Schmidt M, Kennedy BK. Aging: one thing leads to another. Curr Biol. 2012; 22:R1048-R1051.

347. Goldberg AA, Bourque SD, Kyryakov P, Boukh-Viner T, Gregg C, Beach A, Burstein MT, Machkalyan G, Richard V, Rampersad S, Titorenko VI. A novel function of lipid droplets in regulating longevity. Biochem Soc Trans. 2009; 37:1050-1055.

348. Eisenberg T, Knauer H, Schauer A, Büttner S, Ruckenstuhl C, Carmona-Gutierrez D, Ring J, Schroeder S, Magnes C, Antonacci L, Fussi H, Deszcz L, Hartl R, Schraml E, Criollo A, Megalou E, Weiskopf D, Laun P, Heeren G, Breitenbach M, Grubeck-Loebenstein B, Herker E, Fahrenkrog B, Fröhlich KU, Sinner F, Tavernarakis N, Minois N, Kroemer G, Madeo F. Induction of autophagy by spermidine promotes longevity. Nat Cell Biol. 2009; 11:1305-1314.

349. Minois N, Carmona-Gutierrez D, Madeo F. Polyamines in aging and disease. Aging (Albany NY). 2011; 3:716-732.

350. Seo JG, Lai CY, Miceli MV, Jazwinski SM. A novel role of peroxin PEX6: suppression of aging defects in mitochondria. Aging Cell. 2007; 6:405-413.

Appendix

List of My Publications

1. Kyryakov, P., Beach, A., Richard, V.R., Burstein, M.T., **Leonov, A.**, Levy, S. and Titorenko, V.I. Caloric restriction extends yeast chronological lifespan by altering a pattern of age-related changes in trehalose concentration. Front. Physiol. (2012) 3:256.

2. Beach, A., Burstein, M.T., Richard, V.R., **Leonov, A.**, Levy, S. and Titorenko, V.I. Integration of peroxisomes into an endomembrane system that governs cellular aging. Front. Physiol. (2012) 3:283.

3. Burstein, M.T., Kyryakov, P., Beach, A., Richard, V.R., Koupaki, O., Gomez-Perez, A., **Leonov, A.**, Levy, S., Noohi, F. and Titorenko, V.I. Lithocholic acid extends longevity of chronologically aging yeast only if added at certain critical periods of their lifespan. Cell Cycle (2012) 11:3443- 3462.

4. Beach, A., Burstein, M.T., Richard, V.R., Gomez-Perez, A., **Leonov, A.**, Iouk, T. and Titorenko, V.I. A modular network regulates longevity of chronologically aging yeast. Cell Biol. Res. Ther. (2013) 2:1000e110.

5. Richard, V.R., **Leonov, A.***, Beach, A., Burstein, M.T., Koupaki, O., Gomez-Perez, A., Levy, S., Pluska, L., Mattie, S., Rafeh, R., Iouk, T., Sheibani, S., Greenwood, M., Vali, H. and Titorenko, V.I. Macromitophagy is a longevity assurance process that in chronologically aging yeast limited in calorie supply sustains functional mitochondria and maintains cellular lipid homeostasis. Aging (2013) 5:234-269. **** Equally contributed 1st co-author.***

6. **Leonov, A.** and Titorenko, V.I. A network of interorganellar communications underlies cellular aging. IUBMB Life (2013) 65:665-674.

7. Beach, A., Richard, V.R., **Leonov, A.***, Burstein, M.T., Bourque, S.D., Koupaki, O., Juneau, M., Feldman, R., Iouk, T. and Titorenko, V.I. Mitochondrial membrane lipidome defines yeast longevity. Aging (2013) 5:551-574. **** Equally contributed 1st co-author.***

8. Sheibani, S., Richard, V.R., Beach, A., **Leonov, A.**, Feldman, R., Khelghatybana, L., Piano, A., Greenwood, M., Vali, H. and Titorenko, V.I. Macromitophagy, neutral lipids synthesis and peroxisomal fatty acid oxidation protect yeast from "liponecrosis", a previously unknown form of programmed cell death. Cell Cycle (2014) 13:138-147.

9. Arlia-Ciommo, A., **Leonov, A.**, Piano, A., Svistkova, V. and Titorenko, V.I. Cell- autonomous mechanisms of chronological aging in the yeast Saccharomyces cerevisiae. Microbial Cell (2014) 1:164-178.

10. Richard, V.R., Beach, A., Piano, A., **Leonov, A.**, Feldman, R., Burstein, M.T., Kyryakov, P., Gomez-Perez, A., Arlia-Ciommo, A., Baptista, S., Campbell, C., Goncharov, D., Pannu, S., Patrinos, D., Sadri, B., Svistkova, V., Victor, A. and Titorenko, V.I. Mechanism of liponecrosis, a distinct mode of programmed cell death. Cell Cycle (2014) 13:3707-3726.

11. Arlia-Ciommo, A., Piano, A., **Leonov, A.**, Svistkova, V. and Titorenko, V.I. Quasi-programmed aging of budding yeast: a trade-off between programmed processes of cell proliferation, differentiation, stress response, survival and death defines yeast lifespan. Cell Cycle (2014) 13:3336-3349.

12. Beach, A., **Leonov, A.**, Arlia-Ciommo, A., Svistkova, V., Lutchman, V. and Titorenko, V.I. Mechanisms by which different functional states of mitochondria define yeast longevity. Int. J. Mol. Sci. (2015) 16:5528-5554.

13. **Leonov, A.**, Arlia-Ciommo, A., Piano, A., Svistkova, V., Lutchman, V., Medkour, Y. and Titorenko, V.I. Longevity extension by phytochemicals. Molecules (2015) 20:6544-6572.

14. Beach, A., Richard, V.R., Bourque, S., Boukh-Viner, T., Kyryakov, P., Gomez-Perez, A., Arlia-Ciommo, A., Feldman, R., **Leonov, A.**, Piano, A., Svistkova, V. and Titorenko, V.I. Lithocholic bile acid accumulated in yeast mitochondria orchestrates a development of an anti-aging cellular pattern by causing age-related changes in cellular proteome. Cell Cycle (2015) 14:1643-1656.

15. Arlia-Ciommo, A., Dakik, P., **Leonov, A.**, McAuley, M., Medkour, Y., Mohammad, K., Iouk, T., Simard, É. and Titorenko, V.I. Mechanisms through which chemical compounds produced by mammals or plants delay chronological aging in yeast. Austin Biol. (2016) 1:1011.

16. **Leonov, A.**, Arlia-Ciommo, A., Bourque, S.D., Koupaki, O., Kyryakov, P., Dakik, P., McAuley, M., Medkour, Y., Mohammad, K., Di Maulo, T. and Titorenko, V.I. Specific changes in mitochondrial lipidome alter mitochondrial proteome and increase the geroprotective efficiency of lithocholic acid in chronologically aging yeast. Oncotarget (2017) 8:30672-30691.

17. **Leonov, A.**, Feldman, R., Piano, A., Arlia-Ciommo, A., Lutchman, V., Ahmadi, M., Elsaser, S., Fakim, H., Heshmati-Moghaddam, M., Hussain, A., Orfali, S., Rajen, H., Roofigari-Esfahani, N., Rosanelli, L. and Titorenko, V.I. Caloric restriction extends yeast chronological lifespan via a mechanism linking cellular aging to cell cycle regulation, maintenance of a quiescent state, entry into a non-quiescent state and survival in the non-quiescent state. Oncotarget (2017) 8:69328-69350.

18. Arlia-Ciommo, A., **Leonov, A.**, Beach, A., Richard, V.R., Bourque, S.D., Burstein, M.T., Kyryakov, P., Gomez-Perez, A., Koupaki, O., Feldman, R. and Titorenko, V.I. Caloric restriction delays yeast chronological aging by remodeling carbohydrate and lipid metabolism, altering peroxisomal and mitochondrial functionalities, and postponing the onsets of apoptotic and liponecrotic modes of regulated cell death. Oncotarget (2018) 9: in press.